QUASICLASSICAL STUDIES OF CHEMICAL REACTION DYNAMICS WITH INCLUSION OF TUNNELING AND NONADIABATIC TRANSITION

OLUWAPONMILE OLOYEDE

Doctor of Philosophy

Department of Functional Molecular Science
School of Mathematical and Physical Science
THE GRADUATE UNIVERSITY FOR ADVANCED STUDIES

September 2005

Thesis supervisor: Professor Hiroki Nakamura

GRADUATE UNIVERSITY FOR ADVANCED STUDIES
Okazaki, Aichi, Japan.

CERTIFICATE OF APPROVAL

PH.D. THESIS

This is to certify that the Ph.D. thesis of

OLUWAPONMILE OLOYEDE

has been approved by the Examining Committee
for the thesis requirement for the Doctor of
Philosophy degree in Functional Molecular Science at the
September 2005 graduation.

Thesis committee: _____
Thesis supervisor

_____
Member

_____
Member

_____
Member

_____
Member

_____
Member

_____
Member

Dedicated to the memory of Alice Kehinde Oloyede, as an eternal gratitude to the priceless virtue of her selflessness.

ACKNOWLEDGMENTS

The completion of a doctoral thesis is a most auspicious moment to pay the author's various debts of gratitude. It would have been almost impossible to carry out the work presented here without the kindness, guidance and generosity of spirit of several people.

Firstly, Professor Hiroki Nakamura's assistance to me has been unquantifiable. Most notable, are his efforts, along with those of Mrs. Nakamura, at enabling me settle down in Japan. He went to every extent to provide me with an enabling environment to carry out my research successfully. In spite of his understandably busy schedule, he did all he could to offer me advice and suggestions at the most appropriate times. When required, he never failed to give me the nudge necessary to shove me out of my bouts of complacency. And he showed an unbelievable measure of patience even when my conducts were plainly intolerable. He has also been helpful materially and even offering a listening ear whenever I needed one. I am grateful that he offered me a place in his group where I have had the opportunity to learn and meet many people who have impacted me considerably, most important among whom is Dr. Gennady Mil'nikov.

Words are not enough to capture the enormity of the debt I owe Dr. Mil'nikov. Ever since I arrived in Okazaki, all green with practically nothing but my enthusiasm, he has done his best to help me with my research, even showing more concern about me than I ever showed myself. I remember vividly his first encounter with me; his first act was to ask me if I could tell him the spectrum of the hydrogenic atom; at our very first meeting, barely 1 hour after my arrival in Japan! He has been a mentor, guardian, 'pro bono' consultant, tutor of Mathematics and Physics, amongst his many other roles. He has even helped a couple of times with my stylistics! I thank him most sincerely and deeply appreciate his every attempt to make me a better scientist.

Other members of the Nakamura group have also been most helpful and kind. I offer my heartfelt thanks to Dr. Yi Zhao, Dr. Alexey Kondorskiy, Dr. Chaoyuan Zhu, Dr. Shinkoh Nanbu, Dr. Toshimasa Ishida, Dr. Shimpei Chikazumi, Dr. Shiyang Zou, Dr Hiroyuki Tamura, Dr. Hirsohi Fujisaki, Dr Hideyuki Kamisaka, Dr. Artur Ishkhanyan, Dr. E. A. Solov'ev and Dr. V. Osherov. Dr Shinkoh Nanbu deserves special mention for his help

with computational facilities and offering me technical assistance whenever I needed it. I also wish to put on record the collegiality I enjoyed with many members of the Theoretical Studies Department and the kindness of the secretaries.

My former teachers also deserve a place here for the various roles they played in helping me achieve my dreams of a postgraduate education. These include Professors Olu Ogboja, J.U. Nwalor, T. Ajayi, A. Ogunbayo, A.S.B. Gimba, J. Cable, C. Gilmer, M. Rodgers, H. Xi, T. Kinstle and many others too numerous to mention.

My parents have given me the kind of understanding that almost defies human logic. They have never for once questioned my chosen paths, always displaying the attitude that my judgement needed no substitution with theirs. Most poignantly, I remember my mother who willingly let me pursue my work, suppressing the urge to make demands of me that would well have been within her maternal rights. My achievement of a doctoral degree amounts to nothing without the garland of her sweet memory. I also seize the opportunity to thank my brother, Ope, my wife, Bukola, Auntie Funke and the girls, and all my younger siblings for their moral support. And to Alhaja Akinboro, I hope you find fulfillment in this as yet another testament to your wisdom.

I extend my deep appreciation to the Ministry of Education of the Japanese Government for providing me with financial support that allowed me concentrate on my work without worrying about my sustenance.

And to all old friends and benevolent spirits, thanks for being the constant wind beneath my wings.

TABLE OF CONTENTS

CHAPTER 1

GENERAL INTRODUCTION

The subject of chemical dynamics typically consists of two different but complementary steps. First, one desires to know the behavior of the potential energy between interacting species, and secondly, one needs to study how this potential energy surface influences the chemical reactions between these chemical species. The former is the focus of a large number of active researchers who have adapted the tools of quantum chemistry to obtain chemically-accurate potential energy surfaces which have been used to reproduce results of various experiments in spectroscopy, chemical reaction studies etc. The latter effort, using equations of motion derived from physical laws for reactions studies, is the subject matter of this thesis.

Along with the elegant approximations and simpler formulations which have enabled a better understanding of the physics and chemistry of these problems, the sophistication of modern computers have also played quite a role in pushing advances in this field to its current state. The availability and development of increasingly fast computers with bigger storage capabilities continue to influence the course of chemical dynamics studies in no small measure; researchers therefore consider this bit of good fortune as an invitation to tackle systems which are progressively larger and more complicated than those that were being studied a decade or two ago.

The sheer power of these computational resources does not, however, obliterate the difficulty to contend with, if one intends to treat a large system (like the smallest of proteins or enzymes) with a fully quantum-mechanical scheme. The quantum mechanical equations to describe these many-body systems become so large and unwieldy that the expectation of using a wholly quantal approach to routinely study those systems remains an impractical undertaking.

Nonetheless, the approaches which are based on the solution of the classical equations of motion continue to offer recourse to studying chemical dynamics in systems of various size and complexity. The earliest calculations based on the solution of the classical equations of motion were carried out by Wall, Hiller and Mazuron [1] to determine the transition probability for a simple chemical reaction. Some years later they also pioneered the use of the pseudo-random numbers in selecting initial condition for collision[2], completing the groundwork for what has become the standard technique for implementing classical trajectory computations.

As experimental results from crossed molecular-beam studies of chemical reactions became more available, people like Blais et al [3], and Karplus et al [4], became more interested in further testing the validity of classical methods. In a simple, but notable study of an A+ BC type reaction, Karplus and co-workers introduced the quasiclassical assumption that the initial molecular states were quantized properly. This replaced the earlier practice of taking the energy levels as continuous as suggested by classical mechanics, marking the start of attempts at situating a bit of quantum effects within classical simulations. However, the presence of more critical quantum effects like interference and tunneling at low energies, demonstrated that classical mechanics, as a stand-alone technique, was inherently flawed. In chemical reactions, the pertinent quantum effects one needs to consider include the zero-point energy problem, tunneling, resonance[5], nonadiabatic transitions, amongst others.

In a series of papers[6, 7], Miller, inspired by earlier works by Ford and Wheeler[8], developed the concept of the classical S-matrix theory which uses classical mechanics to construct the classical limit of the quantum mechanical transition amplitude and manipulate it quantum mechanically[9]. The goal was to show how classical trajectories could be used to obtain a classical approximation to the S-matrix elements in order to compute the quantum mechanical cross sections. Similar ideas were put forward by Pechukas[10] who used the path integral of Feynman to derive a semiclassical scattering theory, while Marcus[11] employed a WKB-type method to directly calculate the S-matrix for inelastic and reactive collisions. These efforts were the first of the many imaginative pursuits that have come to mark the attempts at grafting quantum effects into the simpler task of computing classical trajectories, and together, are considered among the highlights of semiclassical research endeavors.

For routine work however, it is more practical to revert to more straight-forward applications of classical simulations because as far as the overall reaction probabilities are concerned, it is expected that a little averaging goes a long way in washing out the quantum interference effects.[9] This guarantees that classical trajectory methods, with nonadiabatic transitions and tunneling taken into account, would be very much useful and feasible for chemical dynamics especially for large systems.

The search for such a simple approximation that could act as an accessory to the full trajectory simulation of the chemical dynamics motivated the paper by Tully and Preston[12]. They formulated what has become known as the Trajectory Surface Hopping Method in order to include multi-surface effects in classical calculations. In this scheme, the nuclear motion is treated classically on a single adiabatic potential energy surface, and on reaching an avoided crossing between the potential energy surfaces, the trajectory is split into different branches which follow the different potential energy surfaces. Since this work was published, there have been several modifications regarding how to choose a better criterion for hopping location or hopping probability, but the central idea has endured. Examples of related works are those of Miller and co-workers[13], Truhlar and co-workers[14], Stine and Muckerman[15], Zhu and co-workers[16, 17].

In a similar fashion, Makri and Miller[18], proposed an approximate way to treat tunneling just as Tully and Preston had done for nonadiabatic transition. They relaxed the requirement that the model be rigorously accurate, when compared to previous theories like the complex-valued trajectories[19], the classical S-matrix theory[7], or the instanton model[20], because they were more concerned with the ease of applicability. A classical trajectory is made to evolve in a classically-allowed region of space and on encountering an intervening barrier between two separated classically-allowed regions, it has a probability to make an instantaneous transition in real time. The model gave a fair description of tunneling phenomena under a wide variety of conditions providing a simple but practical starting-point for adding tunneling to classical methodology.

It is obvious from the foregoing, that making classical simulations better has been the goal of an extensive number of research efforts and we argue here that, there is even a whole lot more to be achieved with classical simulations. This is especially true if we have good semiclassical analytical theory to deal with the important quantum effects such as nonadiabatic transitions and tunneling. These issues provide the motivation for the theme of this thesis where I report the several dynamical studies that have been carried out, in

some sense, to push the envelope further in the use of classical trajectory methods by using improved semiclassical theories of quantum effects.

In Chapter 2, I report on our study of finding caustics-an important feature in semiclassical analysis, in multi-dimensional space. The study of caustics is important not only because they are geometrical objects in their own right, but because they mark the points where the behavior of the WKB wavefunction becomes intractable. Since the momentum vanishes at these caustics, it is clear that they are points at which tunneling paths emerge and therefore are crucial to the attempts at adding tunneling effects to classical simulations. There has not been any simple and systematic way of finding caustics but the present theory can present a general method that works for any system.

To complete chapter 2, we present numerical demonstrations of how to locate caustics of trajectories in the Henon-Heiles potential and also extended the same to the caustics in a potential of a triatomic system undergoing reaction. This extension to chemical reaction systems, called for a retooling of our method, since the condensation region of the reaction process has caustics happening almost simultaneously in different regions of configuration space. The final method[21] capably treats this case of multiple caustics and therefore is a good candidate for use in studying multi-dimensional systems. The light masses of the constituent atoms in the H_3 system makes it a good testing ground for many tunneling theories. With this realization, I seize the advantage offered by the caustics-locating method, merging it with a simple "straight-line tunneling path" method to calculate the thermal rate constant of the H_3 system. Our method proves especially useful because the direction of tunneling used in this calculation, can be easily obtained from a by-product quantity of our caustics method.

Chapter 3 concerns the semiclassical study of nonadiabatic transition. I report here, an improvement and generalization of the Trajectory Surface Hopping Method of Tully and Preston which was briefly mentioned above. In the original method, the hopping points were dictated by the location of the seam surface and the probability of hop was determined by integrating the time-dependent coupled equations or by using the Landau-Zener formula. The small size of the DH_2^+ [16] system permitted the use of an analytical expression to determine the seam surface for the system. [The seam surface is the locus of the points along the potential surface of a system which defines the points where hopping can take place]. For large and complicated systems, this geometrical construct is not easily defined and hence, cannot be easily obtained for use in calculation. Also, the Landau-Zener formula

for curve-crossing has been known to be quite inaccurate in a wide variety of situations and its use has been a weakness of previous surface hopping implementations.

The method presented in this chapter, avoids these problems by seeking a generalized method which does not require the knowledge of the seam surface. This is particularly desirable if one intends to extend the scope of problems which surface hopping methods can tackle. The use of the Zhu-Nakamura theory[8] is also introduced, with the approximation that the nonadiabatic transition can be reduced to a one-dimensional problem. The Zhu-Nakamura theory adds a crucial advantage to classical treatments of nonadiabatic transitions because the theory is valid for classically-forbidden hops. These hops arise when the energy of the classical trajectory is not enough to reach the crossing point. Other methods fail completely at treating such non-classical scenarios and this underlines the crucial modification which the work in this thesis adds to classical simulations. Even the fewest switches method of Tully[22], which has been recently proposed and quite widely used, cannot fully take into acount these transitions. I present the results of the application of the improved surface hopping method to two systems; first is the simple test case of DH_2^+ system which features only the Landau-Zener type hops and secondly, a conical intersection system which has a richer variety of transitions.

The goal of chapter 4 is the extension of the aforementioned quasiclassical methodologies to the subject of the real chemical reactions O + HCl $\longrightarrow$ OH + Cl, H + ClO, in the OHCl system which is an important molecule in atmospheric chemistry[23]. The ground $1\ ^1A'$ potential surface has two deep wells corresponding to HClO and HOCl and there are two other excited potential surfaces, the $1^1A''$ and the $2^1A'$ which participate in the reactions. The differential cross section, branching ratio and product internal state distribution of this system are of utmost interest and have been measured experimentally. However, since the possible mediating effects of the two excited surfaces have never been considered in quasiclassical calculations, the results of this chapter should help in clarifying the reaction dynamics in important atmospheric events.

In the final chapter, I present the conclusion and offer my conjectures as to what the future holds for quasiclassical methods. My submission is that classical approaches remain very relevant to the practice of chemical dynamics as long as it is carefully coupled to semiclassical theories. Developments in semiclassical theories is expected to encourage even more imaginative use of classical trajectories in dynamical studies for a long time to come, especially in the future when they should prove essential to the study of large systems.

REFERENCES

[1] F. T. Wall, L. A. Hiller, Jr., J. Mazur, J. Chem. Phys., **29**, 255 (1958)

[2] F. T. Wall, L. A. Hiller, Jr., J. Mazur, J. Chem. Phys., **35**, 1284 (1961)

[3] N.C. Blais, D.L. Bunker, J. Chem. Phys., bf 37, 2713 (1962); ibid. **39**, 315 (1963); ibid. **41**, 2877 (1964)

[4] M. Karplus, R.N. Porter, R.D. Sharma, J. Chem. Phys., **43**, 3259 (1965)

[5] G. C. Schatz, Ann. Rev. Phys. Chem., **39**, 317 (1988)

[6] W. H. Miller, J. Chem. Phys., **53**, 1949 (1970); ibid. **53**, 3578 (1970); ibid. **54**, 5386 (1971); C.C. Rankin and W.H. Miller, ibid. **55**, 3150, (1971)

[7] W.H. Miller, Adv. Chem. Phys., **25**, 69 (1974); ibid. **30**, 74 (1975)

[8] K.W. Ford, J.A. Wheeler, Ann. Phys. **7**, 259, (1959)

[9] W. H. Miller, Acc. Chem. Res., **4**, 161, (1971)

[10] P. Pechukas, Phys. Rev., **181**, 166,(1969) ; ibid. **181**, 174, (1969)

[11] R.A. Marcus, Chem. Phys. Lett. **7**, 525 (1970); J. Chem. Phys., **53**, 3965 (1971); J.N.L. Connor and R.A. Marcus, J. Chem. Phys., **55**, 5636 (1971); W. H. Wong and R.A. Marcus, J. Chem. Phys., **55**, 5663 (1971); R.A. Marcus, J. Chem. Phys., **56**, 311 (1972); J. Stine and R. A. Marcus, Chem. Phys. Lett. **15**, 536 (1972); R.A. Marcus, J. Chem. Phys., **57**, 4903 (1972)

[12] J.C. Tully and R. K. Preston, J. Chem. Phys., **55**, 562 (1970)

[13] H.D. Meyer, W.H. Miller, J. Chem. Phys., **72**, 2272; ibid. **71**, 2156,(1979); C.W. McCurdy, H.D. Meyer and W.H. Miller, ibid. **70**, 3177, (1979)

[14] D.G. Truhlar and N.C. Blais, J. Chem. Phys., **79**, 1334 (1983); ibid. **106** (21): 8699 (1997); J. Phys. Chem. A **102**, 1666 (1998); ibid. **103**, 6309 (1999)

[15] J.R. Stine and J.T. Muckerman, J. Chem. Phys., **65**, 3975, (1976); ibid. **68**, 185, (1978); ibid. **84**, 1056, (1986)

[16] C. Zhu, K. Nobusada and H. Nakamura, J. Chem. Phys., **115**, 3031 (2001); ibid. **116**, 3234 (2001)

[17] C. Zhu, H. Kamisaka and H. Nakamura, J. Chem. Phys.,**116**, 3234 (2001)

[18] N. Makri, W.H. Miller, J. Chem. Phys., **91**, 4026, (1989)

[19] J. D. Doll, T. F. George, and W. H. Miller, J. Chem. Phys., **58**, 1343 (1972)

[20] A. O. Caldeira, A. J. Legget, Ann. Phys., **149**, 374 (1983)

[21] P. Oloyede, G.V. Mil'Nikov, H. Nakamura, J. Theo. Comp. Chem., **3**, 91,(2004)

[22] J. C. Tully, J. Chem. Phys., **93**, 1061, (1990)

[23] S. Nanbu, M. Aoyagi, H. Kamisaka, H. Nakamura, W. Bian and K. Tanaka, J. Theo. Comp. Chem., **1**, 263, (2002)

[24] W.H. Miller, T.F. George, J. Chem. Phys., **56**, 5637, (1972); H.D. Meyer, W.H. Miller, ibid. **70**, 3214, (1979)

[25] H. Nakamura, *Nonadiabatic Transitions, Concepts, Basic Theories and Applications* (World Scientific, 2002)

CHAPTER 2

CAUSTICS OF CLASSICAL TRAJECTORY

2.1 INTRODUCTION

A widely-employed tool for visualizing systems of 2 degree of freedoms is the surface-of-section method pioneered by Poincaré[1] and which was used to great effect by Henon and Heiles. This method displays the curves of the integrable system in the form of a map and the trace left by these curves as they pierce the 2-dimensional submanifold. However, for systems with dimensions greater than 2, (the dimension of the surface of section, m has 2N-2 degrees of freedom) visualization in the form of these sections are immensely difficult. Despite attempts by Martinet and Magnenat[2], and by Froeschelé[3] to obtain projections on 4-dimensional surface of section, the problem of visualizing of such system is still far from solved. However, since the nature of integrability or otherwise of a general Hamiltonian system of n$\geq$3 system can be obtained from the behavior of the projection of the boundary which are the caustics, a method to determine caustics should offer a very useful approach to obtain the information which are unavailable using the Poincaré surface-of-section method. The contents of this chapter address these issues.

Apart from their nature as important semi-classical geometrical objects worthy of study in their own rights, the importance of caustics for practical dynamical studies is crucial to the thematic thrust of this thesis. Caustics arise in diverse fields of physics and chemistry especially when semiclassical approximations are used to describe a system. For instance, in the short-wavelength limit of the theory of semiclassical interferences, the divergences between the classically-allowed and classically-forbidden regions correspond to the caustics in the diffraction pattern[4]. Other examples of the significance of caustics arise in the

application of semiclassical quantization schemes[5], in astronomy and astrophysics[2, 6], in chemical reaction dynamics and in many other fields. Caustics are important in the study of multi-dimensional systems because they are the multidimensional analogues of the turning point in 1-dimensional system.

In chemical reaction dynamics, the clever use of classical mechanics has generated great interest because of its low computational cost when compared to the alternative of using the quantum mechanical approach, particularly in large systems. Important quantum mechanical effects such as tunneling, phase interference and nonadiabatic transition should, of course, be taken into account[7, 8]. Tunneling, both potential tunneling and dynamic tunneling, play vital roles in multi-dimensional chemical dynamics and several workers have suggested different methods to include its effects into conventional classical trajectory propagation. (See, for example, review by Takatsuka et al[9] and references therein). In any case, non-classical propagation beyond the classically-allowed region is required and a logical starting point for such propagations is the boundary between the classically-allowed and -forbidden areas. By devising a method to locate the caustics, this boundary can be accurately identified.

It is well known that in a $2N$-dimensional phase space, the N-dimensional Lagrange manifold is generated by a continuous set of the map of coordinates and momenta in time, $\{q(t), p(t)\}$. On projecting this manifold onto the configuration space, almost all points are diffeormorphic while some points show up as singularities. These singularities can be mathematically written in two forms: either $\frac{\partial q(t)}{\partial q(0)} = 0$ or $\frac{\partial p(t)}{\partial q(t)} = \infty$. This formal description suggests two approaches for numerical determination of the location of caustics.

One approach is to propagate $\frac{\partial q(t)}{\partial q(0)}$, a minor of the monodromy matrix which is the solution of certain coupled linear differential equations[10, 11]. This system of coupled equations is reducible to a 2^{nd} order differential equation equivalent to the equation for linear deviation of a classical trajectory. For long propagation time, the solution of such an equation may become unstable due to exponentially growing and decaying terms which can be several orders of magnitude apart. The second approach, adopted in this work, is to propagate $\frac{\partial p(t)}{\partial q(t)}$, which is a solution of a Riccatti-type differential equation [12]. The higher degree of numerical stability common to this type of non-linear differential equation makes this approach particularly appealing, but the divergence of the solution at the caustics persists and hinders solution of this equation beyond the singularity. This divergence is an intrinsic property of the solution and cannot be avoided simply by improving the sophistication of

the numerical recipe. By this reckoning, we propose in this chapter a sequence of canonical transformations capable of avoiding the divergence of the solution of the differential equation while accurately locating the caustics.

The outline of this chapter is as follows; in Section 2.2, we present the basic equations and explain the transformations which ensure the avoidance of singularities. To test its efficiency, the method is first used to locate caustics of trajectories of the 2-D Henon-Heiles potential in both regular and chaotic regimes, and then applied to trajectories used to simulate a triatomic chemical reaction process. The reaction case is of a higher dimension and the distribution of caustics is more complicated, especially in the condensation region of chemical reaction. This includes the appearance of two or more caustics in different spatial coordinates at almost the same instant in time (In a time profile of the eigenvalue of the propagated matrix, these coalescent caustics appear as split peaks). For these reasons, the formulation used in the 2-D case does not adequately handle all the divergences in the higher dimension and needs to be reworked to prevent divergence when successive caustics occur very closely. Our method has been generalized to treat such higher-dimensional problems making it applicable to any arbitrary N-dimensional system. The results of these numerical tests as well as the generalizations used in the higher-dimensional case are discussed in Section 2.3. Some applications of the use of the caustics method are presented in Section 2.4 and concluding remarks are presented in Section 2.5.

2.2 BASIC EQUATIONS AND STRATEGY

In a Lagrange manifold, in order to obtain the matrix of the derivatives $\mathbf{A}_{ij} = \frac{\partial p_i}{\partial q_j}$, i,j=1,2,. . ., N, we consider the family of charactersitics for the Hamilton-Jacobi equation $(q(\gamma),p(\gamma))$ where γ is an N-dimensional parameter. The matrix of the second derivatives $\mathbf{A}_{ij}$ can be written in terms of the derivatives with respect to the dimensional parameter, γ

$$\mathbf{A} = \frac{\partial p_i}{\partial q_j} = \frac{\partial p_i}{\partial \gamma_j}\left(\frac{\partial q_i}{\partial \gamma_j}\right)^{-1}. \tag{2.1}$$

Along the charactertistics, the time derivative of the matrix of second derivative can be written as

$$\frac{d}{dt}\mathbf{A} = \left[\frac{d}{dt}\left(\frac{\partial p_i}{\partial \gamma_j}\right)\right]\left(\frac{\partial q_i}{\partial \gamma_j}\right)^{-1} - \mathbf{A}\left[\frac{d}{dt}\left(\frac{\partial q_i}{\partial \gamma_j}\right)\right]\left(\frac{\partial q_i}{\partial \gamma_j}\right)^{-1}. \tag{2.2}$$

Differentiating Hamilton's equations with respect to the parameter γ, one obtains

$$\frac{d}{dt}\Big(\frac{\partial p_i}{\partial \gamma_j}\Big) = -H_{qq}\Big(\frac{\partial q_i}{\partial \gamma_j}\Big) - H_{qp}\Big(\frac{\partial p_i}{\partial \gamma_j}\Big), \tag{2.3}$$

$$\frac{d}{dt}\Big(\frac{\partial q_i}{\partial \gamma_j}\Big) = H_{pq}\Big(\frac{\partial q_i}{\partial \gamma_j}\Big) + H_{pp}\Big(\frac{\partial p_i}{\partial \gamma_j}\Big) \tag{2.4}$$

where H_{qq}, $H_{qp}\ldots$ are the matrices of second derivative of the Hamiltonian taken along the trajectory, i.e. $\frac{\partial^2 H}{\partial q \partial q}$, $\frac{\partial^2 H}{\partial q \partial p}\ldots$. Inserting these relations to Eq. 2.2, one obtains the following Riccati-type differential equation

$$\dot{A} = H_{qq} + H_{qp}A + AH_{pq} + AH_{pp}A.^{1} \tag{2.5}$$

During propagation of the classical trajectory, the solution of equation 2.5 diverges at the caustics where

$$\mathrm{Det}|A(t_{caustics})| = \infty. \tag{2.6}$$

As stated in the introduction, further solution of the differential equation is not possible beyond this point and we have to reformulate the problem. To achieve this, we propose the following transformations.

2.2.1 Propagation and Transformation of the Matrix **A**.

To clarify the idea behind the proposed transformations, consider a one-dimensional problem with solution, $A = \frac{\partial p}{\partial q}$. At the turning point, $p(q) = 0$ and A diverges. By inverting A to obtain $\tilde{A} = \frac{\partial q}{\partial p}$, the divergence is eliminated and propagation of $\tilde{A}$ proceeds smoothly through the caustics. This inversion is equivalent to a canonical transformation, $(p, q) \rightarrow (-\tilde{q}, \tilde{p})$ (The sign change ensures that the transformation is canonical and that Hamilton's equations of motion remain invariant in the new representation). It is relevant to reiterate that the second derivative coefficients are also changed in the new representation and it can be shown that Eq. 2.5 does not change under the transformation.

The reason is that if the matrix A has an element which is a derivative of an integral-of-motion, such an element vanishes and the inversion of the matrix diverges for reasons not directly related to the presence of caustics. A more workable approach is to selectively invert only the diverging element(s) of the old matrix. If the diverging element is assumed to be A_{NN}, the inversion of this element corresponds to a transformation of type

[1] The preceeding proof is obtained thanks to Dr. G. V. Mil'nikov

$(p_N, q_N) \rightarrow (-\tilde{q}_N, \tilde{p}_N)$ which in the new representation, mixes the momenta and coordinates. The new matrix $\tilde{A}$ formed becomes free of any diverging element and its propagation proceeds smoothly through the caustics.

For numerical implementation, the sequential steps to carry out these procedures are summarized below:
(**1**). For an $N \times N$ matrix, irrespective of the position of the diverging matrix element, a simple rotation ensures the repositioning of the diverging element as the (N, N) element of the matrix. This rotation is a canonical transformation and we note that such a rotation is best achieved using the orthogonal matrix which diagonalizes A. Writing this diagonalizing matrix as S, the rotationally-transformed version of A is obtained by

$$p' = Sp \quad \text{and} \quad q' = Sq \tag{2.7}$$

so that

$$A' = SAS^T. \tag{2.8}$$

(**2**). By invoking the transformation $(p'_N, q'_N) \rightarrow (-\tilde{q}_N, \tilde{p}_N)$, we obtain $A' \rightarrow \tilde{A}$, i.e.

$$\frac{D(p')}{D(q')} \rightarrow \frac{D(\tilde{p})}{D(\tilde{q})} \tag{2.9}$$

where:

$$\tilde{p}_i, \ldots, \tilde{p}_{N-1} = {p'}_i, \ldots, {p'}_{N-1} \tag{2.10}$$

$$\tilde{p}_i, \ldots, \tilde{q}_{N-1} = {q'}_i, \ldots, {q'}_{N-1} \tag{2.11}$$

$${p'}_N = -\tilde{q}_N, \quad \text{and} \quad {q'}_N = \tilde{p}_N. \tag{2.12}$$

Equations 2.9 – 2.12 are then used to compute the matrix elements of $\tilde{A}$ in terms of the elements of A' by evaluating partial derivatives of the new Jacobi matrix $\frac{D(\tilde{p})}{D(\tilde{q})}$. The second derivative coefficients in the new representation are derived by rotating the old coefficients as in Eq. 2.7 for consistency, and then substituting the new momenta and coordinates into the old coefficients. For instance, replacing p_N and q_N with $-\tilde{q}_N$ and $\tilde{p}_N$ respectively give

$$(H_{\tilde{q}\tilde{q}})_{NN} = (H_{pp})_{NN}. \tag{2.13}$$

Similar trivial substitutions are used to compose all the other elements of the second derivatives in the new representation. The newly-composed matrix $\tilde{A}$ also satisfies Eq. 2.5 using the modified second derivatives as coefficients.

In the new form, the singularity has been eliminated and the propagation runs smoothly through the hitherto divergent region and the solution of Eq. 2.5 can be obtained with the added advantage of locating the caustics by monitoring either its determinants or its eigenvalue. Well beyond the point of divergence, the inverse transformation is carried in exact reverse order to revert to the matrix A. The original propagation is then continued at regions far away from caustics.

2.3 NUMERICAL TEST

2.3.1 Caustics in Chaotic case.

To test the ideas presented here, we apply the method to a 2-D Henon-Heiles Hamiltonian (in atomic units)[13]

$$H = \frac{1}{2}(p_x^2 + p_y^2) + \frac{1}{2}(x^2 + y^2) + (x^2 y - \frac{1}{3}y^3). \tag{2.14}$$

For this Hamiltonian, the Poincaré surface section method has been successfully used to distinguish between the regular and chaotic regimes depending on the energy. The destruction of the regular pattern of caustics after the full onset of chaos is a well-known phenomenon and following the work of Stuchi and Vieria-Martin[10], we also seek to locate caustics of these trajectories in both regular and chaotic regimes and compare the picture of caustics in this potential with the surface section at the same initial condition.

The classical trajectory was generated from the turning point ($\vec{p}(0) = 0$) which corresponds to initial condition $A^{-1} = 0$ for Eq. 2.5 After short time propagation of A^{-1} the propagation is continued with matrix A. In the cases considered, the initial x_0 is -0.43 while the y_0 has been taken to be -0.37, -0.39 and -0.41. These cases correspond to a progressive degeneration of a regular trajectory into full chaos as the accompanying figures show. As is well known, in the case of the regular regime (Fig. 2.1), the caustics clearly provide the envelope of the family of trajectories. As the system becomes chaotic, discontinuites (Fig. 2.3) and separatrices (Fig. 2.5) appear in the Poincaré surface section and the caustics is no longer discernible with the tori totally destroyed. The present method works well in all these regimes(See Fig. 2.4).

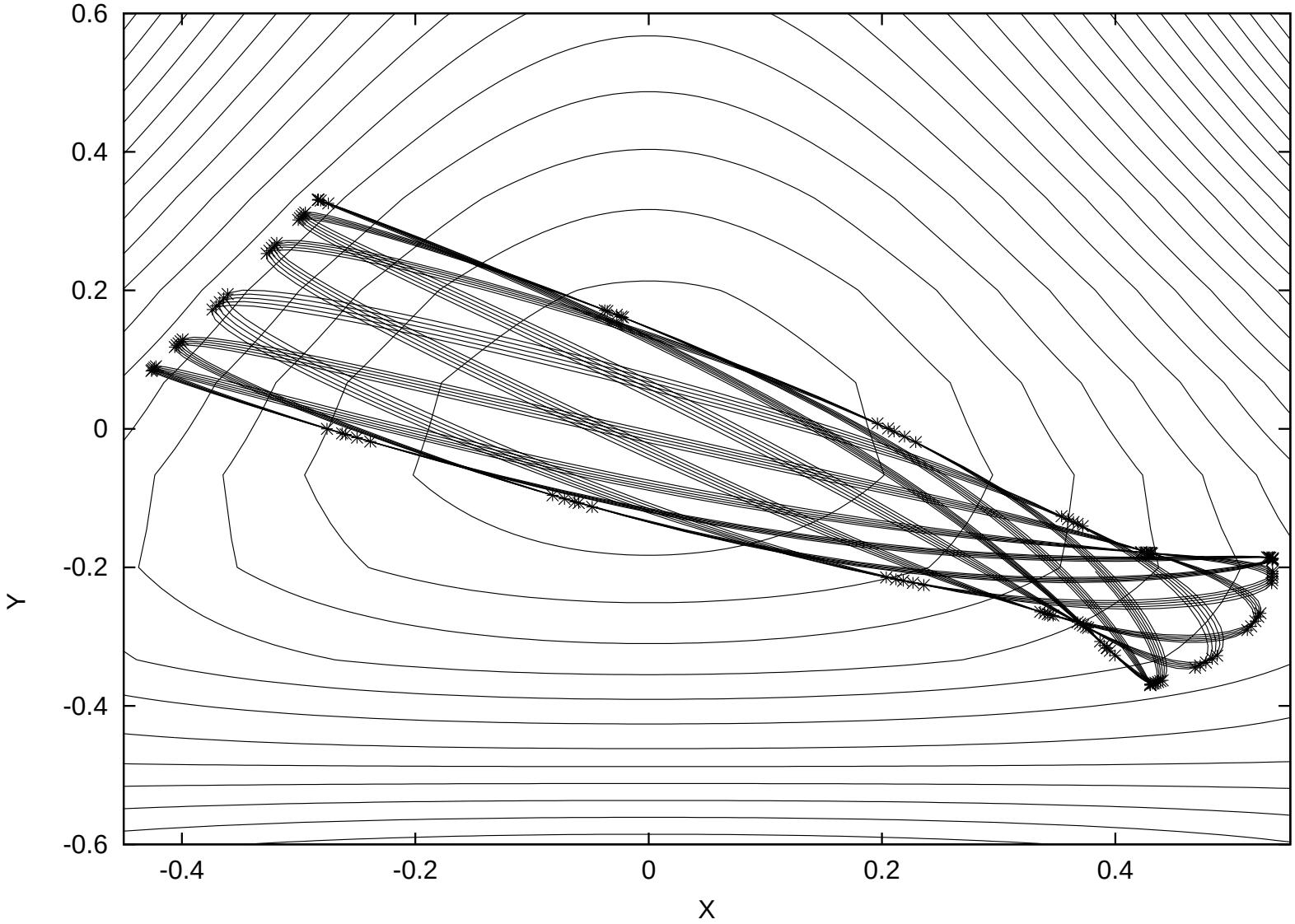

Figure 2.1: Henon-Heiles trajectory for initial condition: x_0=-0.43 and y_0=-0.37. The asterisks indicate location of caustics.

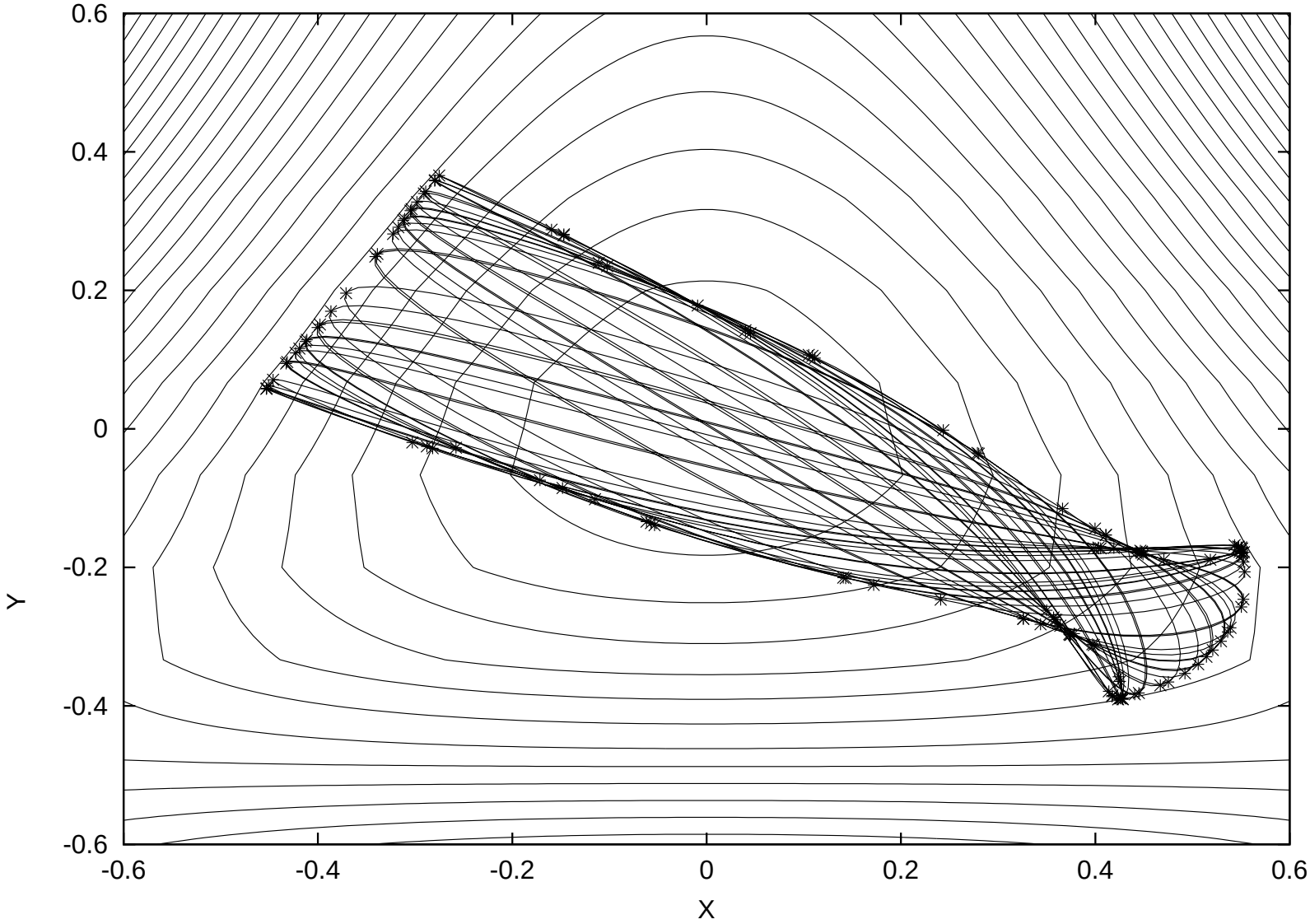

Figure 2.2: Henon-Heiles trajectory for initial condition: x_0=-0.43 and y_0=-0.39. Partial destruction of caustics is seen.

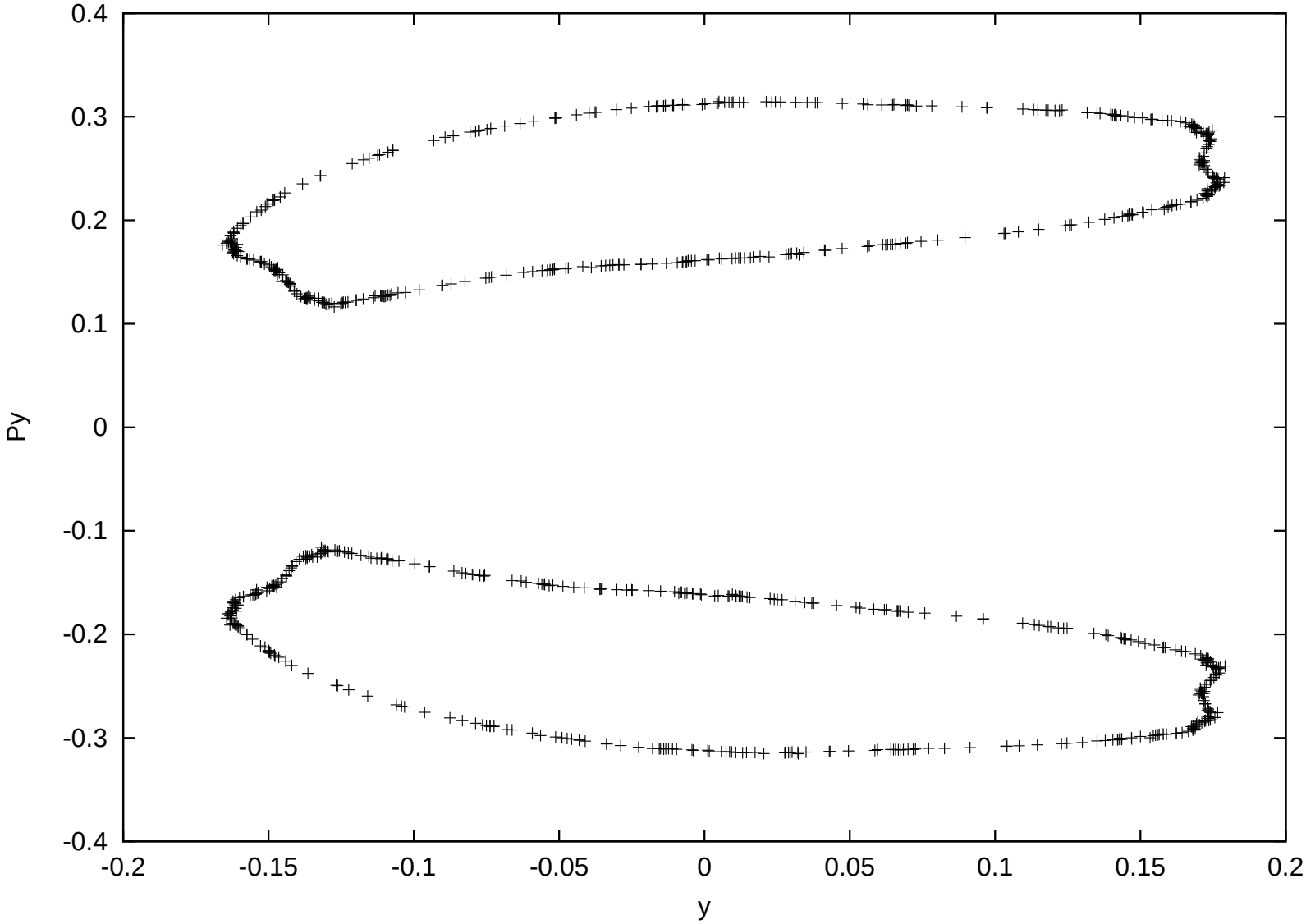

Figure 2.3: Poincaré surface corresponding to Fig. 2.2.

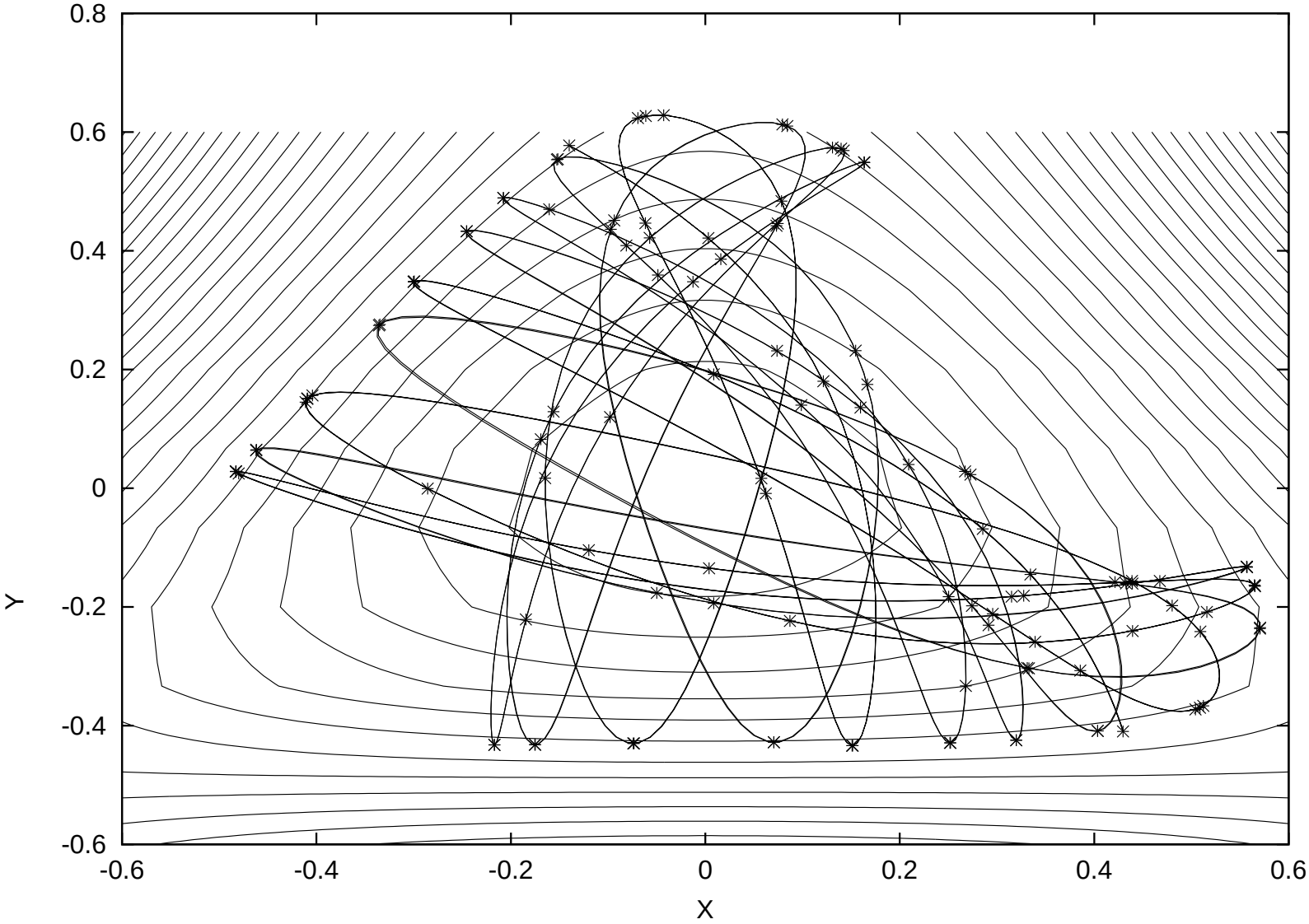

Figure 2.4: Henon-Heiles trajectory for initial condition: x_0=-0.43 and y_0=-0.41. Total destruction of caustics is seen.

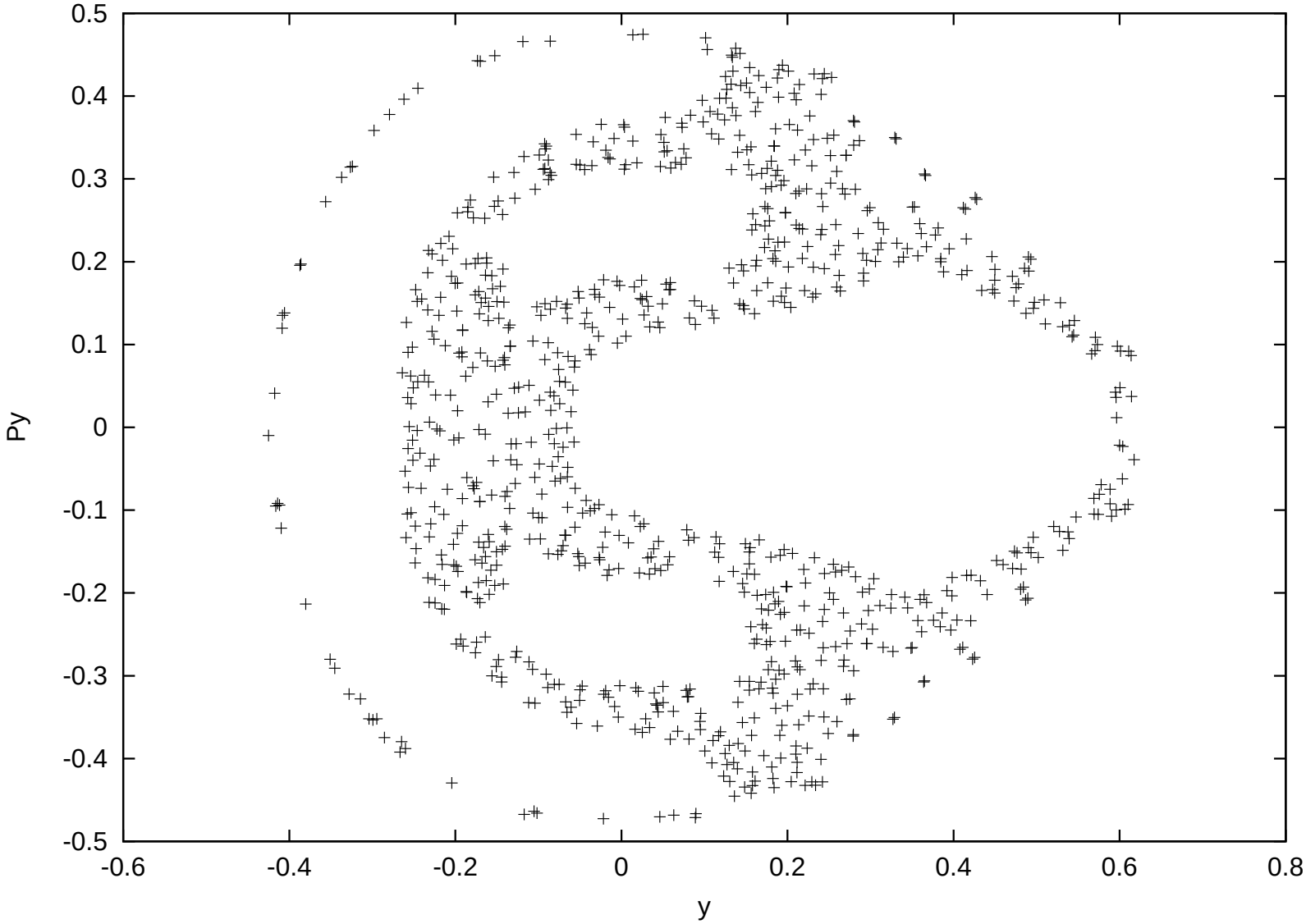

Figure 2.5: Poincaré surface corresponding to Fig. 2.4. Appearance of separatrices denote full chaos

2.3.2 Caustics in Reaction Dynamics

The second example to which we have applied our method is that of a triatomic chemical reaction. The natural motivation here is to construct a recipe which forms an important component in the effort to take into account the effects of tunneling in chemical reaction dynamics in both classical and semiclassical treaments. In order to run tunneling trajectories such as the instanton trajectories in the classically forbidden region[14], it is inevitable to find caustics along each trajectory in the classically allowed region. For the numerical test here, we have used the lowest adiabatic potential energy surface of a DIM(Diatomics-in-Molecule) potential mimicking the CH_2 molecule[15, 16, 17]. Further information about the construction of this potential is provided in Chapter 3. In this chapter, we only provide the important parameters of the potential. The DIM matrix is defined as

$$\mathbf{V} = \begin{pmatrix} g_1 + \frac{1}{2}(g_3 + h_3 + h_2 + g_2) & \frac{1}{2}(g_3 - h_3) & \frac{1}{2}(g_2 - h_2) \\ \frac{1}{2}(g_3 - h_3) & g_2 + \frac{1}{2}(g_3 + h_3 + h_1 + g_1) & \frac{1}{2}(g_1 - h_1) \\ \frac{1}{2}(g_2 - h_2) & \frac{1}{2}(g_1 - h_1) & g_3 + \frac{1}{2}(g_1 + h_1 + h_2 + g_2) \end{pmatrix}, \tag{2.15}$$

where, (h_1, h_2, h_3), and (g_1, g_2 and g_3) represent the ground and excited states of 3 diatomic species respectively. The functional forms of these terms are taken as:

$$\begin{aligned} h_1(r) &= -D_h[1 + \alpha_1(r - r_{H_2}) + \alpha_2(r - r_{H_2})^2 + \alpha_3(r - r_{H_2})^3]\exp^{-\alpha_4(r - r_{H_2})} \\ g_1(r) &= D_g[1 + \beta_1 r + \beta_2 r^2]\exp^{(-\beta_3 r)} \\ h_{2,3}(r) &= B_h(\exp^{-\gamma_h(r - r_{CH})} - 2)\exp^{-\gamma_h(r - r_{CH})} \\ g_{2,3}(r) &= B_g(\exp^{-\gamma_g(r - r_{CH})} - 2)\exp^{-\gamma_g(r - r_{CH})} \end{aligned} \tag{2.16}$$

The parameters r_{CH} and r_{H_2} are 2 a.u and 1.401 a.u respectively. The total angular momentum J, is assumed to be zero while the collision energy and the initial ro-vibrational states are taken to be 1.2eV and (v=0, j=0). It should be noted that the PES has an attractive well of depth about 2.3 eV and thus many trajectories are trapped in the well region for long time as seen in Fig. 2.6. The parameters values used are listed in Table 2.1.

Without loss of generality, a triatomic system can be described by the Jacobi coordinates and then using the assumption that the center of mass is stationary and also the constraint J=0, the system can be described by four coordinates (i.e. the collision is confined to a plane[18]) and thus by a 4 × 4 matrix. These four coordinates are here referred to as X,Y,x

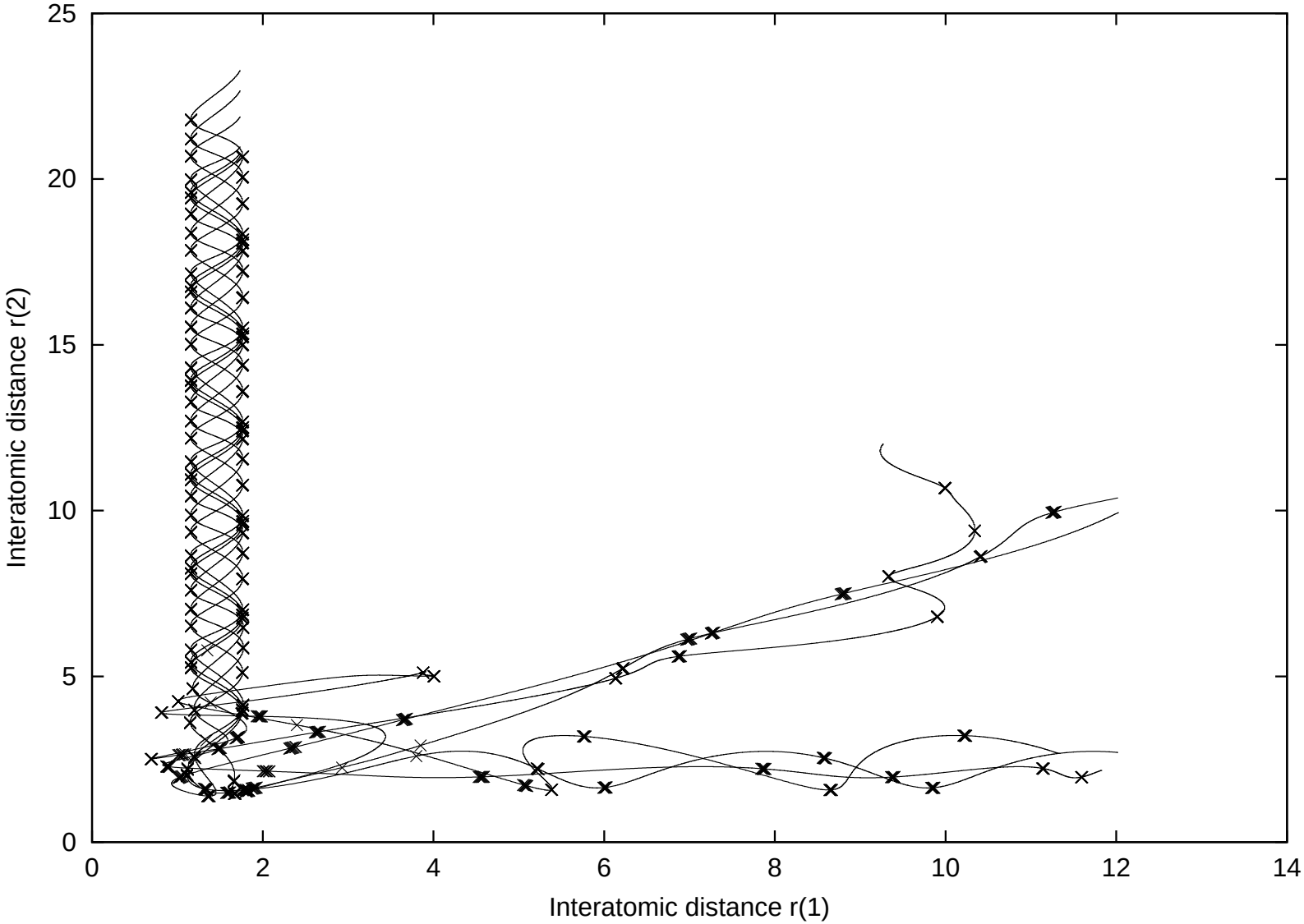

Figure 2.6: Family of reactive trajectories on the ground adiabatic potential energy surface.

Table 2.1: Parameters of the functional form of the potential energy surface of Eqs. 2.15 and 2.16

i	1	2	3	4
α_i	2.1977034	1.2932502	0.64375666	2.835071
β_i	-1.3874149	0.9098728	2.181301	—

j	h	g
D_j	0.15796326	4.502447
B_j	0.13	0.10
γ_j	1.3	1.5

and y.

The initial condition for the A matrix is obtained by using the energy and momentum conservation.

$$\begin{aligned} E_{col} &= \frac{1}{2\mu_{A,BC}}(P_X^2 + P_Y^2) \\ E_{nj} &= \frac{1}{2\mu_{A,BC}}(p_x^2 + p_y^2) + V(x,y) \\ J_z &= (xp_y - yp_x) + (XP_Y - YP_X) \\ J^2 &= (XP_Y - YP_X)^2 + (xp_y - yp_x)^2 \end{aligned} \tag{2.17}$$

Differentiating each of the four conservation equations partially with respect to the four coordinates yields the analytical expression for the matrix $\frac{\mathbf{D}(P_X,P_Y,p_x,p_y)}{\mathbf{D}(X,Y,x,y)}$ in the asymptotic region. The initial condition so obtained is

$$\mathbf{A} = \begin{pmatrix} \mathbf{AA} & \mathbf{0} \\ \mathbf{0} & \mathbf{aa} \end{pmatrix}, \tag{2.18}$$

where

$$\mathbf{AA} = \frac{1}{\mathbf{P_X X} + \mathbf{P_Y Y}} \begin{pmatrix} P_Y^2 & -P_X P_Y \\ -P_X P_Y & P_X^2 \end{pmatrix} \tag{2.19}$$

and

$$\mathbf{aa} = \frac{1}{\mathbf{p_x x} + \mathbf{p_y y}} \begin{pmatrix} -\mu x \frac{\partial V}{\partial x} + p_y^2 & -\mu x \frac{\partial V}{\partial y} - p_x p_y \\ -\mu y \frac{\partial V}{\partial x} - p_x p_y & -\mu y \frac{\partial V}{\partial y} + p_x^2 \end{pmatrix}. \tag{2.20}$$

To solve Eq. 2.5, we have employed the fourth-order Adams-Bashforth-Moulton predictor-corrector scheme where the corrector is iterated until convergence is achieved. This scheme acts as the first check on the validity of the transformations. Namely, the non-convergence can flag an error in the solution of Eq. 2.5 caused by a defective implementation of the suggested canonical transformations.

In order to show the feature of propagation, an example is given in Fig. 2.6 showing a family of reactive trajectories and their numerically-determined caustics. As expected, the caustics occur periodically in the asymptotic region corresponding to the turning points of the vibrational motion. The value of our method is seen in the rearrangement region. Here, the trajectory is no longer periodic and the caustics cannot be easily identified by observation. This method works well to determine those points which are important to incorporate tunneling effects in reaction dynamics.

2.3.3 Case of closely-occuring caustics

As mentioned above, it may happen that two or more eigenvalues of the matrix A almost simultaneously diverge around the same propagation time, especially when the multi-dimensional potential has a deep well. This often occurs in the condensation region of the insertion type of chemical reactions. This requires consecutive multiple canonical transformations to treat concomitantly-occuring divergences. A bit of care is also needed in choosing time step and the divergence criterion. Fig. 2.7 clearly demonstrates this. This is a time-profile of the maximum absolute eigenvalue of the propagated matrix in the condensation region with the peaks signifying the occurence of caustics. In the asymptotic region(not shown), the period corresponds to that of vibrational motion of the diatomic. The value of the method of multiple transformations is highlighted by the detection of the internal structure which breaks the periodicity of caustics. Here the split of the peak corresponds to the situation where three caustics occur within a time-interval of about one-tenth of the period of the caustics in the asymptotic region.

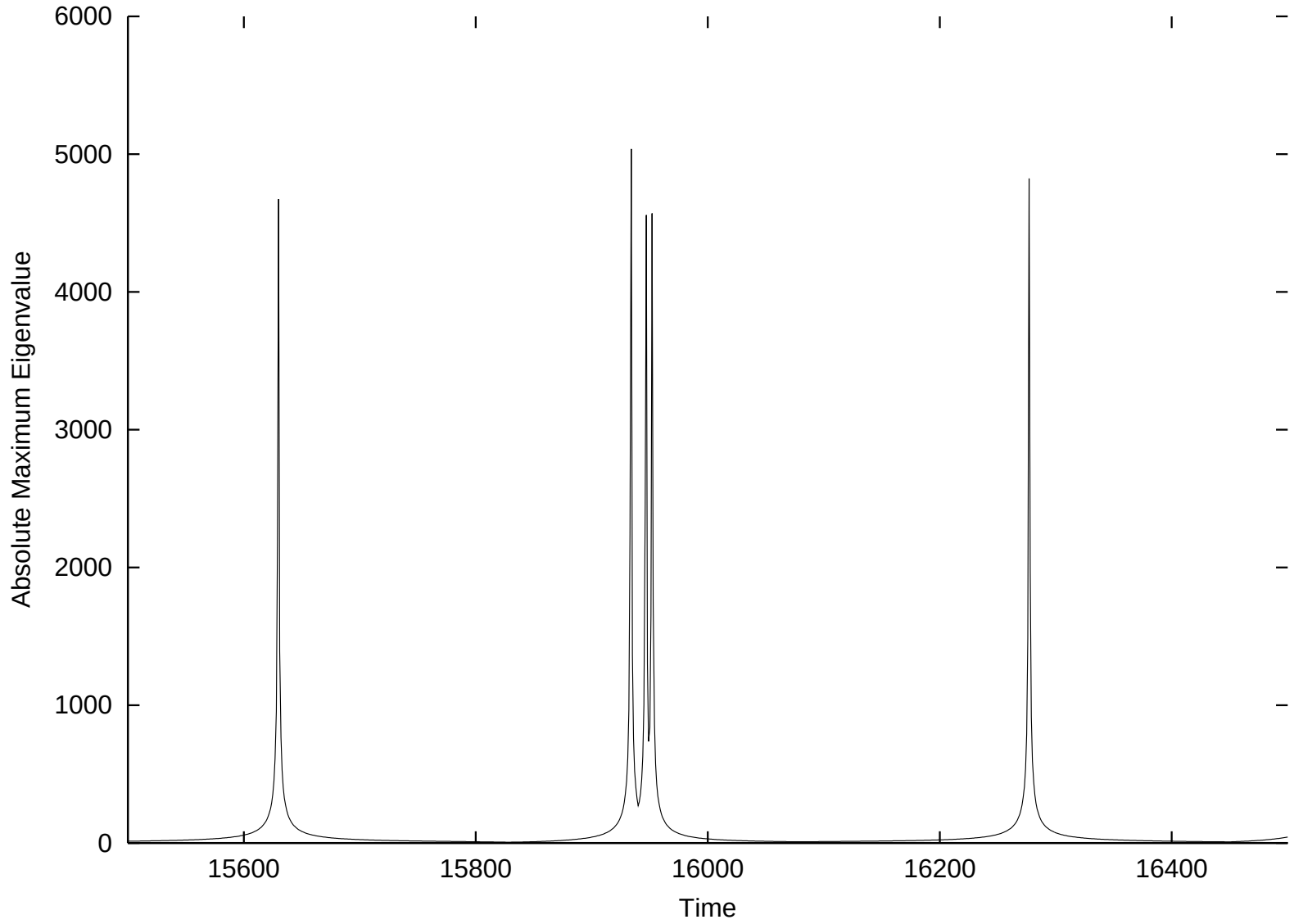

Figure 2.7: Time-profile of the absolute maximum eigenvalue of propagated matrix in the case of reaction. Coalescence of caustics occurs in the condensation region and is seen here as split peaks.

2.4 APPLICATIONS OF THE CAUSTICS METHOD IN TUNNELING

2.4.1 Collinear Tunneling

The H_3 system is the prototypical system for investigating tunneling because of the light masses of the reactant species. We attempt to carry out a test calculation to investigate the adaptability of the caustics method described above when it is incorporated into the conventional quasiclassical trajectory propagation approach. Previous works have studied the effects of tunneling in this system [19, 20, 21] and it is typically regarded as a good testing ground to see how well a tunneling recipe does in including tunneling effects in quasiclassical calculations. No elaborate tunneling trajectory method is proposed here since no rigorously correct method exists at the moment to describe tunneling trajectory. Instead, I have used a simple straight-line path to represent the tunneling between two opposite ends of the barrier. The LSTH potential[22] is a widely-used potential for the H_3 system and its features are equally well-known[cf. Fig. 2.8]. On this potential, the threshold for purely classical trajectory is 0.276 eV and reaction below this point takes place via tunneling.

For the collinear case, the A matrix of Eq. 2.5 is a 2 × 2 matrix and the initial condition of this matrix is obtained using the relevant equations for a collinear system with coordinates X,x and conjugate momenta, P_X and p_x.

$$\begin{aligned} E_{col} &= \frac{1}{2\mu_{A,BC}}(P_X^2) \\ E_{nj} &= \frac{1}{2\mu_{A,BC}}(p_x^2 + V(x)) \end{aligned} \tag{2.21}$$

As the trajectory is being propagated, the solution of the A matrix is also being solved in time. The calculated vibrational period 161.024 a.u which is in excellent agreement with the 161 a.u. obtained from the solution of differential equation.(Fig. 2.9). At the point of caustic, the eigenvector corresponding to the maximum eigenvalue of the A matrix, is used as the direction in which the one-dimensional potential barrier to tunneling is sought. A straight-line path is initiated at the beginning of the barrier and tunneling is considered to terminate when the trajectory "hits" the barrier where the value of the potential equals the value at the starting point. See Fig. 2.10. From the result of this simple test calculation, Fig. 2.11, it is seen that the quantum threshold is well reproduced and the probability agrees quite well if one couples the caustics method and the simple straight-line tunneling method to ordinary quasiclassical methodology.

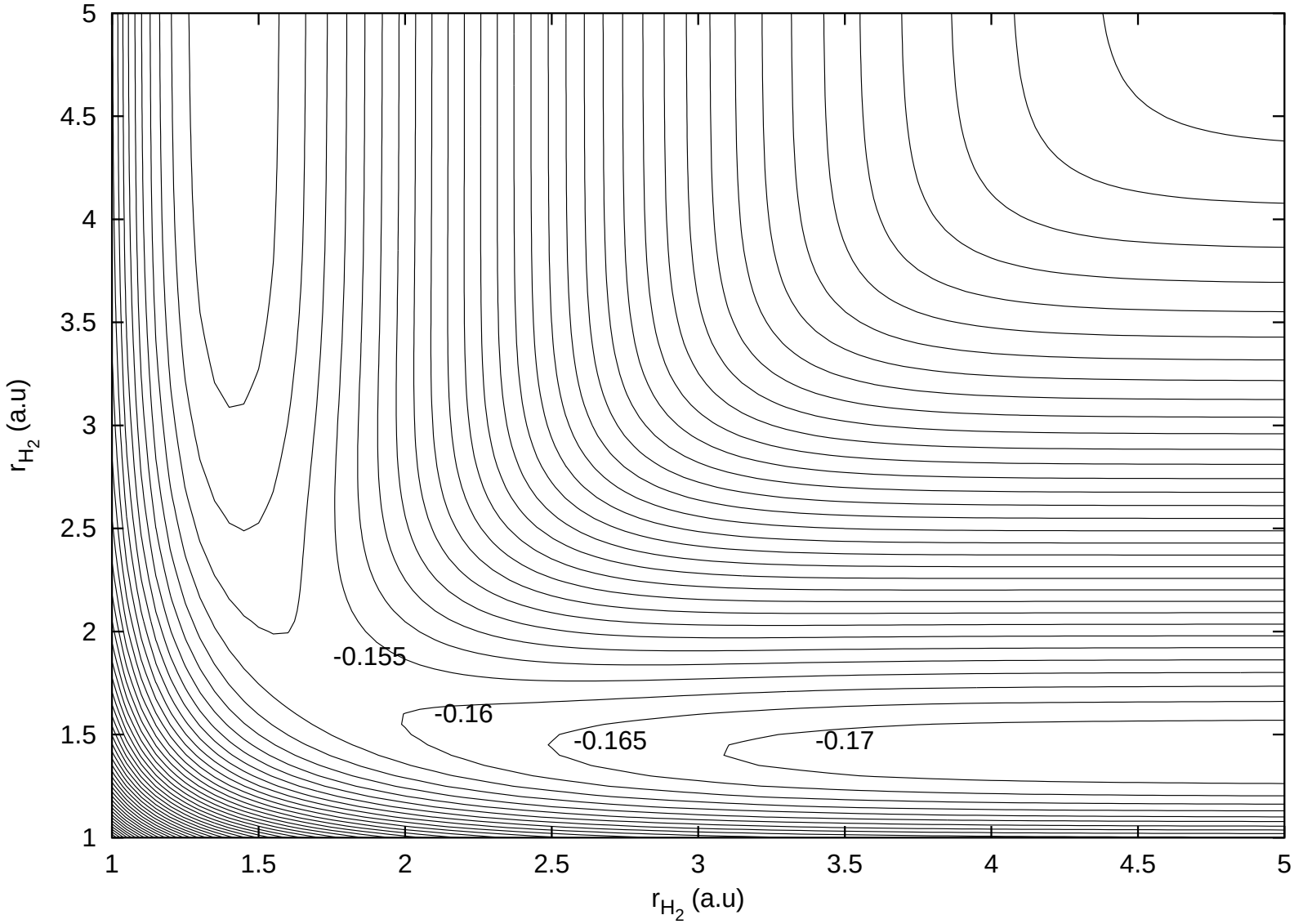

Figure 2.8: Collinear LSTH potential showing energy in atomic units.

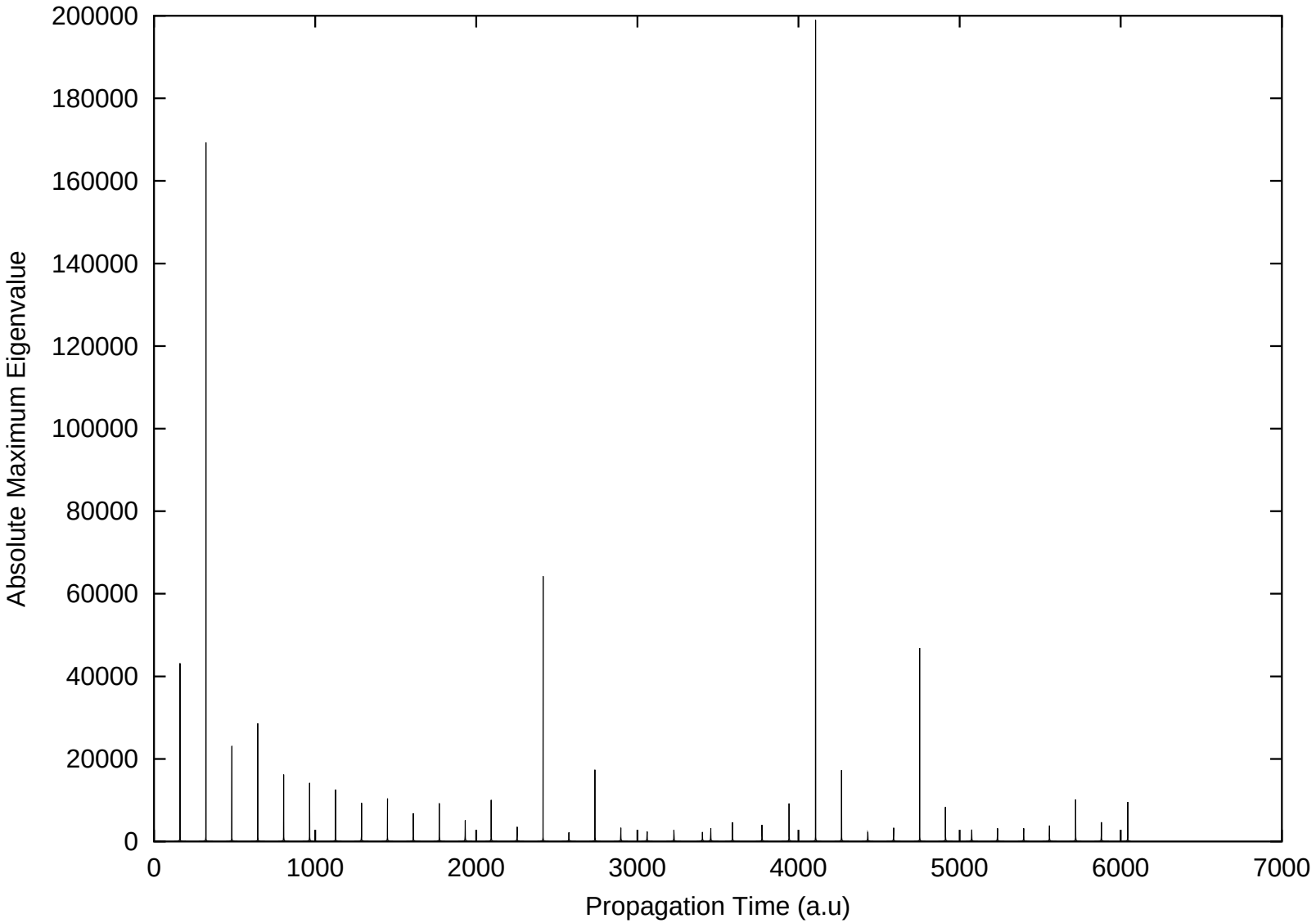

Figure 2.9: Caustic of the H_3 collinear system on the LSTH potential(Full).

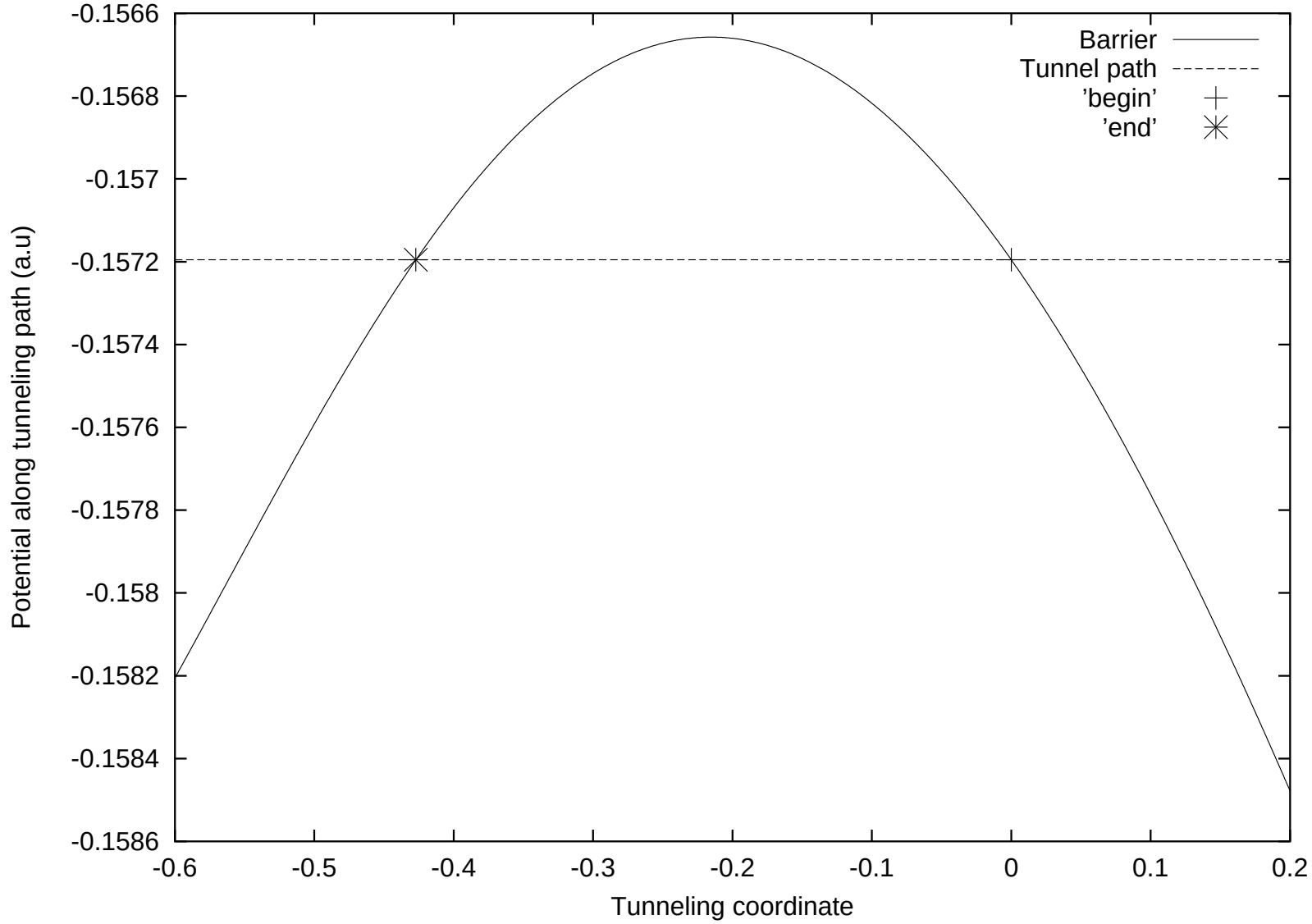

Figure 2.10: Straight line tunneling path across barrier.

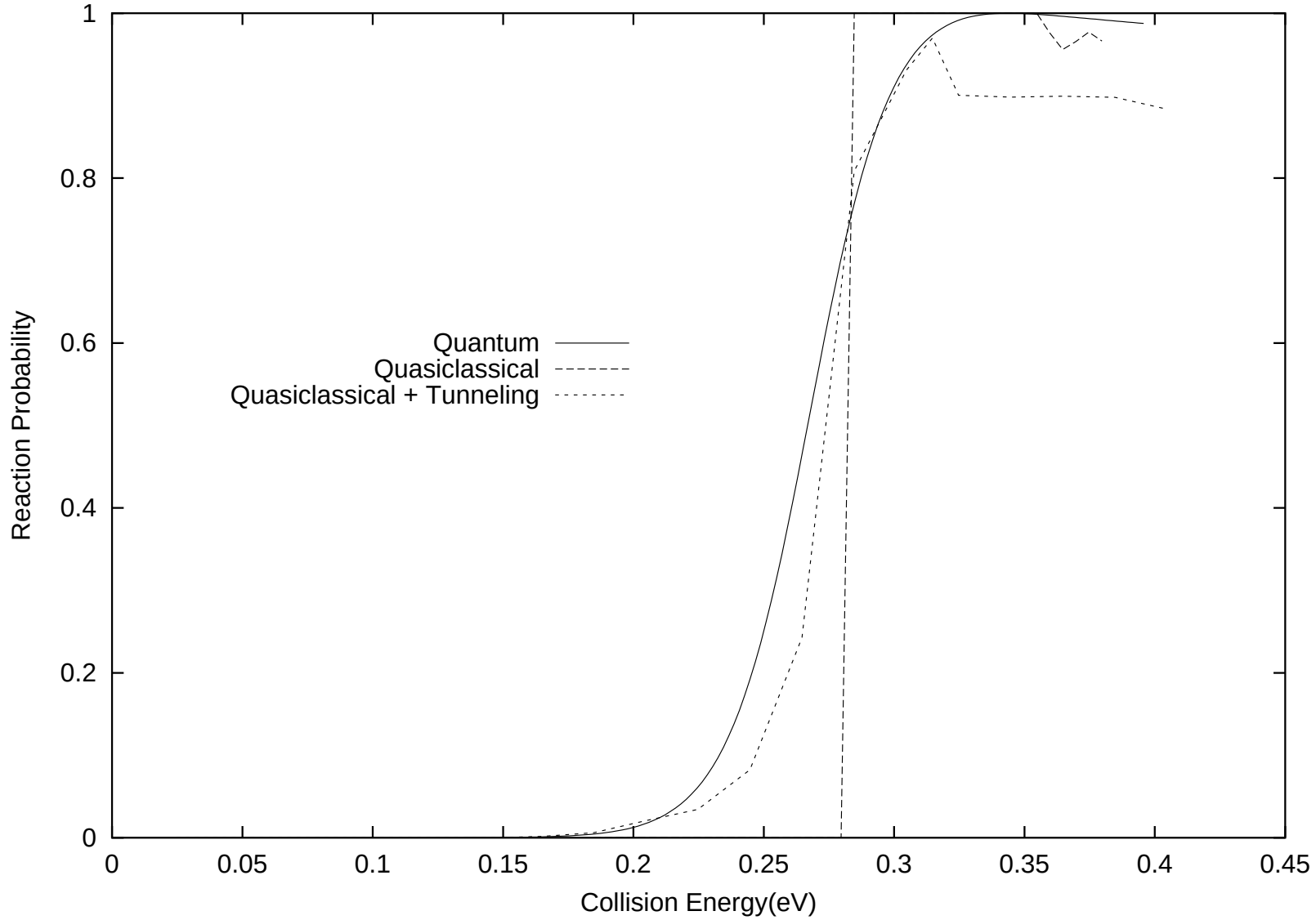

Figure 2.11: Reaction probability of collinear H_3 on LSTH potential.

2.4.2 Thermal Reaction Rate Constant

The collinear case above serves to verify tunneling effects in the H_3 system and most importantly, confirms that the method of this chapter can be very useful in actual dynamical calculations. In this subsection, I proceed to calculate the thermal rate constant of the same system with inclusion of tunneling. The quasiclassical approach to determining the thermal rate constant involves a temperature-averaging over the reaction cross section. The complete procedure involved in the quasiclassical recipe for determining the cross section is well-explained in Chapter 4 and I only present the details related to the temperature averaging in this section. The trajectories to be run to determine the reaction cross section involves summing over all possible impact parameters, i.e. a 3-dimensional problem with a non-zero total angular momentum. A 3-D problem such as this should provide a more exacting test than the collinear system of the previous section because of the multidimensionality. It follows that in this 3-D case, a different initial condition for the A matrix has to be determined. The relevant equations are obtained as always with the assumption that in the asymptotic region the potential is separable. This initial condition of the $\frac{\partial p_i}{\partial q_j}$ matrix for whatever dimension of the system are dictated by writing the conservation equations of the constants of motion of the classical S-matrix. In the 2-dimensional case as seen above, the conservation equations used were those for Energy, Total angular momentum, and the projection of the total angular momentum on a chosen axis. The 6 constants of motion for the 3-dimensional case can be chosen as E_{col}, the collision energy, E_{nj}, the vibrational energy of the diatomic, [n and j are vibrational and rotational level respectively of the diatomic], j_z, the projection of the angular momentum of the diatomic on the z axis, j^2, the total angular momentum of the diatomic, J_z the projection of the total angular momentum of the system on the z axis, and J^2. For an incoming A atom and a vibrating BC diatomic, the equations for these constants of motion are,

$$\begin{aligned}
E_{col} &= \frac{1}{2\mu_{A,BC}}(P_X^2 + P_Y^2 + P_Z^2) \\
E_{nj} &= \frac{1}{2\mu_{A,BC}}(p_x^2 + p_y^2 + p_z^2) + V(x,y,z) \\
j_z &= (yp_z - zp_y)cos\alpha_x + (zp_x - xp_z)cos\alpha_y + (xp_y - yp_x)cos\alpha_z \\
j^2 &= (yp_z - zp_y)^2 + (zp_x - xp_z)^2 + (xp_y - yp_x)^2 \\
J_z &= (YP_Z - ZP_Y)cos\alpha_x + (ZP_X - XP_Z)cos\alpha_Y + (XP_Y - YP_X)cos\alpha_z \\
J^2 &= (YP_Z - ZP_Y)^2 + (ZP_X - XP_Z)^2 + (XP_Y - YP_X)^2
\end{aligned} \tag{2.22}$$

In order to calculate the thermal rate constant, the cross section is calculated [see chapter

5 for complete description] and then averaged over the collision energy. The simple straight line tunneling path is once again coupled to the caustics method in order to account for tunneling effect. Fig. 2.12 confirms the utility value of the caustics-locating technique of this chapter.

2.5 CONCLUDING REMARKS

I have presented an efficient method to determine caustics in multi-dimensional chemical dynamics. The formulation can be easily applied to any general, N-dimensional system. This is a salient point to note because, for any N-dimensional system, the maximum number of divergences which could occur almost in the same time instant is the same as the dimensionality of the system. This method can treat even this extreme case quite capably and is expected to be a potentially powerful complement to future work in the areas of classical and semiclassical multi-dimensional dynamics. In fact, within the limitation of a lack of a rigorous method to propagate tunneling trajectory, tunneling effects have been studied in a prototypical tunneling sysetem with a method which is based on the formulation presented in this chapter. This is quite significant since nonadiabatic transition can be incorporated properly with the use of the Zhu-Nakamura theory both in the TSH(Trajectory Surface Hopping) method and the semiclassical IVR(Initial Value Representation) theory[30, 31], with simultaneous tunneling. Thus, this should become an important candidate for computation so that quantum mechanical effects can now be nicely incorporated in the classical and the semiclassical dynamics theories to deal with large chemical and biological systems.

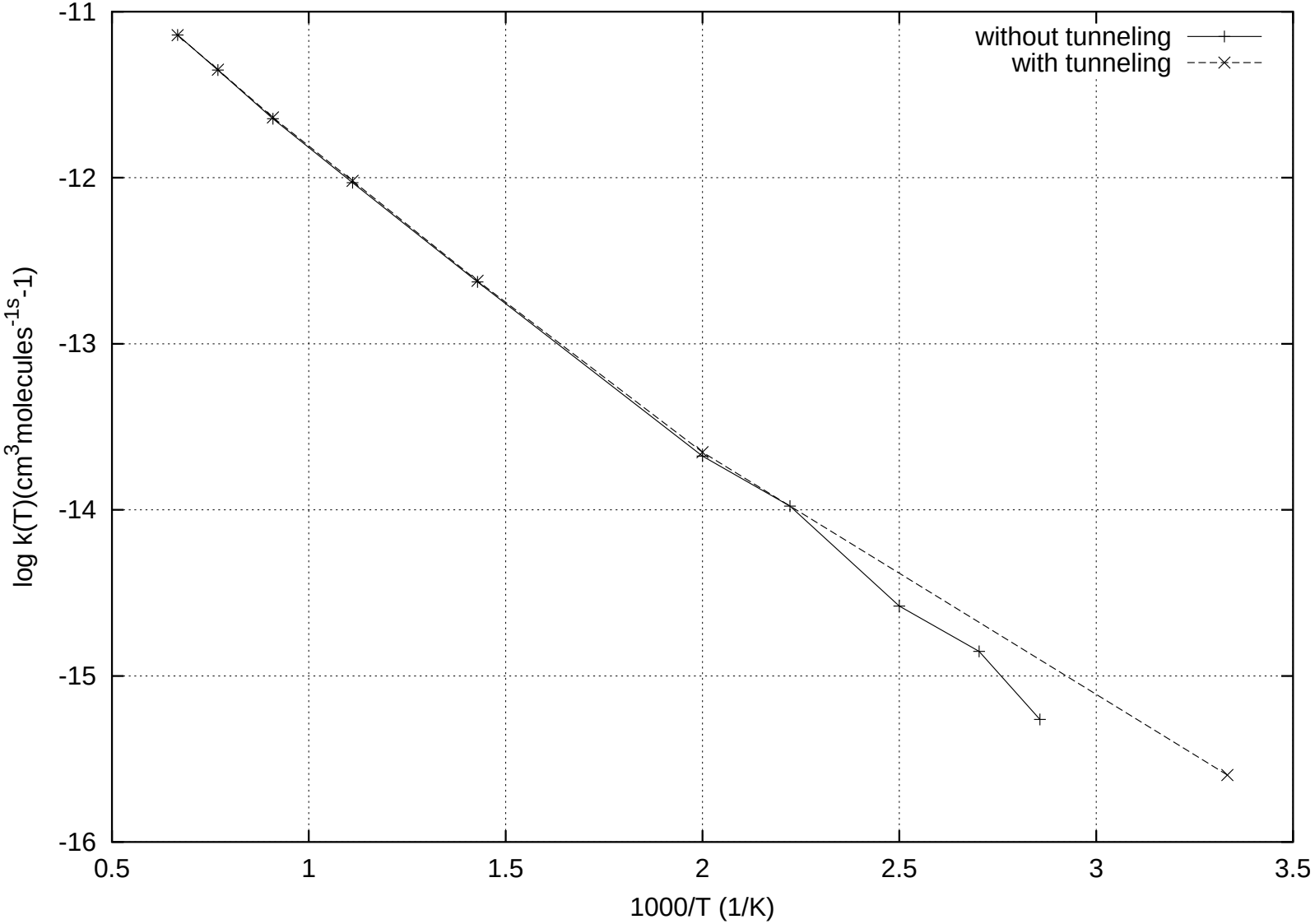

Figure 2.12: Thermal Reaction rate constant of H_3 on LSTH potential.

REFERENCES

[1] M. C. Gutzwiller, *Chaos in Classical and Quantum Mechanics*, (Cambridge,1982)

[2] L. Martinet and P. Magnenat, Astron. Astrophys.**96**, 68, (1981)

[3] C. Froeschelé, Astron. Astrophys.**16**, 172, (1972)

[4] M.S. Child, *Semiclassical Mechanics with Molecular Applications*, (Clarendon,1991)

[5] C.J. Ashton and J.T. Muckerman, J. Phys. Chem. **87**, 2738, (1983)

[6] A.M. Ozorio de Almeida and J.H. Hannay, Ann. Phys. (NY) **138**, 115, (1981)

[7] W.H. Miller, J. Phys. Chem. A,**105**, 2942, (2001)

[8] H. Nakamura, *Nonadiabatic Transition, Concepts, Basic Theories and Applications*, (World Scientific,2002)

[9] K. Takatsuka, H. Ushiyama and A. Inoue-Ushiyama, Phys. Rep. **322**, 5, (1995)

[10] T.J. Stuchi and R. Vieira-Martins, Phys. Lett. **A201**, 179, (1995)

[11] H. Ushiyama, Y. Arasaki and K. Takatsuka, Chem. Phys. Lett. **346**, 169, (2001)

[12] G.V. Mil'nikov and H. Nakamura, J. Chem. Phys. **115**, 6881, (2001)

[13] M. Henon and C Heiles, Astron. J.**69**, 1316, (1964)

[14] W.H. Miller, J. Chem. Phys.,**62**, 1899, (1974)

[15] F.0. Ellison, J. Am. Chem. Soc.,**85**, 3540, (1963)

[16] A.J.C. Varandas, J.D. Silva, J. Chem. Soc. Faraday II **82**, 593 (1986)

[17] K.P Kirby, E.P. VanDishoeck, Adv. At. Mol. Phys., **25**, 437, (1988)

[18] R.D. Levine, R.B. Bernstein *Molecular Reaction Dynamics*, (Clarendon,1974)

[19] T. Takayanagi, N. Masaki, K. Nakamura, M. Okamoto, S. Sato, G.C. Schatz, J. Chem. Phys. **86**, 6133, (1987).

[20] T. Takayanagi, K. Nakamura, S. Sato, J. Chem. Phys. **90**, 1641, (1989).

[21] G.C. Hancock, C.A. Mead, D.G. Truhlar, A.J.C. Varandas, J. Chem. Phys. **91**, 3492, (1989).

[22] P. Siegbahn, B. Liu, J. Chem. Phys. **68**, 2457, (1978); D.G. Truhlar, C.J. Horowitz, J. Chem. Phys. **68**, 2466, (1978); ibid. **71**, 1415(E), (1979).

[23] J. V. José and E. J. Saletan, *Classical Dynamics*, (Cambridge,1998)

[24] I. Percival and D. Richards, *Introdcution to Dynamics*, (Cambridge,1982)

[25] A.M. Ozorio de Almeida, *Hamilton Systems: Chaos and quantization*, (Cambridge,1998)

[26] V. I. Arnold, *Mathematical methods of classical mechanics*, (Springer, Berlin, 1978)

[27] V.G. Ushakov, K. Nobusada, and V.I. Osherov, Phys. Chem. Chem. Phys. **3**, 63, (2001)

[28] A. Ichihara and K. Yokoyama, J. Chem. Phys. **103**, 2109, (1995)

[29] R.Ramaswany and R.A. Marcus, J. Chem. Phys.**74**, 1385, (1981)

[30] C.Zhu, H. Kamisaka and H. Nakamura, J. Chem. Phys. **115**, 11036, (2001); ibid, **116**, 3234 (2002).

[31] H. Nakamura, Invited Talk at the "Symposium in Memory of Professor G.D. Billing" (Copenhagen, August 2003).

CHAPTER 3

TRAJECTORY SURFACE HOPPING(TSH) METHOD WITH USE OF THE ZHU-NAKAMURA THEORY.

3.1 INTRODUCTION

The rapidly-growing interest of physical chemists and chemical physicists in studying chemical processes in biological molecules almost guarantees that the subject of nonadiabatic transitions will continue to engage the attention of researchers in the foreseeable future. This is because apart from its well-known ubiquity in chemical reactions in relatively small molecular systems, it has become accepted that nonadiabatic transitions are also vital in systems as large as amino acids and in transition metal centers in enzymes[1, 3, 4], which are both very crucial to life-sustaining processes. In studying these large systems, fully quantum calculations are still far from becoming routine, with the implication that classical methodologies continue to be the practical and appealing alternative, principally because of their low computational costs and the physical insights they provide into understanding the underlying dynamics of the reaction.

The ideal compromise has always been some kind of mixed quantum-classical techniques, treating nuclear motion classically, and the electronic motions quantum-mechanically. For treating nuclear motion, the choices in literature include the semiclassical initial value representation method[5, 6], the frozen Gaussian methods[7, 8], or the usual single-surface propagation of classical trajectories. When the trajectory reaches a region where electronic

surfaces approach each other closely enough, the effect of possible nonadiabatic transitions is included by solving the time-dependent coupled equations[9], by ab-initio multiple spawning of Martinez et al[10], or using analytical expressions to predict the probability of transitions between adjoining surfaces.

The Trajectory Surface Hopping (TSH) method introduced by Tully and Preston[9] has enjoyed widespread application as a realization of such a quantum-classical recipe. As the nuclei moves on the initial adiabatic potential surface, the time-dependent coupled equations are solved, in order to compute the probability of hopping. At a point which satisfies a set criterion, the decision is made for the trajectory to either hop or remain on the initial surface after comparing the computed probability with a randomly-generated number. In the event of a hop, the nuclear velocity is adjusted to ensure conservation of energy of the system. The simplicity of this technique is its biggest benefit and makes it attractive in studying high-dimensional systems. Also in the same publication, they suggested the use of the famous linear Landau-Zener (LZ) model[11] to compute the transition probability as a way of reducing computational efforts.

While there have been several modifications to the TSH model since this earliest effort[12, 13], its central ideas have remained the same and much research effort continue to be devoted to finding improvements. Solving the coupled-equation is not much of a choice as the system becomes more complicated, while the convenience of using the analytical LZ formula is offset by a number of its shortcomings. [See for instance [14]]. The inadequacy of the LZ formula which is most relevant to our discussion here, is in the event that the region of large nonadiabatic coupling is located where the energy in the hopping direction cannot reach the crossing between the relevant two potential energy surfaces. These hops are commonly known as classically-forbidden hops. If the LZ expression were used for TSH in such a scenario, the results would be clearly wrong. The widely-used fewest switches method of Tully[13] also cannot be employed in treating these classically-forbidden transitions.

The Zhu-Nakamura (ZN) theory [1] provides the complete analytical solution for one-dimensional non-adiabatic transition across a wide range of energies. It thus improves upon the LZ analytical formula since the validity of the ZN theory in low energy regions implies that it works well in treating tunneling effects and can therefore be used to properly include energetically forbidden hops in TSH. Such a modification would make the conventional TSH scheme considerably more powerful as a computationally-cheap and easily implementable

tool to study nonadiabatic dynamics in more complicated system. This new scheme (Zhu-Nakamura Trajectory Surface Hopping or ZN-TSH for short) has been explored in a series of papers by Zhu et al [15, 16, 17] which focused on the collinear H_3^+ and the 3-dimensional DH_2^+ systems. In the current work, we retain the crucial improvements made possible by the Zhu-Nakamura (ZN) theory; but the points of departure between the ideas contained in the current work and that of Zhu et al in Ref.[17] are quite significant.

The first concerns the issue of dimensional reduction. The application of the ZN theory to multidimensional problems requires a careful reduction of the nonadiabatic transition to a 1D problem. For the 3-dimensional DH_2^+, Zhu and co-workers carried out the analysis for the one-dimensional reduction in terms of internal curvilinear coordinate, going so far as to predefine the seam-surface(i.e. locus of the points important for nonadiabatic transition) in terms of these coordinates. Being able to so delineate the seam-surface before the start of actual calculations drastically reduces overall computational time but one important critique of such an approach is that, it is the specific nature of the topology of simple systems like the 3-D DH_2^+ which makes the seam-surface amenable to being so determined analytically. In the DH_2^+ system, the nonadiabatic transitions are induced almost by the one-dimensional vibrational motion away from the asymptotic region, making the treatment of the nonadiabatic transition problem very simple. Chemical systems are seldom so simple and it is strongly required to develop a general method without predefined knowledge of crossing seam-surface.

The next issue is the direction of nonadiabatic transition. In the case of DH_2^+, the geometry of the seam-surface is clear and the direction of the transition is taken to be perpendicular to the seam-surface. The transition in the parallel direction is the non-crossing type and is usually negligible compared to the crossing type. In view of the applications to the large system, this is not very convenient. Here, I propose a method to use the non-adiabatic coupling vector which can be estimated even if its direct knowledge is not available.

The third difference between the work of Zhu et al and the present work, is the manner of treating the conservation of angular-momentum after a classically-forbidden hop. In this case, the energy of the trajectory in 1D on a lower surface is not enough to reach the upper surface and hop cannot ordinarily be made to originate from the lower surface. However, because the ZN theory is valid in computing the transition probability even in this case, we may find a suitable point on the upper surface where the hop terminates while keeping the total energy of the system conserved. Hopping in such manner though, would

be accompanied by a shift of coordinates thereby violating the conservation of angular momentum. We show in section II that finding a suitable matrix to rotate the coordinate is simpler than the method of Ref. [17] and works as well.

The final issue is that in general, both Landau-Zener and Nonadiabatic tunneling types of transitions appear in the same reaction and we have to build up an algorithm to treat both of them properly including the classically-forbidden ones.

To illustrate the present problem and to demonstrate the value of the present method, we make use of a DIM potential matrix constructed to mimic the CH_2 system which has a conical intersection. The behavior of the 1-dimensional cuts of this DIM potential energy surface is also quite interesting because there exists two different types of crossings: in the first type, the two diabatic surfaces cross with the same sign of slope (Landau-Zener (LZ) type) and in the second, the signs of the slope of the diabatic curves are different (Nonadiabatic tunneling (NT) type). Unlike the DH_2^+ system which has only the LZ-type, the presence of both curve-crossing possibilities in our potential surfaces makes the current work to be the first full implementation of the ZN theory and to be applicable to various nonadiabatic processes in large systems.

This chapter is arranged as follows. Section 3.2 provides a detailed description of the theory behind the generalization we propose. Section 3.3 provides a brief summary of the Zhu-Nakamura theory and section 3.4. contains the numerical demonstrations of the generalized recipe and consists of two parts. The first part is the test calculation where we apply our method to DH_2^+ and compare our results with those of Zhu et al. We obtain nice agreement between the results of both approaches confirming the validity of our methodology. The second part of the section goes a step further. We apply the generalized TSH method to the newly-constructed DIM potential surfaces featuring conical intersection and the generalized TSH is shown to compare well enough with quantum results. In this same section, we discuss the results obtained by the generalized TSH and offer concluding remarks in Section 3.5 as well as possible future directions and applications.

3.2 DESCRIPTION OF GENERAL FORMULATION OF ZHU-NAKAMURA TRAJECTORY SURFACE HOPPING METHOD

The steps involved in a typical implementation of the TSH are (i) propagating classical trajectories with sampled initial conditions on an adiabatic surface; (ii) Inclusion of

the nonadiabatic effects by some hopping algorithm and (iii) counting the trajectories after scattering to obtain the probability. The first and the last steps are standard tasks in quasiclassical trajectories methods and we do not provide further details about these here, leaving any further details to the section on numerical demonstrations. The question of the choice of hopping algorithm shall thus be the central focus of this section.

In order to provide a direct contrast between the present methodology and the ideas contained in the previous ZN-TSH by Zhu et al, we provide here more specific details of the ideas involved in their implementation. Zhu et al implemented the 1-dimensional reduction of the potential in terms of the coordinates of 3-dimensional space, (r, R, χ). The seam surface is defined in such a way that the difference ΔV(r, R, χ) between the two adiabatic surfaces V_1(r, R, χ) and V_2(r, R, χ) becomes a minimum along its normal line r=f(R, χ). The differential equation defining this minimum was solved close to the avoided crossing and the solution was found to easily converge to the true seam-surface and obtaining the outline of the effective coupling parameter a^2, of the ZN theory followed easily. All these were done before starting the propagation of trajectories. The predeterminations of the seam-surface and the coupling parameters were used to classify the important diabatic, nonadiabatic and adiabatic zones in the system, and to assign unity or zero probability in the diabatic and adiabatic regions, respectively ensuring that nonadiabatic transition probabilities were computed only in the important nonadiabatic transition zones.

Hops are taken to occur in the direction (e_ρ), perpendicular to the seam surface and in the case of classically-allowed hops, only the component of the momentum, P in the direction, e_ρ changes while P-P.e_ρ does not change. The coordinates of the trajectory similarly do not change. The case of classically forbidden hops is more delicately treated. The discontinuity in trajectory coordinates occasioned by the non-vertical nature of the hops implies a change in the coordinates after the hop which in turn, leads to a violation of the conservation of the total angular momentum. For these non-vertical hops, Zhu and coworkers suggested adjusting all the coordinates other than the internal, without changing the components of the momentum. We will show below that this idea can be generalized to an arbitrary case and a unique general recipe can be formulated.

A generalized TSH method should be usable for any system irrespective of the location of the important nonadiabatic transitions and should provide easy answers to two of the more important practical questions in TSH calculations i.e: what should be the location of hopping and in what direction should the trajectory hop. And the better if such a method

is not limited by the availability of system-defined geometrical features. In answering the first question, a local description of the potential surface separation along the trajectory, suggests itself as an invariably simpler technique for determining the location and time of hopping. This should work reasonably well even for potential energy surfaces with different types of curve-crossings. This implies that, there is actually no need to analytically construct the seam-surface.

To answer the question of finding the direction to be used for the one-dimensional reduction of the potential and thereby obtain the parameters of the ZN theory, two ideas are tested here. First, is to use the nonadiabatic coupling vector. If the diabatic potential is available in a matrix form, the nonadiabatic coupling vector $\left\langle \phi_i \middle| \frac{\partial \phi_j}{\partial r} \right\rangle$ is easily evaluated by using the Hellman-Feynman theorem, where, in the DIM approach, the electronic wavefunctions are written in terms of basis functions which are taken to be orthogonal. To obtain the second approximation of the direction of the nonadiabatic transition, consider the topology of the potential energy surface near the conical intersection. Writing the diabatic Hamiltonian in the vicinity of the conical intersection in the form,

$$\begin{vmatrix} A_i X_i & B_i X_i \\ B_i X_i & -A_i X_i \end{vmatrix}, \tag{3.1}$$

where A_i, B_i = const, $X_i = R_i - R_i^\circ$, where R_i° is the point of conical intersection. From this diabatic matrix, it is easy to obtain $\Delta V = V_2 - V_1$, the difference of the two adiabatic energies. The Hessian matrix of this difference gives

$$\frac{\partial^2 \Delta V}{\partial X_i \partial X_j} = e_i e_j \tag{3.2}$$

where,

$$e_i \sim \sum_{k=1}^{3} (A_i B_k - B_i A_k) X_k. \tag{3.3}$$

At the conical intersection, or at a point on the seam line where the off-diagonal elements of Eq. 3.1 are constant, Eq. 3.2 is exact and is actually equal to the direction dictated by the nonadiabatic coupling vector. In the general case however,

$$\frac{\partial^2 \Delta W}{\partial X_i \partial X_j} \sim e_i e_j (1 + \varepsilon_{ij}). \tag{3.4}$$

The extra matrix ε_{ij} has order of magnitude $\frac{\partial A \cdot A}{\partial A \partial A}$ where A is the element of the DIM Hamiltonian. The closer the trajectory moves to the exact point of conical intersection, the

smaller ε_{ij} becomes, i.e. $(A \to 0)$. In order to evaluate e_i for use in the determination of the nonadiabatic direction, we suggest the following steps :

(i) Diagonalize the $\frac{\partial^2 \Delta V}{\partial X_i \partial X_j}$ matrix.

(ii) Substitute $\{e_i\}$ by the eigenvector corresponding to the maximum eigenvalue of the matrix.

In summary, the steps involved in the generalized-TSH approach are :

(i) Monitoring the adiabatic energy separation along the classical trajectory and initiating hopping at a local minimum.

(ii) Reducing the potential to a 1-dimensional problem by using either of the two methods above. For this generalized ZN-TSH, the reduction is carried out in terms of the generalized cartesian coordinates so that the algorithm is very simple and totally independent of the nature of the system.

(iii) Determination of the transition type i.e.(LZ or NT-type) and the computation of the hopping probability using the appropriate component of the Zhu-Nakamura theory.

(iv) Using the ant-eater method suggested by Tully and Preston[9], a hop/no hop decision judgement based on random numbers is used to determine the surface on which the trajectory continues, and the velocities and coordinates(if necessary as in the case of non-vertical hops) are adjusted in order to conserve energy and total angular momentum.

(v) Counting trajectories after reaction and assignment to final scattering channel.

3.2.1 Classically Forbidden Nonvertical Hopping

One important improvement introduced by the ZN-TSH model is the subject of non-vertical hopping. At the point of hopping, if the energy in the direction of hopping is not enough to make a vertical transition possible, the treatment of non-vertical hops emerges naturally from the ZN theory. These hops result in scenario where for a system of coordinates written in terms of R for relative motion and r for internal motion, the change δR, δr between the coordinates before and after hopping,

$$\delta R, \delta r \neq 0. \tag{3.5}$$

Zhu et al, treated the problem of shift in total angular momentum J, by adjusting the coordinates other than the internal, without changing the components of the momenta. Following Zhu, we want to adjust the final J' (all primed quantities represent quantities after hop) so that δJ =0. Such an adjustment should not of course, change the configuration of the molecule after hop. This corresponds simply to a rotation of the system as shown schematically as

$$R, r, \dot{R}, \dot{r} \xrightarrow{hop} R', r', \dot{R}', \dot{r}' \xrightarrow{rotation} \Omega R', \Omega r', \dot{R}, \dot{r} \tag{3.6}$$

The rotation is determined by three components of the angular velocity (or three angles in the rotation matrix) which are found by fixing the three componenets of J.

1. For the ($\mathbf{J = 0}$) case, motion takes place in the (x, y) plane and Ω signifies the matrix of rotation in this plane. Writing (ΩR, Ωr) as (R″, r″), the angular momentum after hop

$$J' = [\dot{R}' \times R''] + [\dot{r}' \times r''] = 0. \tag{3.7}$$

Since all z-components are zero, before and after hop, we are left with,

$$J'_z = \dot{R}'_x R''_y - \dot{R}'_y R''_x + \dot{r}'_x r''_y - \dot{r}'_y r''_x. \tag{3.8}$$

The expression for rotation,

$$\begin{pmatrix} R''_x \\ R''_y \end{pmatrix} = \begin{pmatrix} \cos\alpha & \sin\alpha \\ -\sin\alpha & \cos\alpha \end{pmatrix} \begin{pmatrix} R'_x \\ R'_y \end{pmatrix} \tag{3.9}$$

and the analogous relation between r″ and r' are substituted into Eq. 3.8, to obtain

$$\tan\alpha = \left[\frac{\dot{R}_x R_y + \dot{r}_x r_y - \dot{R}_y R_x - \dot{r}_y r_x}{\dot{R}_x R_x + \dot{r}_x r_x + \dot{R}_y R_y + \dot{r}_y r_y}\right], \tag{3.10}$$

which provides the angle of rotation that ensures conservation of the total angular momentum.

2. For $J \neq 0$, the conditions $\delta J_{x,y,z}$=0 gives three nonlinear equations with respect to the three angles which parametrize this matrix. The elements of the rotation matrix are

written in terms of direction cosines. At infinitesimal angle of rotation, the relations

$$\lim_{\alpha\to 0} \cos\alpha = 1, \lim_{\alpha\to 0} \sin\alpha = \alpha \tag{3.11}$$

can be used to extract a "linear part" from the nonlinear equation and a final equation in the form,

$$\mathbf{A}\begin{pmatrix} \alpha \\ \beta \\ \gamma \end{pmatrix} = \Delta J + \mathbf{F}(\alpha, \beta, \gamma)$$

can thus be formulated more simply, for a system of arbitrary dimensionality.

For a general (N+1)-dimensional system,

$$R', r' \rightarrow [\Omega \times R], [\Omega \times r] \tag{3.12}$$

$$\dot{R}', \dot{r}' \rightarrow \dot{R}, \dot{r} \tag{3.13}$$

Components of J and Ω can always be found so that $\delta J = 0$.

3.3 ZHU-NAKAMURA THEORY

The Zhu-Nakamura(ZN) theory[1, 2] provides the complete analytical solution to the one-dimensional curve crossing problem. The accuracy of this theory even at collision energies below the crossing point introduces the possibility of improving upon previous quasiclassical treatments of nonadiabatic transitions which employed the Landau-Zener linear model formula. In order to include the ZN theory into quasiclassical propagation, it is necessary to obtain a 1-dimensional energy cut of the potential surface and the ZN theory provides the analytical expression for computing the nonadiabatic transition probability in two different cases, the Landau-Zener type and the Nonadiabatic Tunneling type crossings.

3.3.1 Landau-Zener(LZ) Type Transition

In a 1-dimensional cut of the potential energy surface, when the diabatic curves cross with the same sign of slope, this is known as a Landau-Zener type transition.[See Fig. 3.1]. This case is divided into two regions, i.e. regions where the energy of the trajectory E_i, is higher than the crossing energy, E_x and the other region where E_i is lower. These two regions are covered by two different sets of formulas[1, 2]. R_T^2 and R_T^1 on the figure

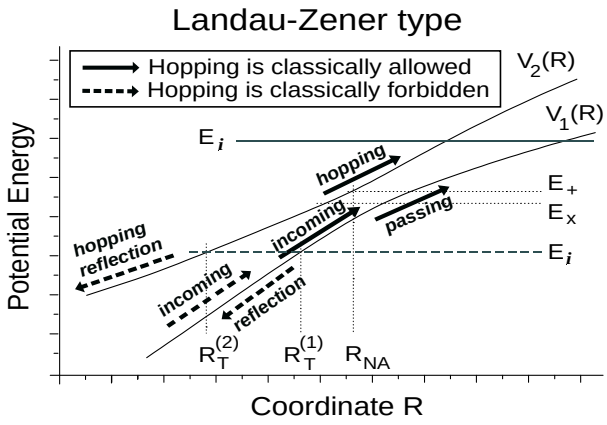

Figure 3.1: Landau-Zener type potential curve-crossing with same sign of diabatic slopes

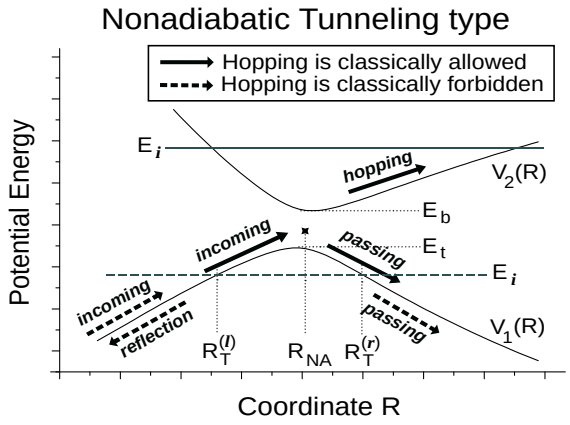

Figure 3.2: Nonadiabatic tunneling type potential curve-crossing with different sign of diabatic slopes

correspond to the turning points on the upper and lower surfaces respectively while R_{NA} is the coordinate at the crossing point and the possible processes are also shown. If the trajectory which is initially on the lower adiabatic surface approaches the 1-D potential from the left of the figure, it could hop onto the upper surface, proceed beyond the crossing point while remaining on the same surface, or become reflected at the hopping point.

3.3.2 Nonadiabatic Tunneling(NT) Type Transition

The Nonadiabatic tunneling type is shown in Fig. 3.2. E_i and R_{NA} have the same definitions as in the LZ case, R_T^l and R_T^r are the left and right turning points respectively, while E_b and E_t denote the bottom and top of the upper and lower adiabatic potential. The

NT-type crossing is covered by three sets of formulas[1, 2], one for region where E_i is higher than the bottom of the higher adiabatic potential, another for the region where E_i is lower than the top of the lower adiabatic potential and a third one for the energy region between the top of the lower adiabatic potential and the bottom of the upper adiabatic potential. In this case, the trajectory approaching from the left on the lower adiabatic surface could hop to the upper surface, proceed adiabatically, tunnel through the barrier or become reflected.

3.4 NUMERICAL DEMONSTRATIONS

3.4.1 DH_2^+

The nonadiabatic charge transfer processes in the 3-D DH_2^+ ($J = 0$) case is the focus of this subsection. The effect of the second intervening potential energy surface on the dynamics of this system and its different isotopic variants, has elicited interest for a long time with the earliest attempts being the series of papers by Tully and Preston[9]. This subsection presents a comparison of our results of our method with those of Ref. [17]

Details of the potential energy surface used are given in Ref. 3 and 4. Contours of this potential is shown in Figs. 3.3 and 3.4 for the ground and excited states at $\angle$(HDH) of 120°. The TSH calculations are carried out on the ground and excited adiabatic surfaces obtained from the DIM diabatic surfaces. As seen in Fig. 3.5, the diatomic potential curves of H_2 and H_2^+ cross at a diatomic distance of $r_s \approx 2.5 a.u.$ Such crossings dominate the potential energy surface of this system, with all the nonadiabatic crossings being only those of the LZ-types and limited around the entrance and exit regions. A system with such topological features only, is simple compared to many other nonadiabatic systems which may have the NT-type crossing in addition to the LZ-type , with nonadiabatic crossings possible over the entire potential energy topography. It is thus the relatively uncomplicated topology that permits the elaborate analytical formulation presented by Zhu et al[17]. Namely, because the true avoided crossing seam of DH_2^+ may be given by an almost straight-line relation, $S(r) = r_s - 2.50 a.u$ [9], where r_s is the smallest of the interatomic distances, the solution of the differential equation in [17] quickly converges to this straight line. It is almost certain that an analogous seam relation will not exist for a system which in spite of a similar dimensionality, possesses richer and more varied nonadiabatic dynamics.

The processes under study here are the charge transfer processes,

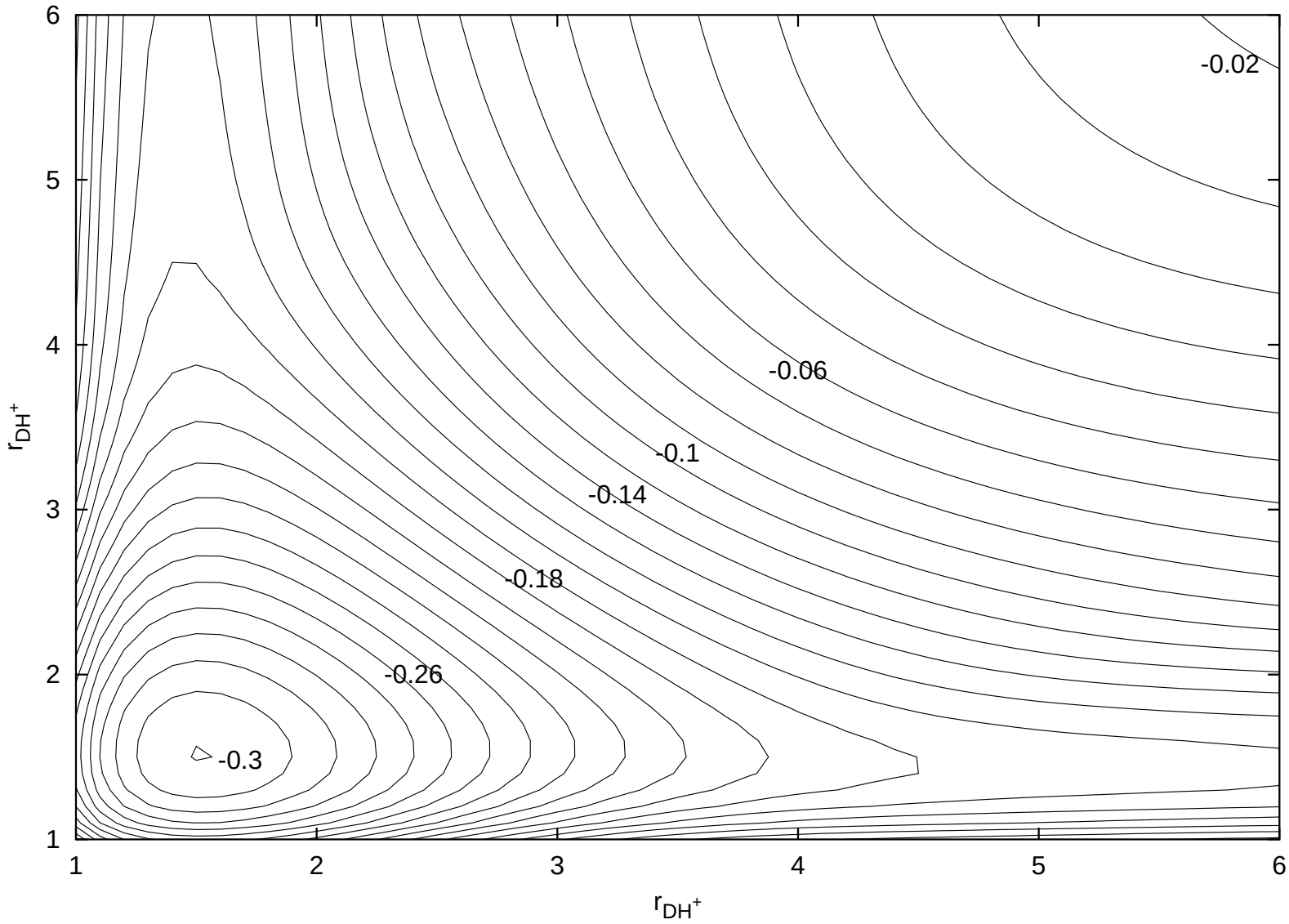

Figure 3.3: Diatomic potential curves(in a.u.) of the DH_2^+ system at angle(HDH)=120°:Ground PES

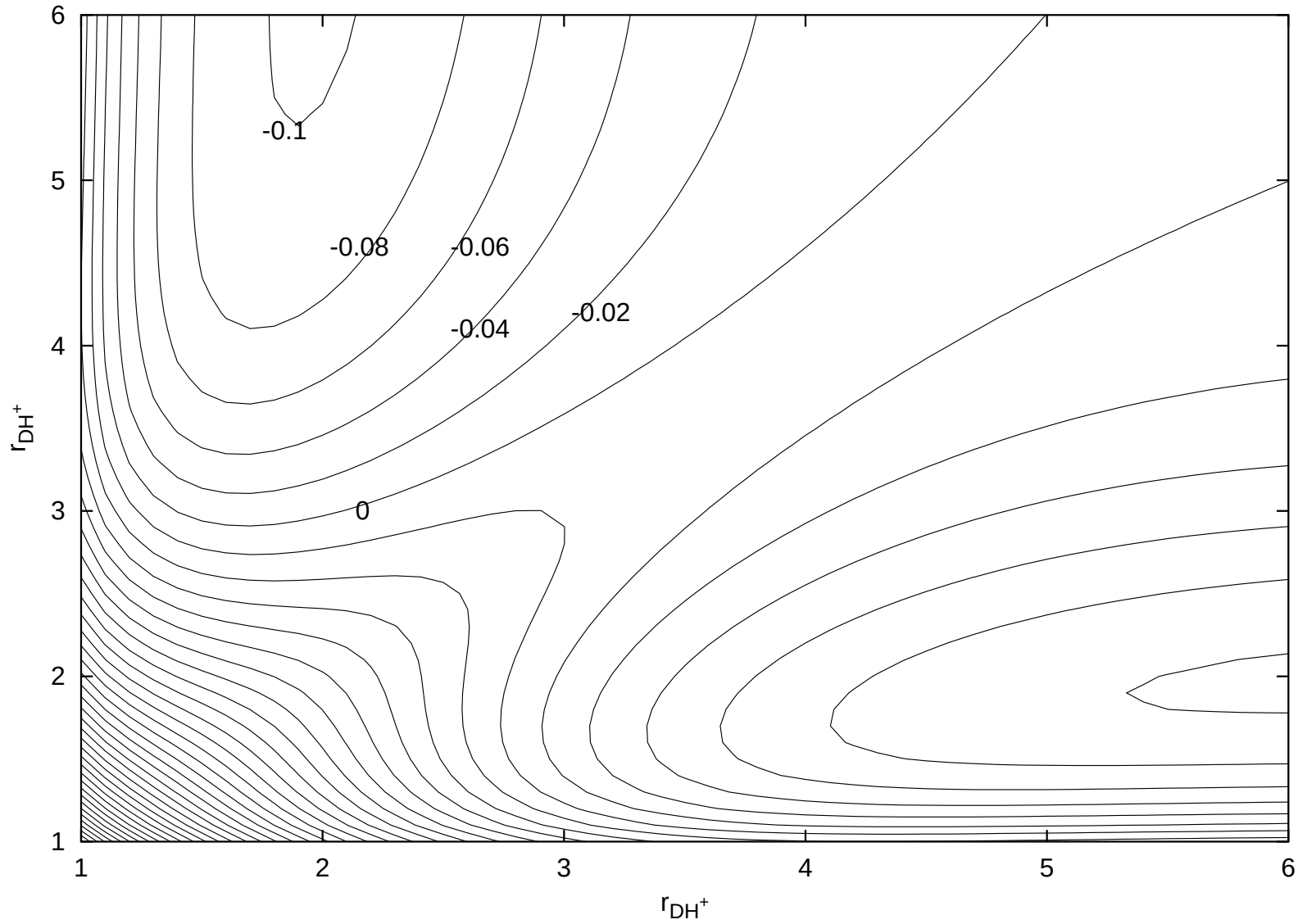

Figure 3.4: Diatomic potential curves(in a.u.) of the DH_2^+ system at angle(HDH)=120°:Excited PES

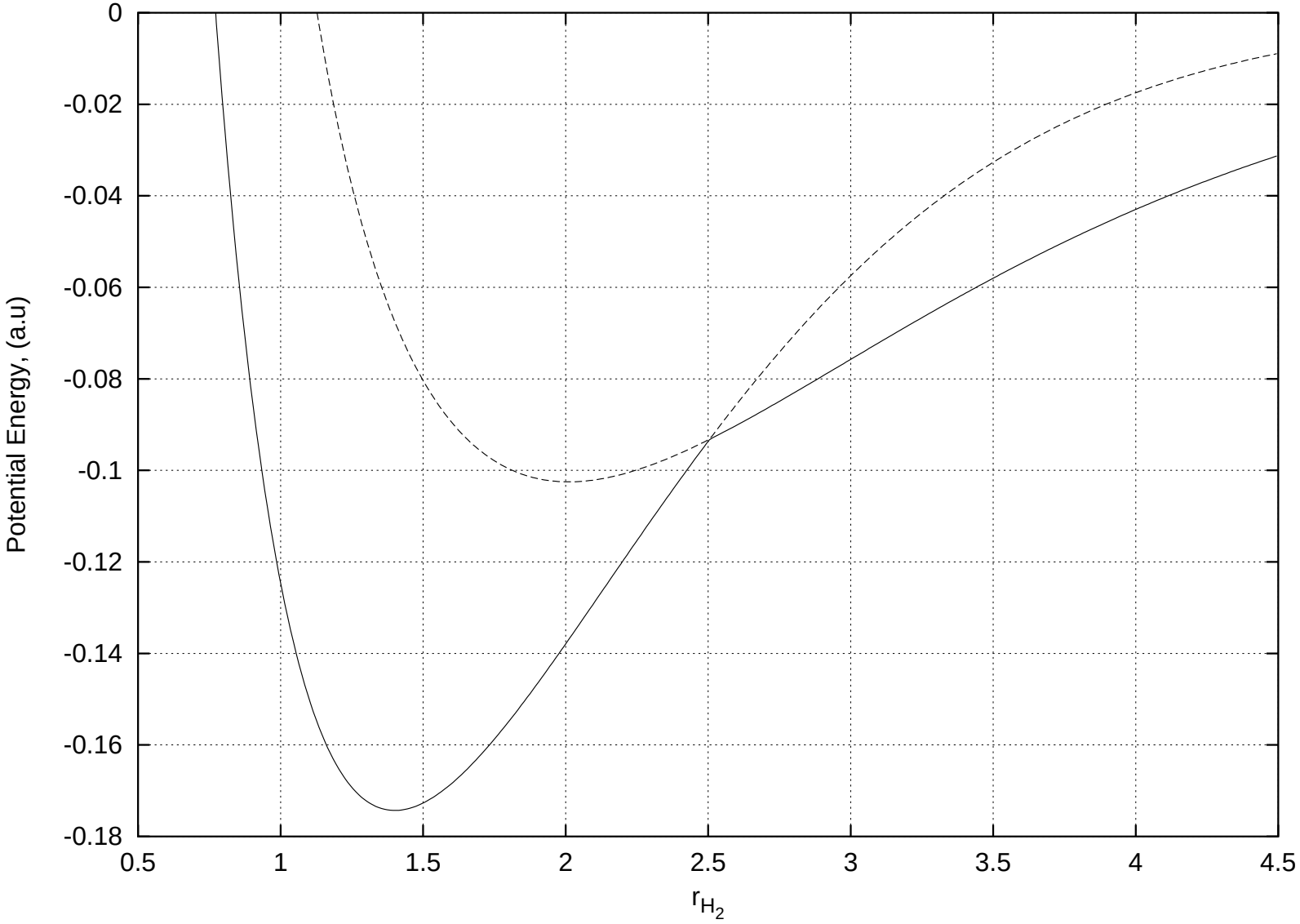

Figure 3.5: Diatomic potential curves of the DH_2^+ system

$$H_2(v,j) + D^+ \rightarrow \begin{cases} HD^+ + H & \text{(reactive)} \\ H_2 + D^+ & \text{(nonreactive)}, \end{cases}$$

Classical trajectories restricted to a plane were generated from the conventional Monte-Carlo procedure for J=0 and the initial energy of each (ν, j) state chosen from the quantized rovibrational levels. Trajectories were propagated on the initial adiabatic surface. The time profile of the separation between the two adiabatic surfaces is monitored and at a local minimum separation, the hopping algorithm is implemented as described above. The trajectories are then counted to assign the products of scattering into the different possible exit channels. The results obtained are shown in Figs. 3.6-3.11 alongside those of Ref. [17]. The good agreement between the present and the more analytical formulation of [17] confirms that the generalization recipe of this chapter works well enough and I go ahead to apply to a system with a more complicated nonadiabatic dynamics.

3.4.2 Model CH_2 System with Conical Intersection

3.4.2.1 Construction of DIM Hamiltonian

The numerical demonstration in the preceeding section was carrried out for a system where the nonadiabatic transition profile is limited only to those of the Landau-Zener types. We therefore construct a new DIM Hamiltonian purposely to obtain potential energy surfaces with interactions that yield a richer variety of nonadiabatic transition events. The surfaces are made to mimic a CH_2 system with conical intersection and also exhibit nonadiabatic tunneling-type transitions. We are thus able to implement the Trajectory Surface Hopping method, exploiting the full use of the various constituent results of the Zhu-Nakamura theory.

Using the DIM method, we choose the basis functions

$$\begin{aligned} \Psi_1 &= |\overline{a}bc|, \\ \Psi_2 &= |a\overline{b}c|, \end{aligned} \tag{3.14}$$

and

$$\Psi_3 = |ab\overline{c}|,$$

where a, b and c represent 1s orbitals located on the three atom centers, with a bar over the orbital denoting β spin and no bar denoting α spin. For A—B, the valence-bond wavefunctions are given by

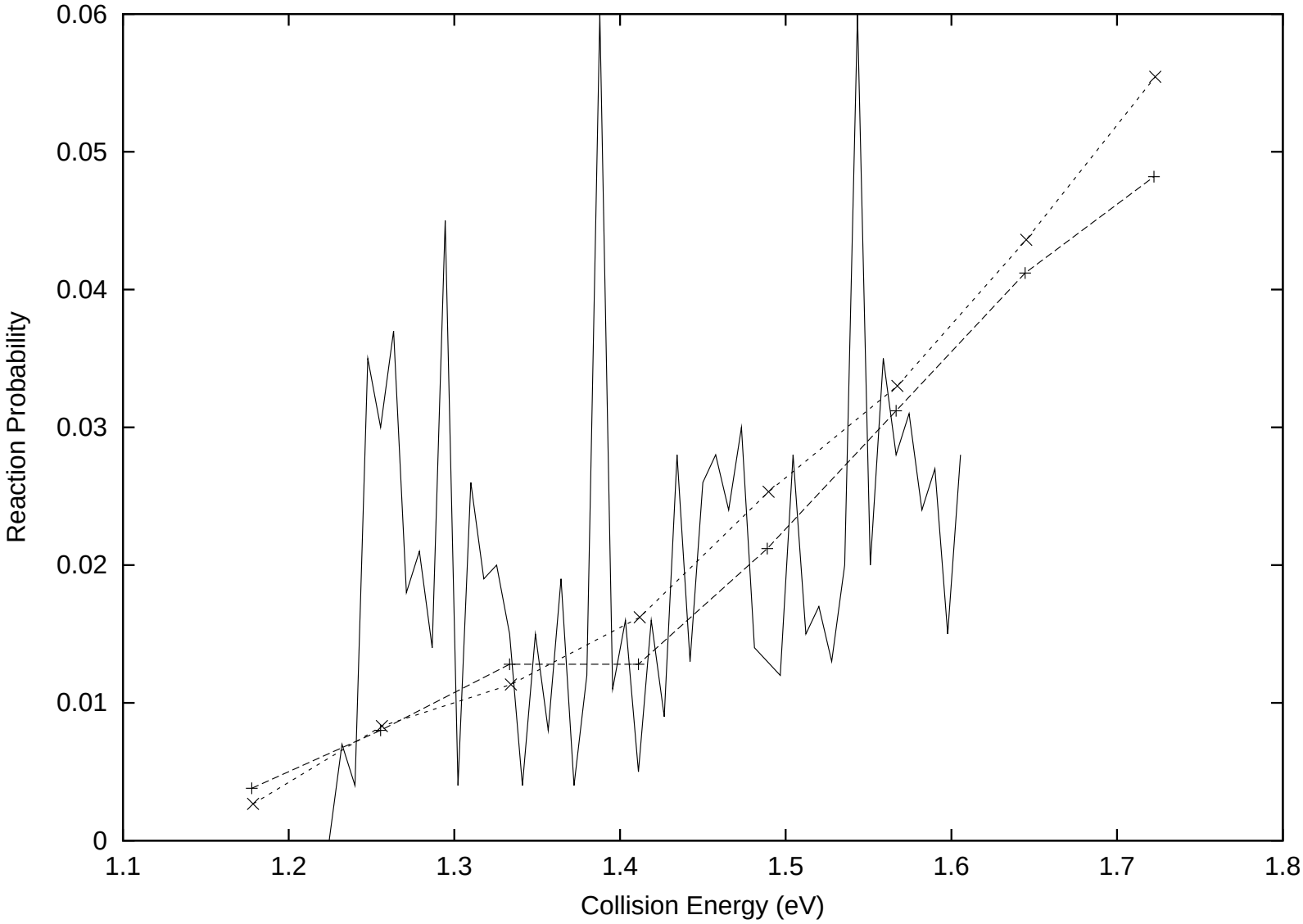

Figure 3.6: $H_2 + D^+ \rightarrow H_2^+ + D$ for $v = 1, j = 2$. Present:(thin short-dashed line with (x)), Zhu et al:(thick long-dashed line with (+)), Quantum:(continuous line)

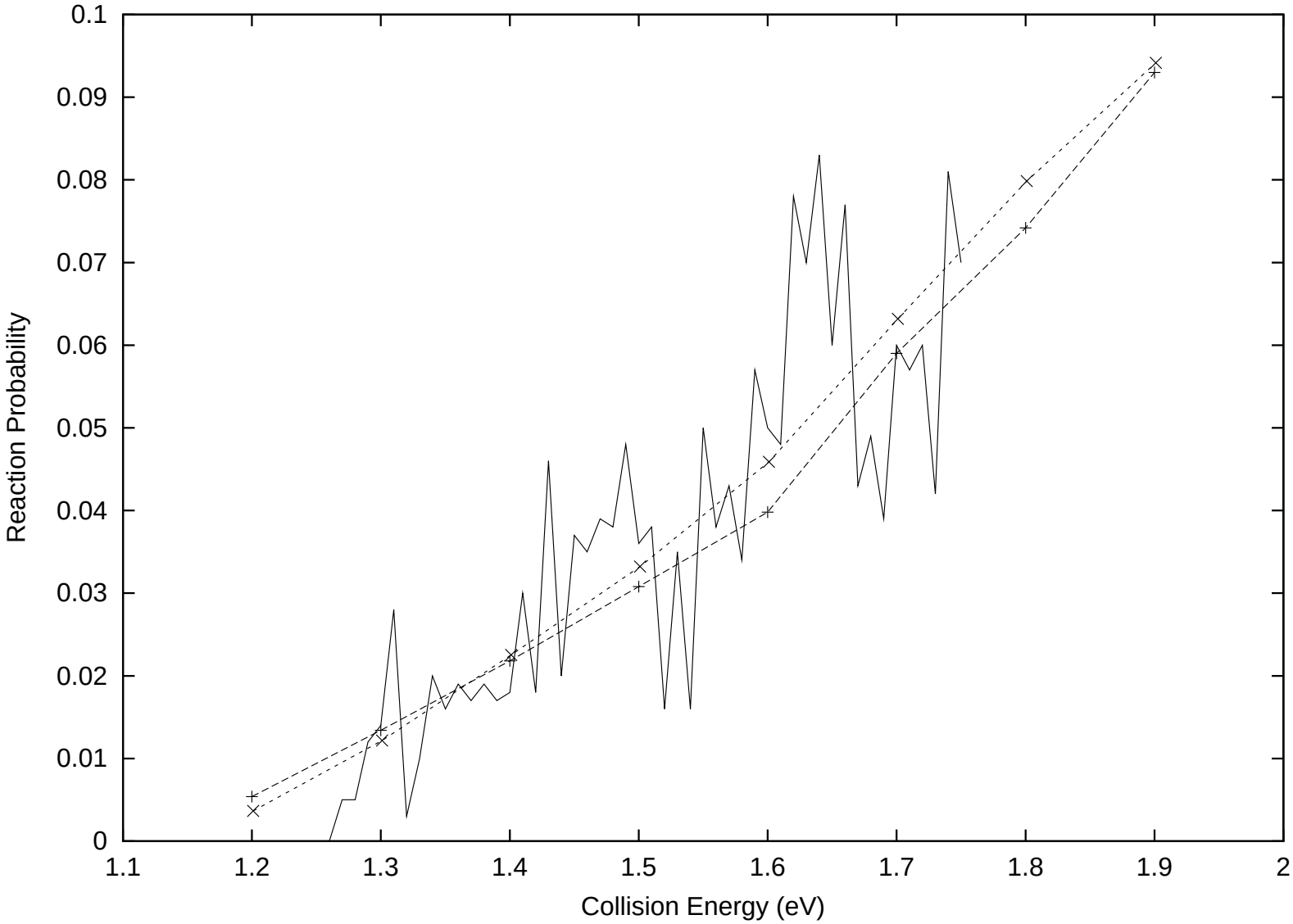

Figure 3.7: $H_2 + D^+ \rightarrow HD^+ + H$ for $v = 1, j = 2$. Present:(short-dashed line with (x)), Zhu et al:(long-dashed line with (+)), Quantum:(continuous line)

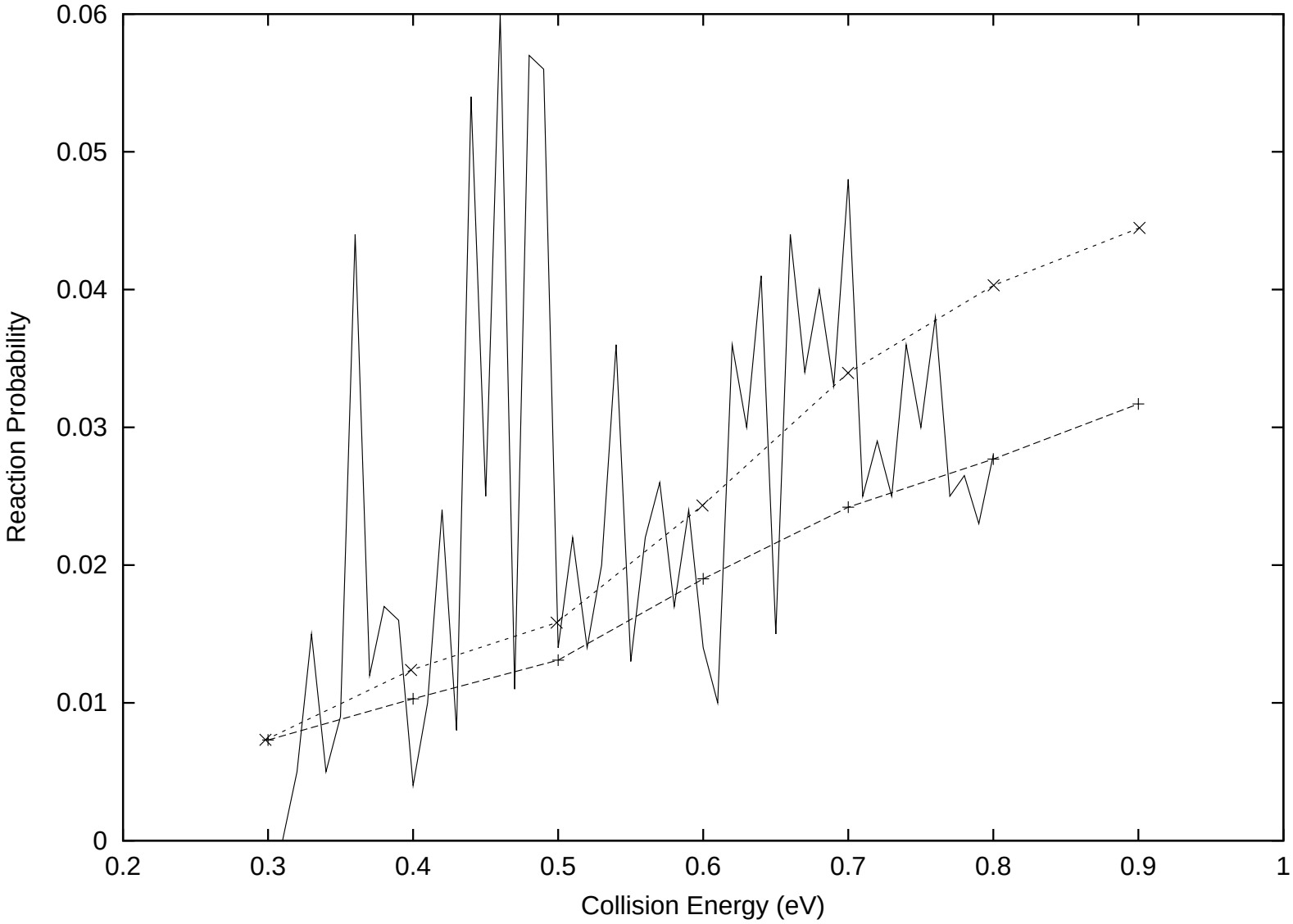

Figure 3.8: $H_2 + D^+ \rightarrow H_2^+ + D$ for $v = 3, j = 2$. Present:(short-dashed line with (x)), Zhu et al:(long-dashed line with (+)), Quantum:(continuous line)

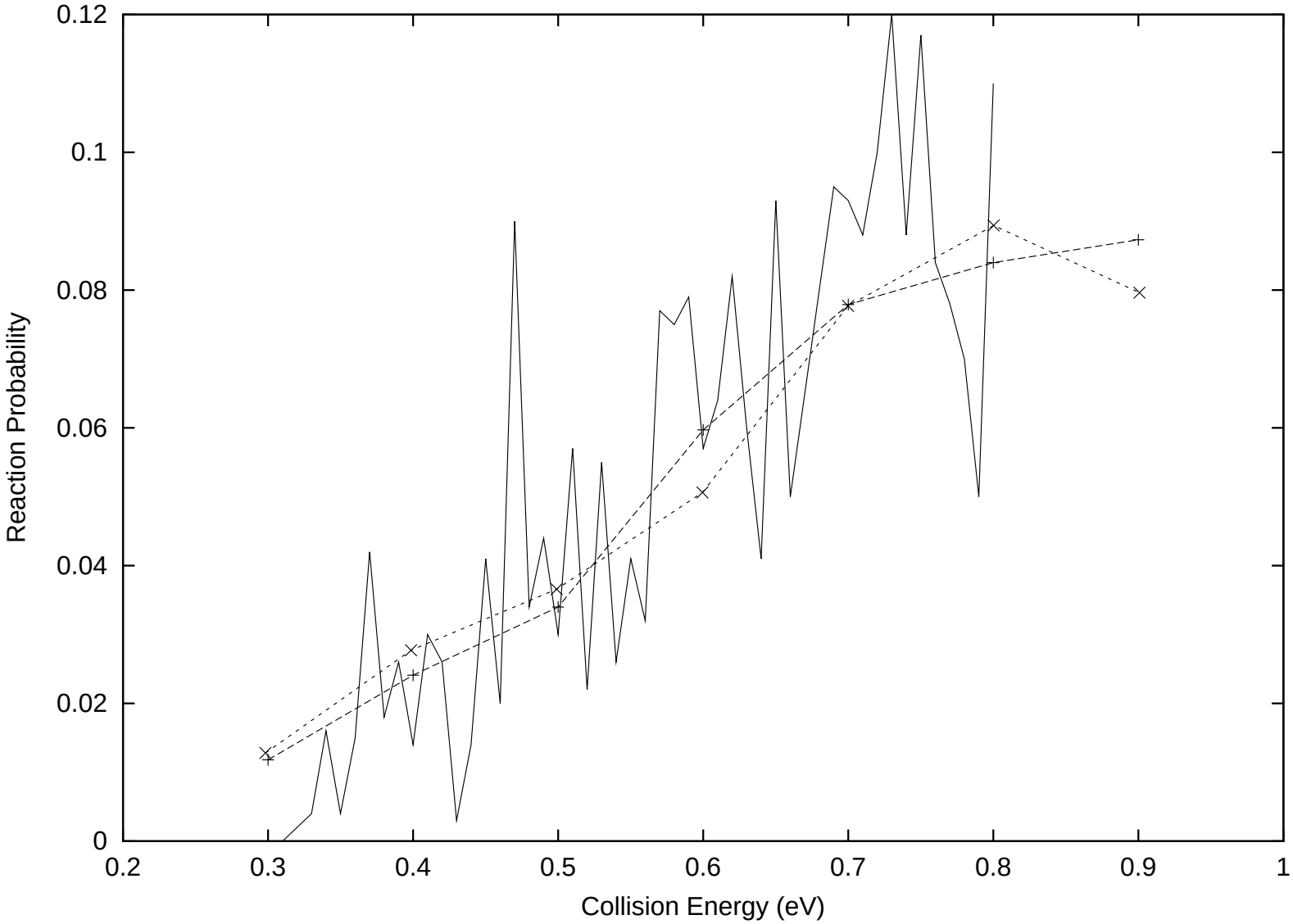

Figure 3.9: $H_2 + D^+ \rightarrow HD^+ + H$ for $v = 3, j = 2$. Present:(short-dashed line with (x)), Zhu et al:(long-dashed line with (+)), Quantum:(continuous line)

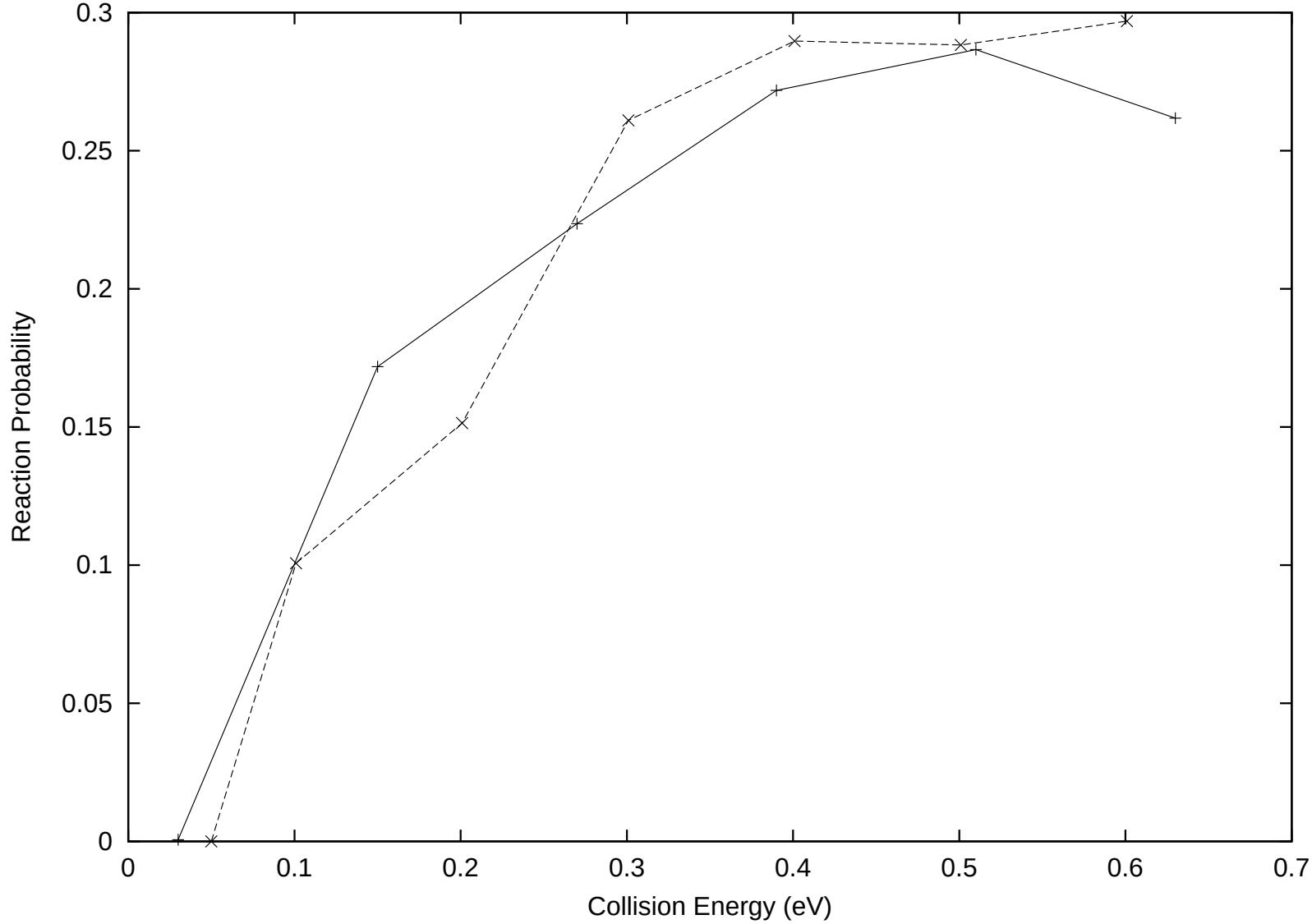

Figure 3.10: $H_2 + D^+ \rightarrow H_2^+ + D$ for $v = 5, j = 2$. Present:(short-dashed line), Zhu et al:(continuous line)

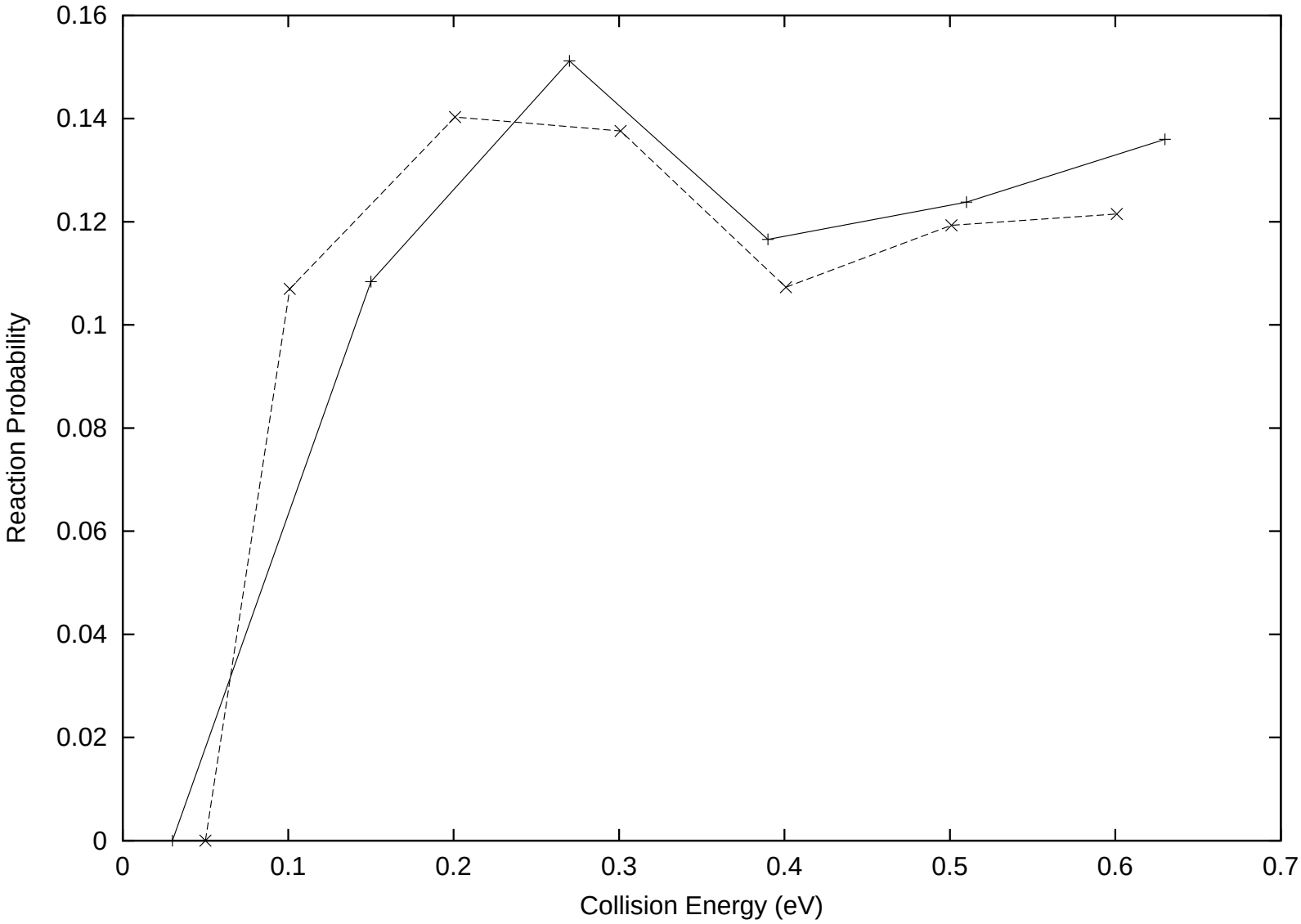

Figure 3.11: $H_2 + D^+ \rightarrow HD^+ + H$ for $v = 5, j = 2$. Present:(short-dashed line), Zhu et al:(continuous line)

$$\begin{aligned}\Phi_1^{AB} &= |a\overline{b}| + |\overline{a}b|,\\ \Phi_2^{AB} &= |a\overline{b}| - |\overline{a}b|,\\ \Phi_3^{AB} &= |ab|, \qquad (3.15)\end{aligned}$$

and

$$\Phi_4^{AB} = |\overline{a}\overline{b}|.$$

The Hamiltonian in terms of those of the atomic and the diatomic constituents of the ABC system is

$$H = H_{AB} + H_{AC} + H_{BC} - H_A - H_B - H_C \qquad (3.16)$$

The 3×3 matrix is calculated directly by taking the relevant matrix elements in terms of the basis functions, $\Psi_i, i = 1, 2, 3$. As an example,

$$\begin{aligned}H_{AB}\Psi_1 = H_{AB}|abc| &= H_{AB}\hat{A}_{AB}\hat{A}_{(AB)}abc\\ &= \hat{A}_{(AB)}H_{AB}|ab|c \qquad (3.17)\end{aligned}$$

where $\hat{A}_{AB}$ is the operator which antisymetrizes the electrons belonging to AB, and $\hat{A}_{(AB)}$ is the rest of the antisymmetrization operator.

Using $|ab| = \frac{\phi_1^{AB}+\phi_2^{AB}}{2}$ and $\mathrm{H}_{AB}\phi_{1,2}^{AB} = \mathrm{E}_{1,2}^{AB}\phi_{1,2}^{AB}$, one easily obtains

$$\begin{aligned}H_{AB}\Psi_1 &= \hat{A}_{(AB)}H_{AB}\frac{\phi_1^{AB}+\phi_2^{AB}}{2}C\\ &= \hat{A}_{(AB)}\frac{1}{2}\Big[E_1^{AB}\phi_1^{AB} + E_2^{AB}\phi_2^{AB}\Big]C\\ &= \hat{A}_{(AB)}\Big[E_1^{AB}(|ab| - |ab|) + E_2^{AB}(|ab| - |ab|)\Big]C\\ &= \frac{E_2^{AB} - E_1^{AB}}{2}\Psi_2 + \frac{E_2^{AB} - E_1^{AB}}{2}\Psi_1. \qquad (3.18)\end{aligned}$$

So that,

$$< \Psi_1|H_{AB}|\Psi_1 >= \frac{E_2^{AB} - E_1^{AB}}{2}S_{12} + \frac{E_2^{AB} - E_1^{AB}}{2}S_{11},$$

where $S_{ij} \equiv < \Psi_i|\Psi_j >$ and the overlap matrix, $S_{ij} = \delta_{ij}$.

Using the DIM method, the matrix elements of the 3×3 diabatic Hamiltonian is obtained

as

$$\mathbf{H} = \begin{pmatrix} H_{11} & H_{12} & H_{13} \\ H_{21} & H_{22} & H_{23} \\ H_{31} & H_{32} & H_{33} \end{pmatrix},$$

where

$$\begin{aligned} H_{11} &= E_2^{BC} + \frac{1}{2}(E_2^{AB} + E_1^{AB} + E_2^{AC} + E_1^{AC}), \\ H_{22} &= E_2^{AC} + \frac{1}{2}(E_2^{AB} + E_1^{AB} + E_2^{BC} + E_1^{BC}), \\ H_{33} &= E_2^{AB} + \frac{1}{2}(E_2^{AC} + E_1^{AC} + E_2^{BC} + E_1^{BC}), \\ H_{12} &= H_{21} = \frac{1}{2}(E_2^{AB} - E_1^{AB}), \\ H_{13} &= H_{31} = \frac{1}{2}(E_2^{AC} - E_1^{AC}), \\ and H_{23} &= H_{32} = \frac{1}{2}(E_2^{BC} - E_1^{BC}). \end{aligned} \tag{3.19}$$

(E_1^{BC}, E_1^{AB}, E_1^{AC}), and (E_2^{BC}, E_2^{AB} and E_2^{AC}) represent the ground and excited states of diatomic which makes up the molecule as is conventionally done in DIM approaches. However for this particular case, we have only subsituted the atomic masses with those of Carbon and 2 Hydrogen atoms. The diatomic potentials are those of a rescaled E_{CH} and E_{H2}. The rescaling of the diatomic potential was done to ensure that (1) the potential well is reduced in the condensation region to ~ 0.6 eV in order to simplify quantum scattering calculations and (2) to introduce a 50/50 chance for the occurence of LZ-type and NT-type transitions. In our actual calculations for this CH_2 model, we reduce the dimensionality of the DIM Hamiltonian to a 2×2 matrix as follows:

Noting that the original basis functions of Eq. 3.14 are not independent, we can reduce the 3×3 DIM matrix by choosing another basis

$$\phi_1 = \psi_1 - \psi_2 \tag{3.20}$$

and

$$\phi_2 = \psi_2 - \psi_3$$

which in matrix form is

$$\begin{pmatrix} \phi_1 \\ \phi_2 \end{pmatrix} = \begin{pmatrix} 1 & -1 & 0 \\ 0 & 1 & -1 \end{pmatrix} \begin{pmatrix} \psi_1 \\ \psi_2 \\ \psi_3 \end{pmatrix}. \tag{3.21}$$

In terms of $\phi_1\phi_2$, the DIM matrix then becomes,

$$\mathbf{H_{2\times 2}} = \begin{pmatrix} 1 & -1 & 0 \\ 0 & 1 & -1 \end{pmatrix} \mathbf{H_{3\times 3}} \begin{pmatrix} 1 & 0 \\ -1 & 1 \\ 0 & -1 \end{pmatrix}, \tag{3.22}$$

and the overlap matrix is

$$\mathbf{S_{2\times 2}} = \begin{pmatrix} 1 & -1 & 0 \\ 0 & 1 & -1 \end{pmatrix} \begin{pmatrix} 1 & 0 \\ -1 & 1 \\ 0 & -1 \end{pmatrix}. \tag{3.23}$$

The final 2×2 Hamiltonian matrix is obtained by removing the overlap matrix by $\mathrm{H}_{2\times 2} \Longrightarrow \mathrm{S}^{-1/2}\mathrm{H}_{2\times 2}\mathrm{S}^{-1/2}$, where

$$\mathbf{S_{2\times 2}} = \begin{pmatrix} 1+\frac{1}{\sqrt{3}} & 1-\frac{1}{\sqrt{3}} \\ 1-\frac{1}{\sqrt{3}} & 1+\frac{1}{\sqrt{3}} \end{pmatrix} \tag{3.24}$$

3.4.2.2 Topology of DIM Potential Surface

Fig. 3.12 shows a cut in the DIM potential surface obtained at $\angle(HCH)$= 110°. The corresponding 2D-contour diagrams at the same angle is shown in Figures 3.13 and 3.14. Fig. 3.15 and 3.16 are potential contours of the same surface but at $\angle(HCH)$= 150°. The two sets of figures give a fair idea of the general features of the potential energy surfaces. The conical intersection is found on the straight line r_{CH_a} =r_{CH_b} and this line has been projected on the contour diagrams in Figs.3.13 and 3.14 . The conical intersection point corresponding to the angle here is identified with a (+) sign. For the ground potential surface, at small angles of about 30°-60°, a well is found close to the potential wall and the saddle points are well separated from the condensation region positioned about

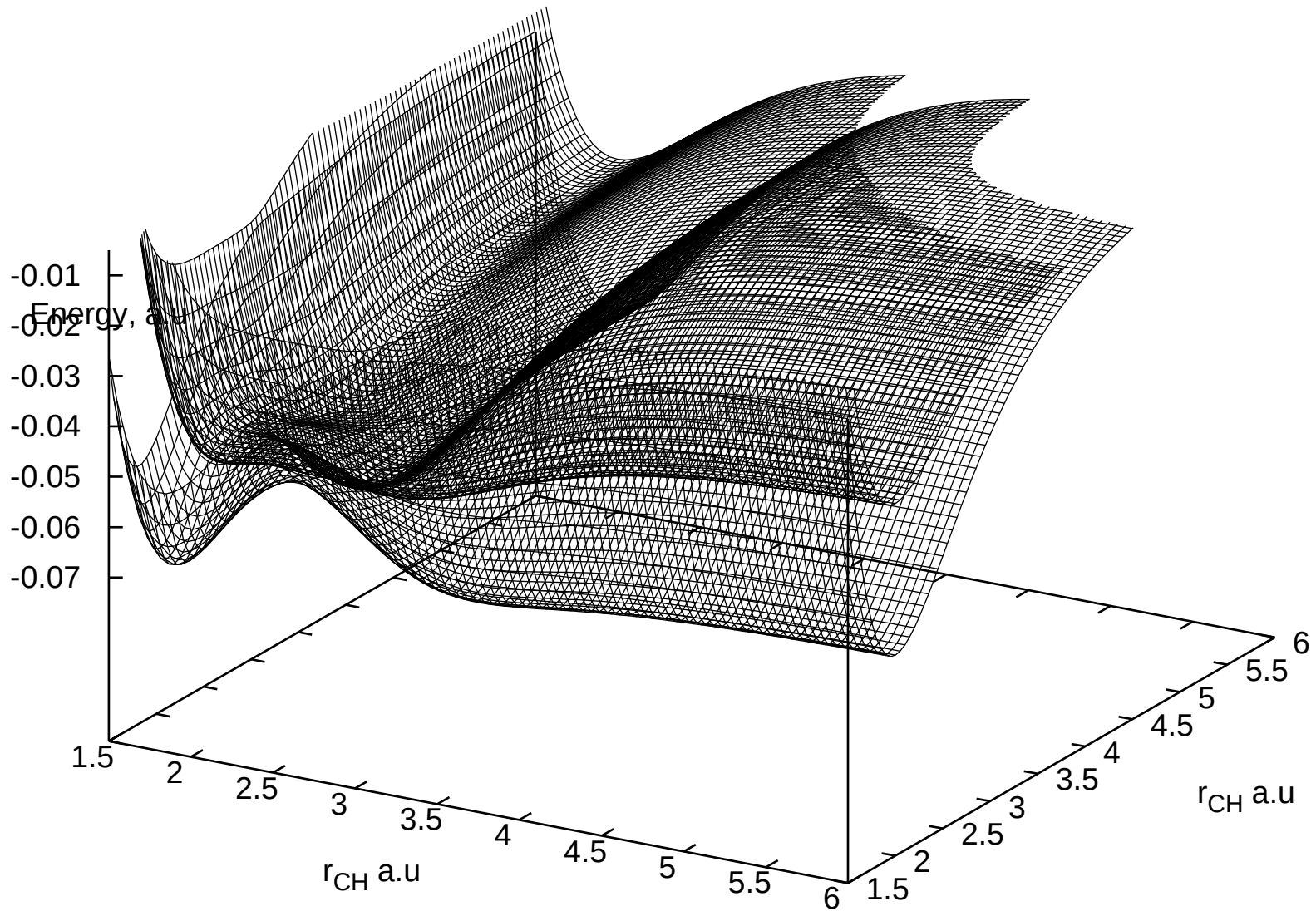

Figure 3.12: Adiabatic potential surface of the model DIM potential at angle(HCH)=110°

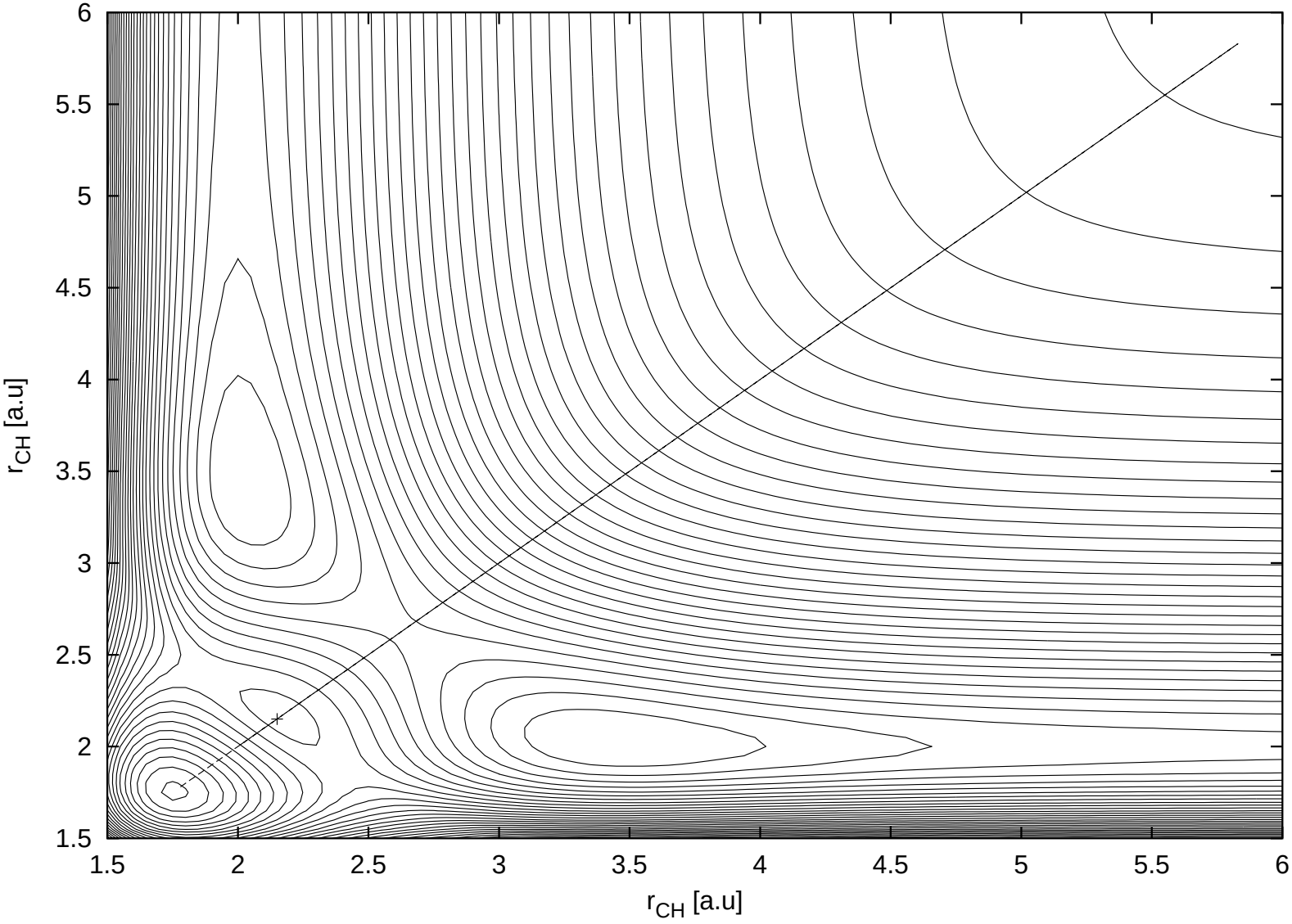

Figure 3.13: Contour of ground surface at same angle as Fig. 3.12. Cross shows point of conical intersection.

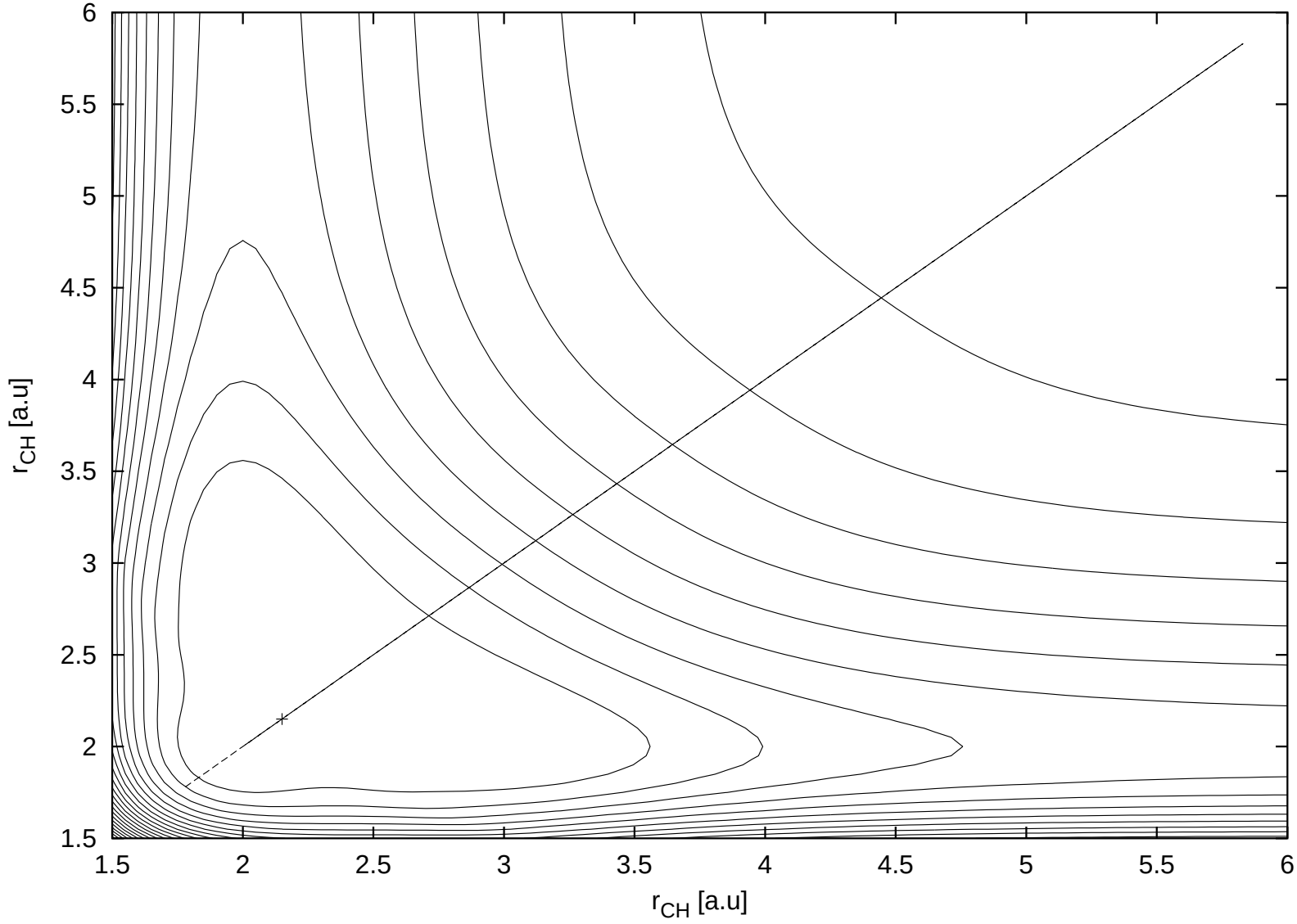

Figure 3.14: Contour of excited surface at same angle as Fig. 3.12. Cross shows point of conical intersection.

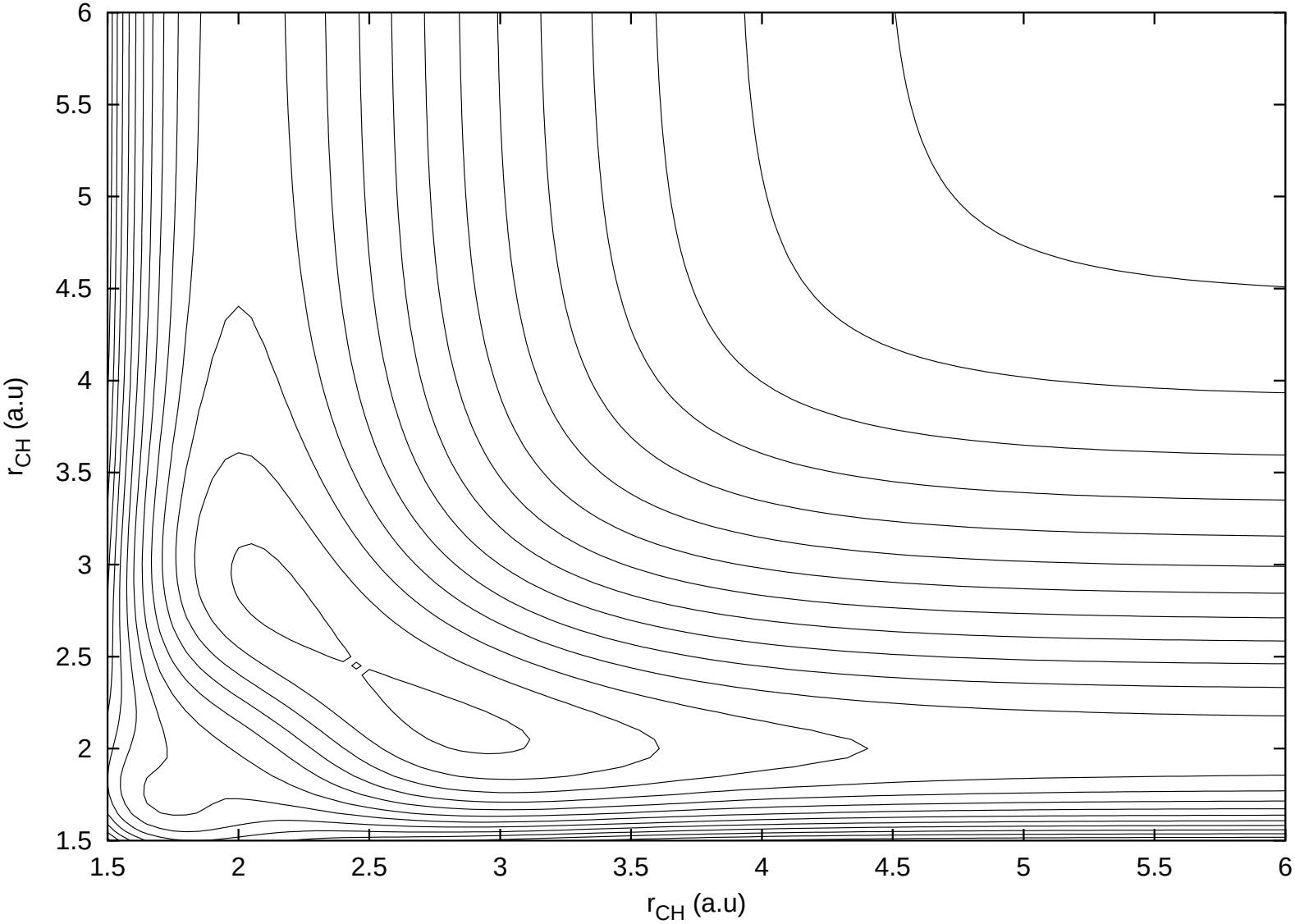

Figure 3.15: Contour of ground surface at angle(HCH)=150°.

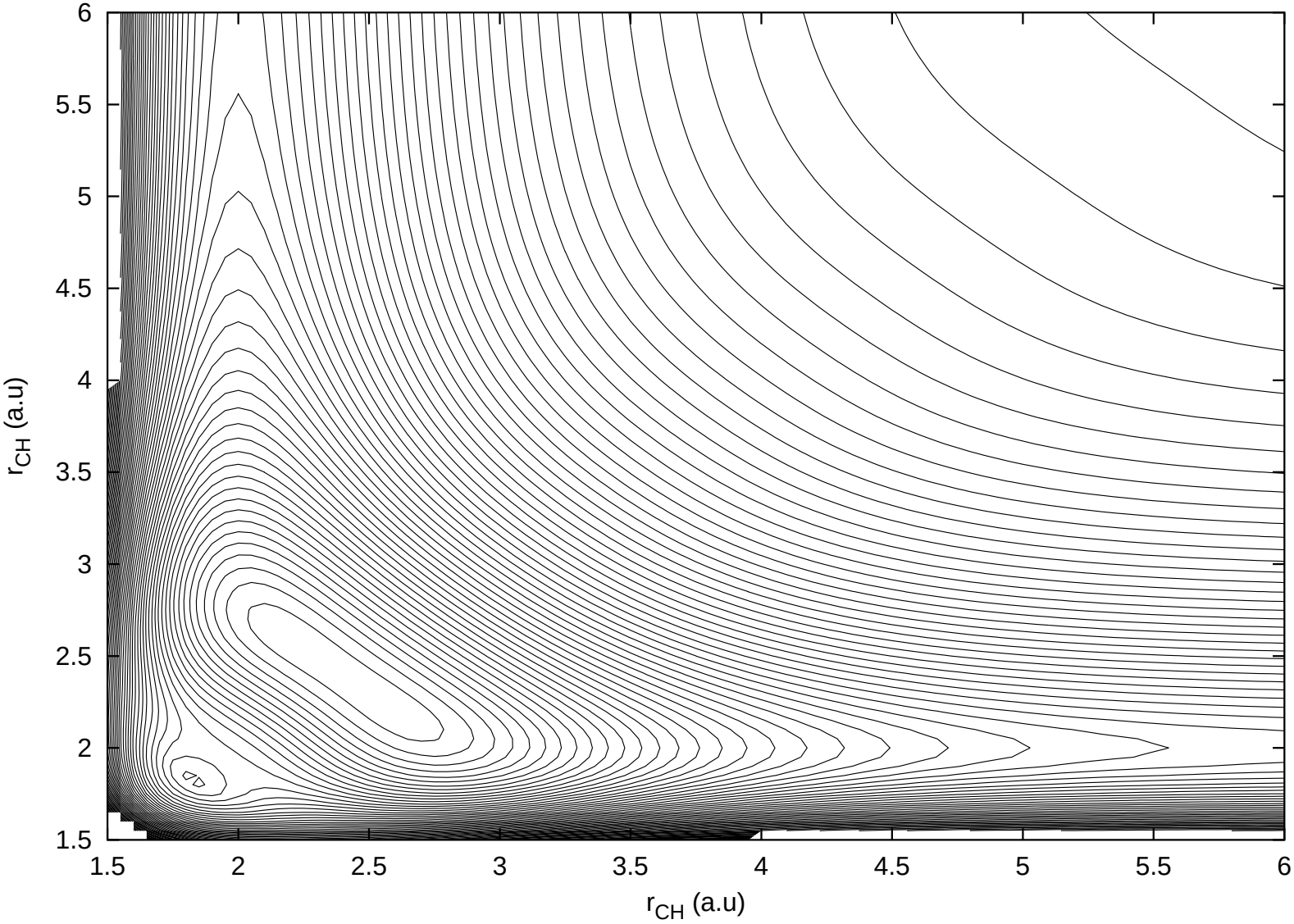

Figure 3.16: Contour of excited surface at angle(HCH)=150°.

$r_{CH_a} = r_{CH_b} > 2.5$ a.u. As the angle between the two C−H bonds becomes wider, to between 90°-130°, the well situated close to the potential wall passes through its deepest which is about -0.07 a.u, and the saddle shift inwards moving towards the well. In between the point on the minimum energy path and the potential energy wall, the surfaces arches upwards, touching the bottom of the upper potential surface to form the point of closest approach between the two surfaces. At about the same range of angles, the upper potential surface has a wide, flat bottom which is less than 0.01 a.u higher than the lowest point in the condensation region. The processes considered are:

$$C + H_2(v, j, i) \rightarrow \begin{cases} H + CH(f) \\ C + H_2(f) \end{cases}, \tag{3.25}$$

and

$$H + CH(v, j, i) \rightarrow \begin{cases} H + CH(f) \\ C + H_2(f), \end{cases} \tag{3.26}$$

(i, f) represent the initial and final surfaces respectively. On the second surface, the H_2 channel is closed because of the repulsiveness mentioned above.

Initial conditions of classical trajectories were chosen as with those in the DH_2^+ case and are similarly propagated. For each initial state, 10,000 trajectories were propagated using a time-step of 1 a.u. As usual, at the point along the trajectory where the criterion for hopping is satisfied, the hopping algorithm is implemented and trajectory propagation continues either on the same surface as it was before reaching the hopping region, or on the new surface where it has emerged. In this CH_2 case, it is necessary to note that an important part of the hopping algorithm is making the judgement of whether the transition is of an LZ or NT-type in order to employ the appropriate Zhu-Nakamura expressions[1] to compute nonadiabatic probabilities. For the first process, the only possible initial surface is (i=1); for process 3.25a, the channels on the ground and excited surfaces are both open while for process 3.25b, the channel on the excited state is closed. For processes 3.26, both (i=1,2) are considered and 3.26a may have (f=1,2) while 3.26b like 3.25b has the (f=2) channel closed. In both processes, the initial seclected channels were those for (v=0,1) while the final channels were summed over all rovibrational states.

3.4.3 Quantum Mechanical Result

The results of the quasiclassical method described is compared with quantum results obtained by using the Hyperspherical elliptic coordinate approach. For a fuller description,

see [18]. A brief outline of the method follows. In the hyperspherical elliptic coordinate system, the hypersphere is parametrized by the hyperradius ρ and the hypershperical elliptic angles (ξ, η). The Schrödinger equation for J (total angular momentum) $= 0$ can be written as

$$[K(\rho) + H_{ad}(\xi, \eta; \rho) - \mu\rho^2 E]\psi(\rho, \xi, \eta) = 0, \tag{3.27}$$

where $K(\rho)$ represents the kinetic energy relative to ρ, H_{ad} is the adiabatic Hamiltonian composed of the angular kinetic energy and the potential is defined at fixed ρ, μ is a characteristic mass factor, and E is the total energy measured from the ground rovibrational state of the H_2 diatomic potential of the model potential. Solving the eigenvalue equation

$$[H_{ad}(\xi, \eta; \rho) - \mu\rho^2 E]\Phi_\nu(\xi, \eta; \rho) = 0, \tag{3.28}$$

yields the adiabatic potential curves $U_\nu(\rho)$ and the adiabatic channel eigenfunctions $\Phi_\nu(\xi, \eta; \rho)$. The good separability of the hyperspherical elliptic angle coordinates is utilized in obtaining a step-by-step solution of this eigenvalue problem. Eq. 3.28 is first solved with respect to the ξ-motion which represents the vibrational motion of the reactants and the products:

$$[h_{ad}(\xi : \eta, \rho) - \mu\rho^2(\cos\eta - \cos\eta)u_{n\xi(\eta,\rho)}]\phi_{n\xi}(\xi; \eta, \rho) = 0, \tag{3.29}$$

where h_{ad} is the adiabatic hamiltonian defined at fixed ρ and η, $u_{n\xi}$ is the vibrationally adiabatic potential and n_ξ represents the corresponding vibrational quantum number. The eigenfunctions of the adiabatic channel can be expanded in terms of $\phi_{n\eta}$ as

$$\Phi_\nu(\xi, \eta; \rho) = \sum_{n_\xi} f^\nu_{n_\xi}(\eta; \rho)\phi_{n_\xi}(\xi; \eta, \rho). \tag{3.30}$$

Then the total wavefunction $\Psi(\rho, \xi, \eta)$ can be expanded in the form,

$$\Psi(\rho, \xi, \eta) = \rho^{-5/2} \sum_\nu F_\nu(\rho)\Phi_\nu(\xi, \eta; \rho). \tag{3.31}$$

Actual computations of Eqs. 3.27 and 3.29 are carried out by using the slow-variable-discretization (SVD)method[18]. The obtained total wavefunction in each sector of ρ is propagated to the asymptotic region by employing the R-matrix propagation method. This is then used to obtain the S-matrix elements which is compared with the results of the quasiclassiclal recipe above.

3.4.4 Discussion of Results

Figs. 3.17-3.21 are the first set of published results using the Zhu-Nakamura theory to study systems where nonadiabatic transition events are to a large measure more pronounced in the exchange region of the potential energy surfaces and where hops of different nature (i.e. LZ-types and NT-types) are treated simultaneously in a single system. In all the cases shown, the calculations are run at a total energy of 0 - 1.1 eV.

The results presented are compared with quantum results. Since the threshold of the nonadiabatic processes in every case is at total energy value of 0.8 eV, comparisons made for the nonadiabatic transition-induced processes are for energies between 0.8–1.1 eV. The processes shown in Figs. 3.17 and 3.18, i.e. those with C + H_2 reactants(v=0,1), agreees quite well with quantum results. In the case of the H + CH(v=0,j=0) shown in Fig.3.17 for the nonadiabatic processes on the upper surface, the ZN-TSH results have similar trend with quantum results and provides quite a good average of the quantum results. For the adiabatic processes on the lower surface, the resonances are not well reproduced. This is not surprising since quasiclassical methodology can generally not treat resonances well and actually, the long-lived trajectories are killed in the present calculations. However, the trends on this surface is equally good not just qualitatively but quantitatively as well.

In Fig. 3.18, we see the same channel but with vibrationally-excited reagents, the results become a lot better than the v=0 case. The little discrepancy seen at the high energy end in Fig. 3.17 is no longer the case here. It was mentioned above that the locus of the points of conical intersection in this system is located on the symmetric $r_{CH_a} = r_{CH_b}$ line which means that this line is on the path of the incoming diatomic. It can then be said that a higher vibrational energy favors reaction for a diatomic approaching the reaction zone in the direction of this line. Figs. 3.19 is the result for the H + CH initial channel at $v = 0, j = 0$. The nonadiabatic probability for this process is low compared with Fig. 3.20, helping to confirm the importance of vibrational excitation in the success or failure of the trajectory reaching the important non-adiabatic region. The final plot, Fig.3.21 is the result of the only process started on the second surface. In this H + CH(i=2) entrance channel case, the nonadiabatic transition probability for the H + CH(f=1) product channel is much higher than H+CH(f=2) process. This makes clear that the bottleneck to nonadiabatic transition is the complicated topology on the lower surface where the highest point on the potential surface touches the bottom of the upper surface at the conical intersection and the wells surrounding the points of conical intersection prevent transitions from being easily accomplished. The almost flatness of the upper surface, precludes any such complicated

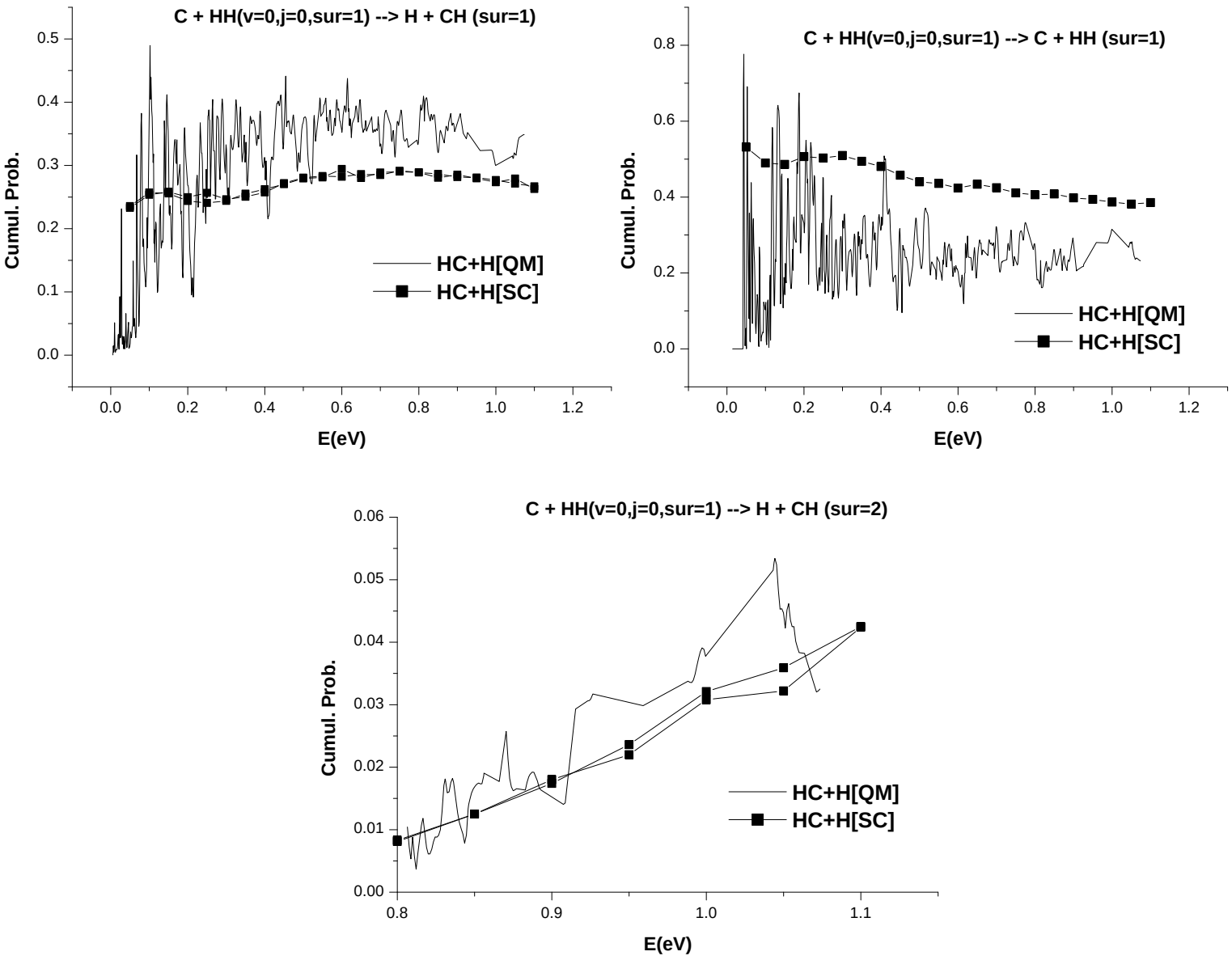

Figure 3.17: initial channel:C + $H_2(v = 0, j = 0$,surface=1)

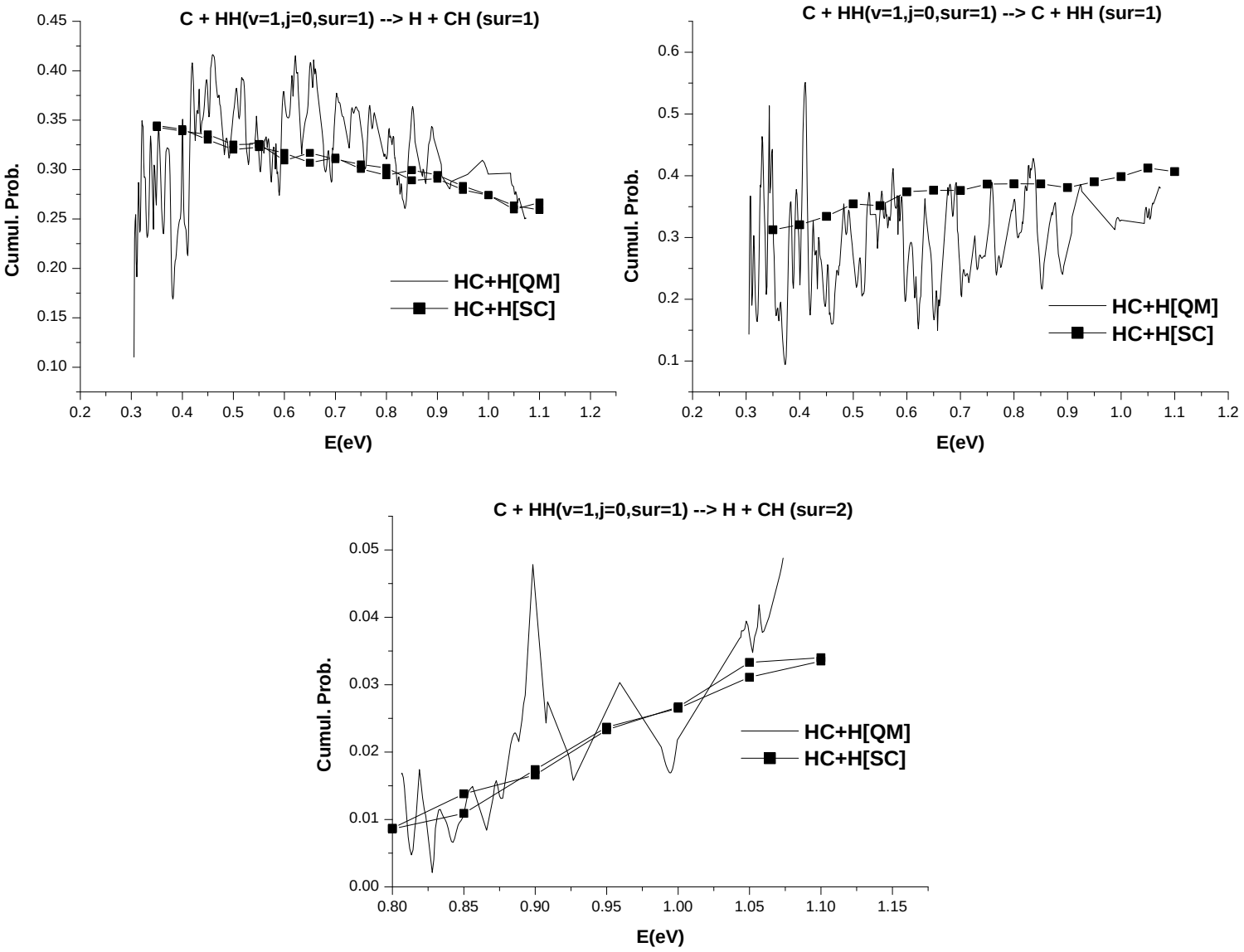

Figure 3.18: initial channel:C + H_2($v = 1, j = 0$,surface=1)

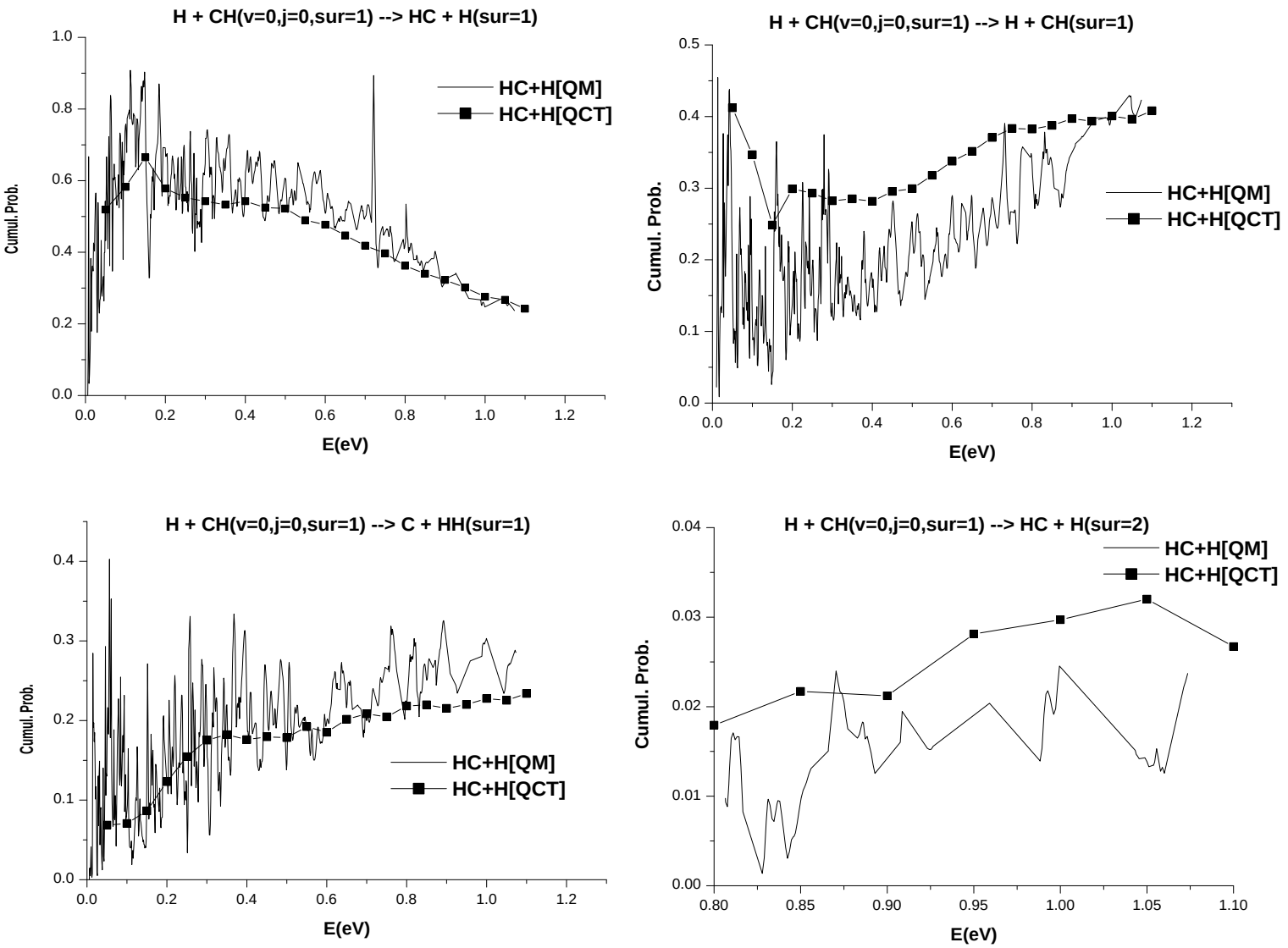

Figure 3.19: initial channel:H + CH($v = 0, j = 0$,surface=1)

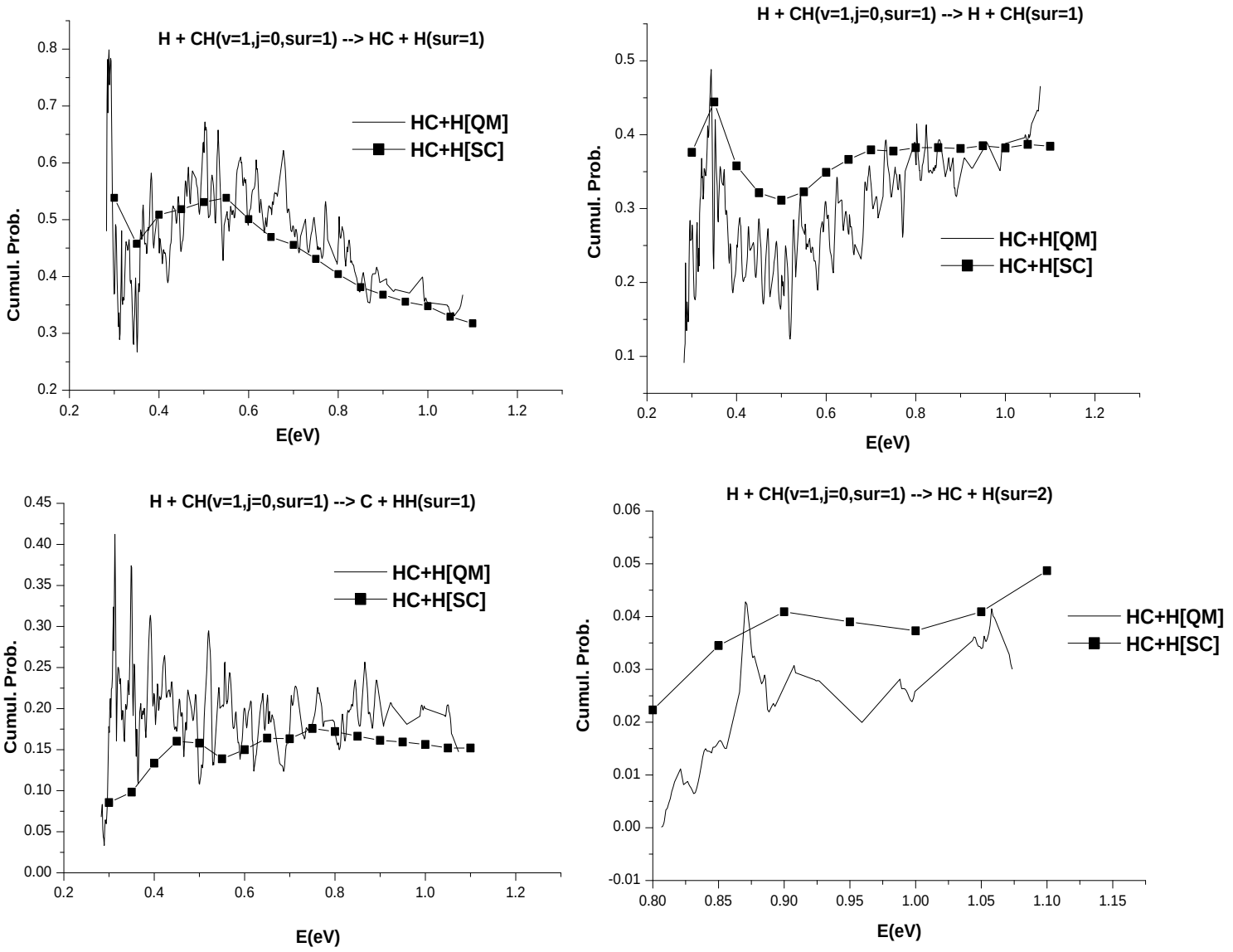

Figure 3.20: initial channel:H + CH($v = 1, j = 0$,surface=1)

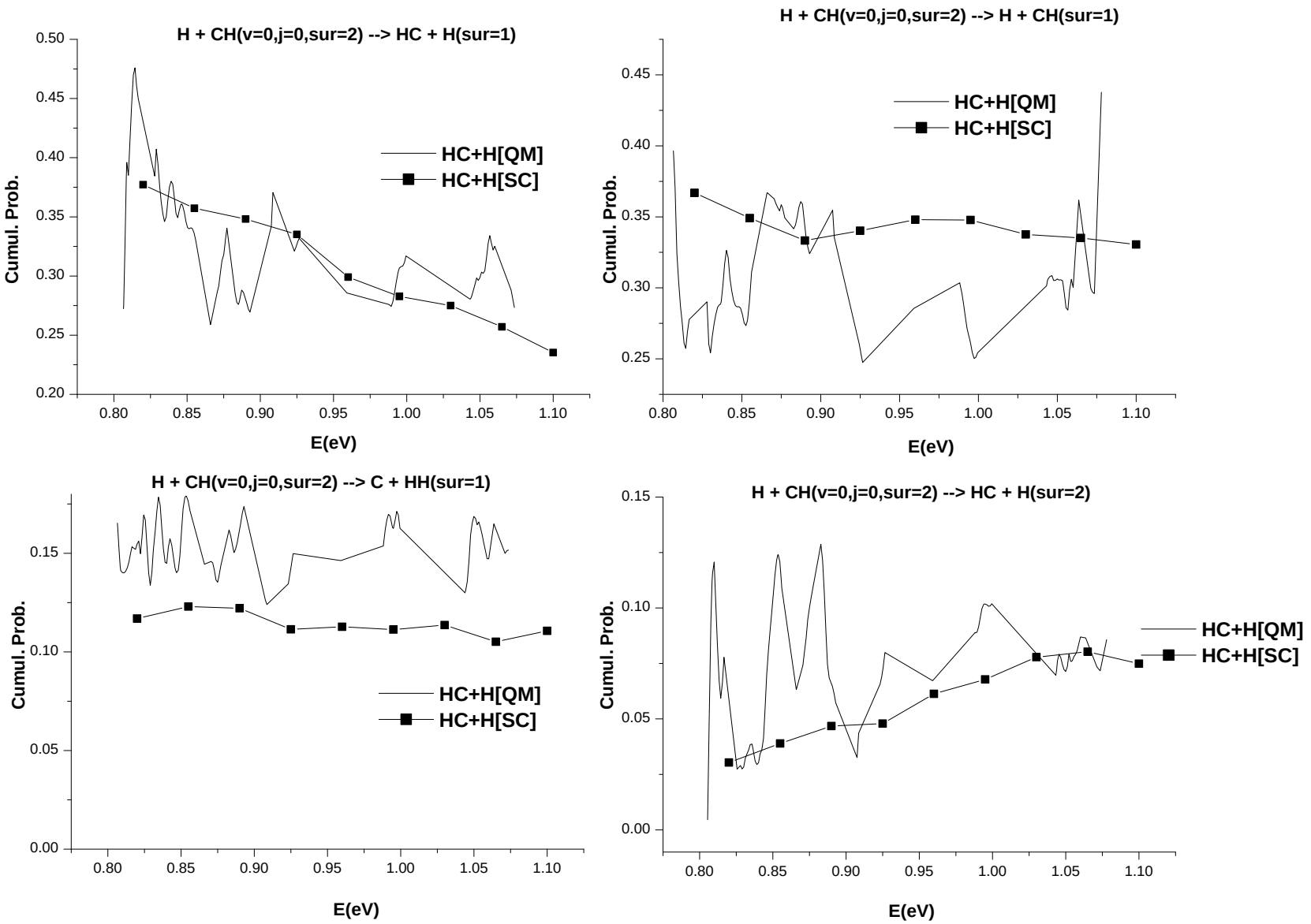

Figure 3.21: initial channel:H + CH($v = 0, j = 0$,surface=2)

mechanism from influencing adiabatic and nonadiabatic reactions.

In general, for the processes occuring on these surfaces, one may propose a simplified picture for the mechanism leading to nonadiabatic reactions as follows: a trajectory approaches from the entrance channel, and on entering the condensation region, hops to the second surface, and exits into the reflection or the exchange channel. As mentioned earlier, the topology of the second potential surface features a wide-bottomed well and it is expected that trajectories may be trapped in this well and afterwards become rather statistically distributed into the two channels on the second surface.

3.5 CONCLUDING REMARKS

In an attempt to generalize the TSH method so that it can nicely applied to large systems, I have improved upon the conventional method in the following respects:

1. Any type of transitions (LZ and NT) can be treated by full use of the Zhu-Nakamura theory.

2. Use of minimum energy separation to detect transition point.

3. Direction of transition along the coupling vector which can be roughly estimated even if it is not available.

4. Simple algorithm to conserve total angular momentum, J.

We restate that the generalized method presented here is more valuable because of the ease of its applicability since detailed analysis of the potential energy surface before hand is not necessary. Since the Zhu-Nakamura theory is accurate, even classically forbidden cases can be properly treated. Except for the case of resonances, the method is quite accurate with encouraging results in comparison with quantum. The agreement with the quantum mechanical results is not perfect, of course, because of the limitations of the treatment such as the reduction of dimensionality, the approximate direction of transition and neglect of phases(resonances). However, we can probably safely conclude that the present simple and general TSH method can be applied to complicated systems. Namely, it should be the case that the possibility of obtaining, at the very minimum, a rough description of how nonadiabaticity mediates processes in complicated multidimensional systems should become more and more closer to fruition. We hope to continue with this approach in our future endeavors.

REFERENCES

[1] H. Nakamura, *Nonadiabatic Transitions, Concepts, Basic Theories and Applications*, (World Scientific,2002)

[2] C. Zhu, G. Mil'nikov, and H. Nakamura, *Modern Trends in Chemical Reaction Dynamics(Advanced Series in Physical Chemistry), ed. K. Liu and X. Yang*, (World Scientific,2002)

[3] J. Michl and V. Bonacic-Koutecky, *Electronic Aspects of Organic Photochemistry*, (Wiley,1990)

[4] J.R. Bolton and N. Mataga and G. Mclendon, *Electron Transfer in Inorganic, Organic and Biological Systems*, (American Chemical Society,1991)

[5] W.H. Miller, J. Chem. Phys. **53**, 3578, 1970.

[6] W.H. Miller and X. Sun, J. Chem. Phys. **106**, 916, 1997.

[7] E.J. Heller, J. Chem. Phys. **94**, 2723, 1991.

[8] A.R. Wolton and D. E. Manolopoulos, Mol. Phys. **84**, 961, 1996.

[9] J. Tully and R.K. Preston, J. Chem. Phys. **55**, 562, 1971.

[10] M. Ben-Nun and T. Martinez, J. Chem. Phys. **108**, 7244, 1998.

[11] L.D. Landau, Phys. Zts. Sov. **2**, 46, 1932, C. Zener, Proc. Roy. Soc. **A137**, 696, 1932.

[12] M. S. Topaler, T. C. Allison, D. W. Schwenke, and D. G. Truhlar, J. Phys. Chem. **A 102**, 1666, 1998.

[13] J. C. Tully, J. Chem. Phys., **93**, 1061, 1990

[14] E. E. Nikitin, Ann. Rev. Phys. Chem. **50**, 1, 1999.

[15] C. Zhu and K. Nobusada and H. Nakamura, J. Chem. Phys. **115**, 3031, 2001.

[16] C. Zhu and H. Kamisaka and H. Nakamura, J. Chem. Phys. **115**, 11036, 2001.

[17] C. Zhu and H. Kamisaka and H. Nakamura, J. Chem. Phys. **116**, 3234, 2002.

[18] K. Nobusada et al, J. Mol. Str. (Theochem) **461-462**, 137, 1999.

CHAPTER 4

CHEMICAL REACTIONS IN THE OHCl SYSTEM

4.1 Introduction

There has been a sustained interest in studying the dynamics of the $O(^1D)$ + HCl system for a period which stretches back over the past 3 decades[1, 2, 3, 4, 5, 6, 7, 8, 9].The reasons for these interest is not far-fetched since it is well-known that OHCl is known to be of great importance in atmospheric processes[10, 11]. HOCl, which is an intermediate in this system is known for its role in the balance of ozone in the stratosphere in the polar regions of the earth. It is especially believed that HOCl helps in the depletion of the stable chlorine reservoir in their conversion into more reactive species in polar clouds.[12]. These processes are further helped by the intense UV radiation which enhances the release of $O(^1D)$ by photodissociation of oxygenated species. Taken together, these processes play crucial role in Ozone layer depletion which is an issue that has become an issue of high priority for environmental policy-makers.

The chemical reactions of the $O(^1D)$ with HCl are:

$$\begin{aligned} O(^1D) + HCl(^1\Sigma^+) &\rightarrow OH(^2\Pi) + Cl(^2P), \Delta H_0 = -44 \text{ kcal/mol} \\ &\rightarrow OCl(^2\Pi) + H(^2S), \Delta H_0 = -6 \text{ kcal/mol} \end{aligned} \tag{4.1}$$

The first reaction which has a larger rate constant compared to the second is known to be a good sink in the conversion of chlorine into free radicals[13]. The second reaction is of considerably less exoergicity. Both of these reactions, apart from their practical importance, are also important in resolving fundamental chemical dynamical questions. Are the reactions of insertion or abstraction type ? What is the branching ratio of the two

product channels ? And what role if any, do the excited state potential surfaces play on the reactions. In this chapter, I intend to report on the dynamical studies which have been carried out on this system using the quasiclassical methodology.

4.2 POTENTIAL ENERGY SURFACES (PES)

Nanbu and co-workers [14] have presented, for the first time, the three lowest potential energy surfaces (symmetry of electronic configuration: $1^1A'$, $1^1A''$ and $2^1A'$) which correlate asymptotically to O(^1D) + HCl and OCl + H. Previous potential energy surfaces of this system have been presented by Peterson[12, 15, 16] and Martinez[13, 17]. Both potential energy surfaces constructed by Peterson et al and Martinez et al were obtained using the CASSCF(Complete Active Space Self-Consistent field) and MRCI(Multi-Reference Configuration Interaction) quantum-chemical methodology. But while Martinez et al used the double-zeta + polarization basis set, Peterson et al employed three different basis sets in the extrapolated complete basis set limit with the three basis sets being the double, triple and quadruple of the diffuse-function augmented, correlation consistent, polarized valence, zeta basis sets. The potential energy surface of Nanbu et al, which is used for the chemical dynamical studies reported in this chapter, were computed by using the MRCI method with the Davidson correction (MRCI+Q). The reference functions are constructed by the CASSCF calculations using the diffuse functions-augmented quadruple-zeta basis sets and the computations are carried out for almost 5000 conformations of the molecule on each of the potential surface. These potential energy surfaces by Nanbu et al, is the first report of the potential energy surface for the two excited states, $1^1A''$ and $2^1A'$. The ground surface is as accurate as Peterson's in the well regions, and is supposed to be more accurate in the asymptotic regions which are important for chemical reaction dynamics. In order to obtain a global surface suitable for use in chemical dynamical studies, the ab-initio potential surfaces are finally interpolated using the interpolant moving least squares (IMLS) method combined with Shepard Interpolation[19]. Further details of the energetics and topology of these surfaces are provided below.

4.2.1 Energetics of $1^1A'$, $1^1A''$, and $2^1A'$ surfaces

The correlation diagram constructed from the final interpolated potential energy surfaces is shown in Fig. 4.1. The dissociation limit of O(^1D) + HCl is taken as the zero of energy. There are two deep wells on the ground state which are found in the bent geometries coresponding to the HOCl and HClO molecules. These wells are labelled P1 and P3 respectively, in the diagram. The depth of P1 is 4.38 eV, that of P3 is 1.94 eV, while between

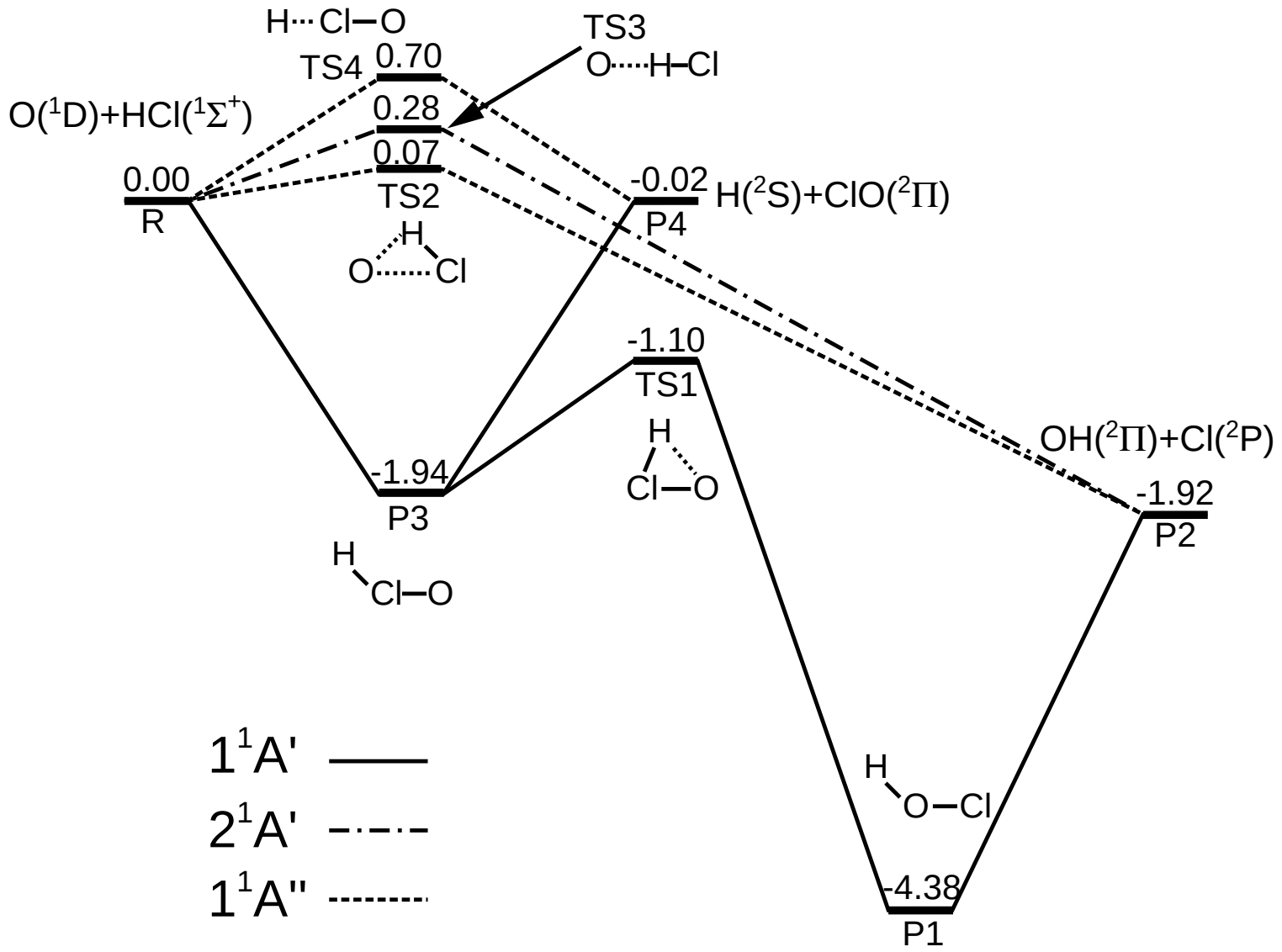

Figure 4.1: Correlation Diagram for the O(^{1}D) + HCl reaction[Reproduced with the kind permission of Dr. Shinkoh Nanbu]

these two wells, the barrier to isomerization from the HClO side is about 0.84 eV. The excess energy of formation for the OH($^2\Pi$) + Cl(^2P) channel is -1.92eV (Experimental=-1.93 eV[20, 21, 22]) while that for the H(^2S) + ClO($^2\Pi$) is -0.02eV (Experimental=-0.13eV). The experimental value is obtained from a thermodynamical cycle. The OCl channel excess energy of formation is in agreement with the exoergicity of the channel as predicted by experiment. [note the endoergicity($\sim$ 0.33eV) of the ClO channel in the potential energy surface used by Schinke[24]]. Two transition states TS2 and TS4 on the $1^1A''$ PES correlate to OH + Cl and H + ClO channels respectively. The TS2 is triangular while the TS4 is linear. The energetic differences between these two transition states imply that their contributions to the final channels are dissimilar. Through TS2, the $1^1A''$ easily contributes to the OH + Cl channel while the TS4 which has a height $\sim$ 0.70eV implies that the contribution of $1^1A''$ to the ClO channel will be limited unless the collision energy is high. The $2^1A'$ has no direct correlation leading to the ClO channel.The only transtion state, labelled TS3 in the diagram, correlates to the OH+Cl and its relatively low height of 0.29eV, implies possible appreciable contribution to the overall dynamics of the reaction.

4.2.2 Topology of $1^1A'$, $1^1A''$, and $2^1A'$ surfaces

Fig. 4.2 shows the two minima on the $1^1A'$ surface at the conformation corresponding to the bent HOCl and bent HClO complexes with the HOCl well about 2.5 eV deeper. Fig. 4.3a is a contour map of the $1^1A''$ with the bond geometry fixed at the geometry of the transition state, TS2. The location of the transition state at the O+HCl entrance channel, suggests that the reaction mechanism is an early-barrier type. Such a reaction would lead to backward scattering due to the late release of excess energy. Fig. 4.3b shows the second transition, TS4 which is of linear conformation as mentioned above. This is located at the interaction region of the potential surface. However, because of the presence of the wells on the $1^1A'$ surface, the reaction mechanism is expected to be different between these two surfaces. Fig. 4.4 shows the contour map of the $2^1A'$ around the TS3 transition state shown in the correlation diagram. The profile of the surface at this configuration is similar to that of the TS2 on the $1^1A''$, i.e. an abstraction-type reaction with early barrier and late energy release. The barrier heights, though, are different on the two surfaces. As a whole, from the topological features of these potential energy surfaces, it can be surmised that the OH + Cl production, can be affected by the excited surfaces. Also, at collision energies higher than 0.6 eV, the $1^1A''$ will play an important role in ClO production. However, the absence of wells on the excited states would imply that the mechansim on the excited states are expected to be less of the statistical-type and more of the state-selected variety.

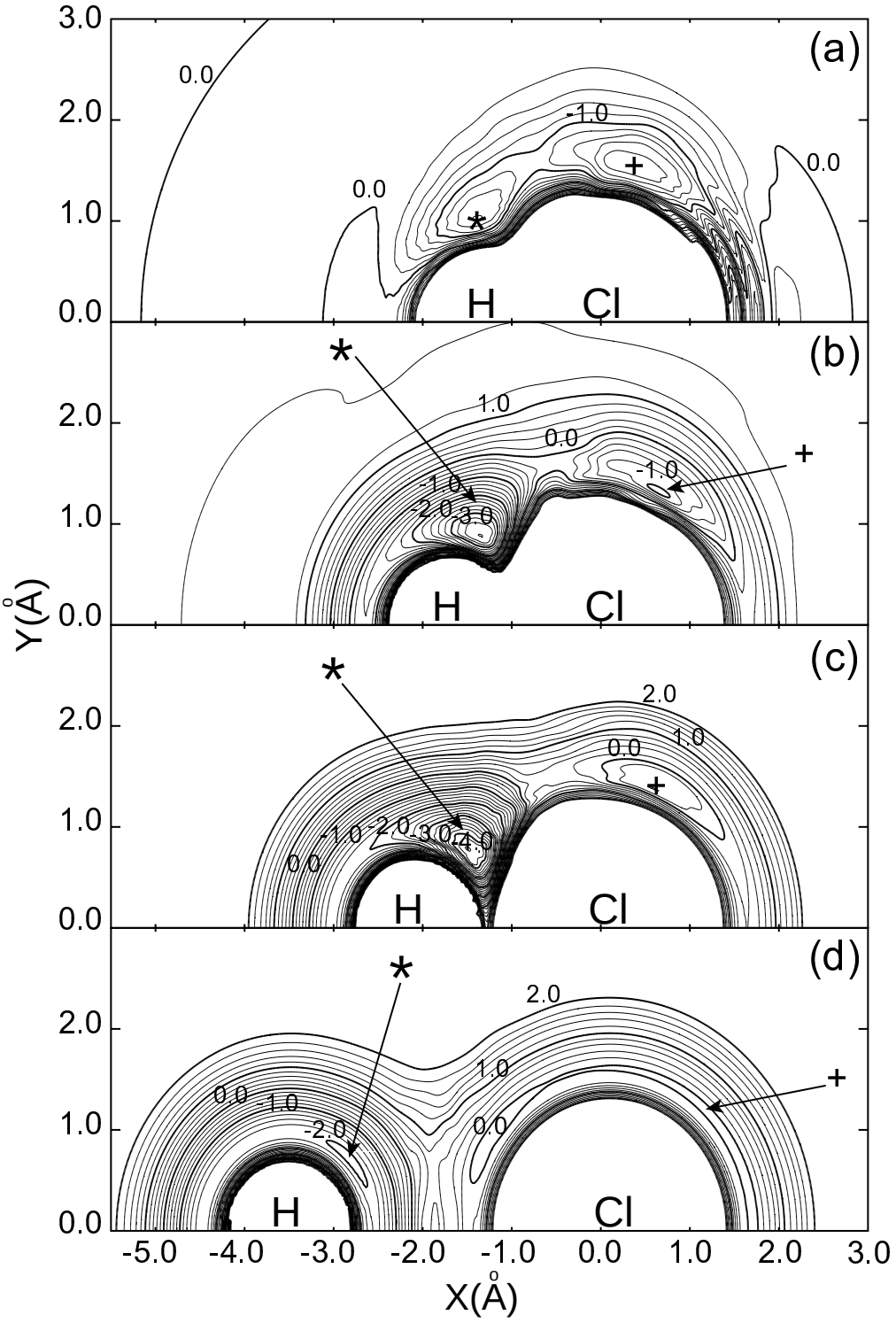

Figure 4.2: Contour plots of the $1^1A'$ electonic state for H-Cl distance (a) r = 1.3 Å (b) r = 1.7 Å, (c) 2.1 Å and (d) r = 3.6 Å. Contours are drawn in steps of 0.2 eV. [Reproduced with the kind permission of Dr. Shinkoh Nanbu]

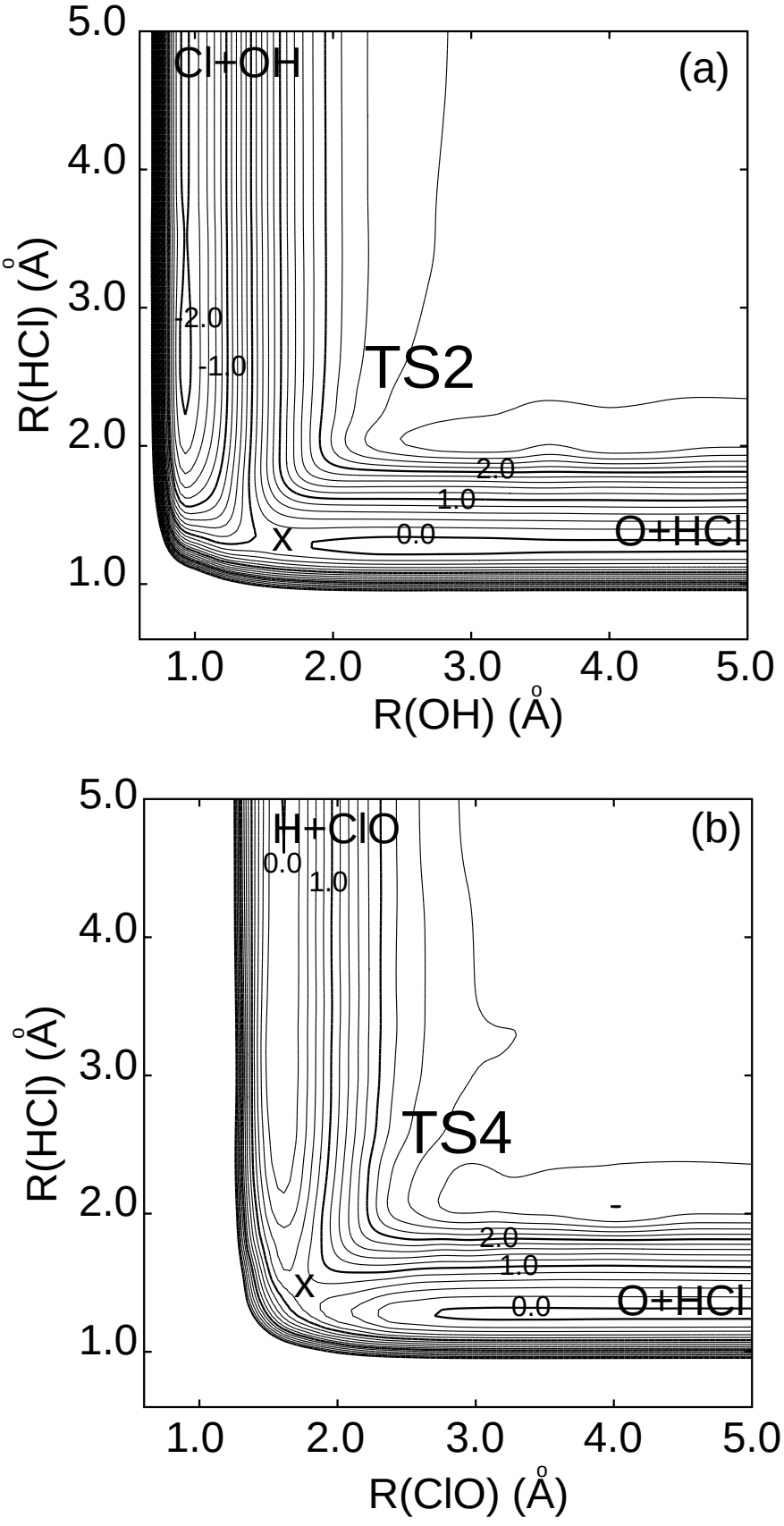

Figure 4.3: Contour plots of the $1^1A''$ electonic state around two transition states (a) the potential around TS2 at angle(OHCl)=130°; (b) the potential around TS4 in the linear geometry. Contours are drawn in steps of 0.2 eV. [Reproduced with the kind permission of Dr. Shinkoh Nanbu]

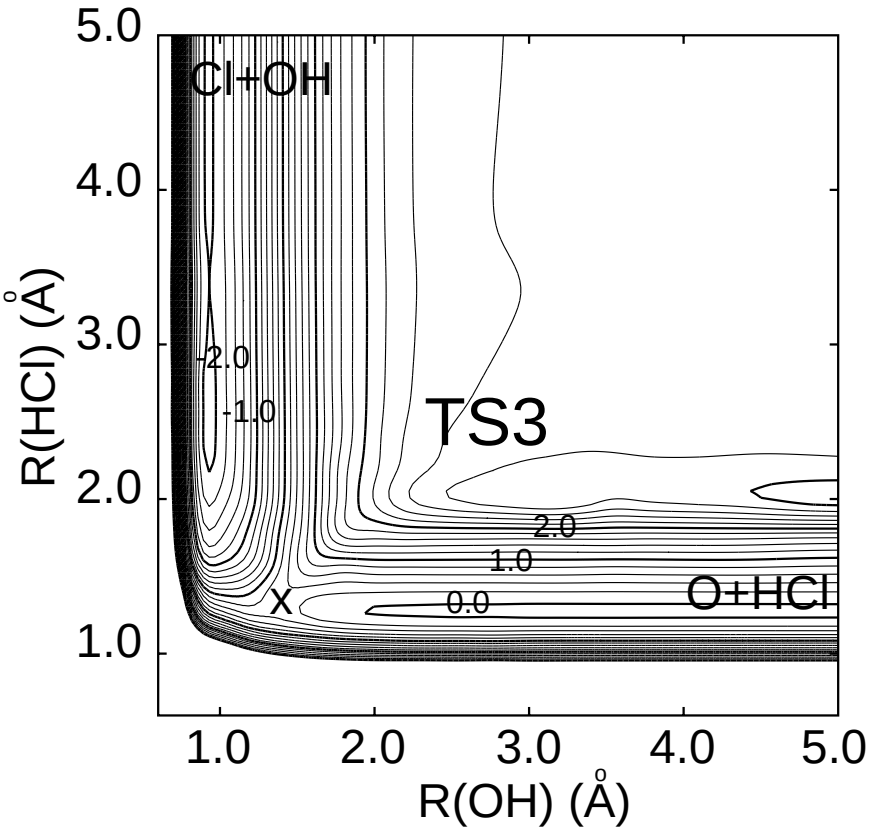

Figure 4.4: Contour plots of the $2^1A'$ electonic state around the TS3 transition state in the linear geometry. Contours are drawn in steps of 0.2 eV. [Reproduced with the kind permission of Dr. Shinkoh Nanbu]

4.3 OTHER EXPERIMENTAL AND THEORETICAL RESULTS

4.3.1 Brief Summary of Experimental Results

At 12.2 kcal/mol collision energy, Balucani, et al carried out an angular distribution measurement of the ClO product from the O(^{1}D) + HCl reaction using a crossed-molecular beam study. Their measurement yielded a backward-forward symmetric scattering, with slight favoring of the backward scattering. Also, they reported a branching ratio $\frac{\sigma_{ClO}}{\sigma_{OH}}$ of 0.34. This particular experiment is of interest to us because QCT calculations have been performed at the same collision energy. Also, the group of Toshinori Suzuki in RIKEN, Japan has measured the OH product angular distribution at a collision energy of 0.26 eV at which we have also carried out another QCT calculation. The RIKEN group have kindly provided us with the measurement of the OH product differential cross section as well as its internal energy distribution.

4.3.2 Brief Summary of two Quasiclassical Calculations (QCT) and Quantum Mechanical Calculations for $J = 0$

There are some previous calculations, relevant to this chapter, which have been carried out for the O(^{1}D) + HCl system using different potential surfaces[16, 17, 24]. These three works employed the quasiclassical trajectory approach as is done in this chapter. However the results of Schinke has a clear discrepancy compared to the other two because of the endoergicity of the potential surface which clearly contradicts the exoergicity predicted by experiment. Also, since the work of Schinke is not carried out at either of the collision energies of interest in this chapter, the results are not shown here. Some properties of the different PESs used for the different QCT studies is shown in Table. 4.1

Table 4.1: Comparison between energetics reported from on the $1^1A'$ PES for the O + HCl sytem. Values are in eV

	R ef .[14]	Ref. [16]	Ref. [17]
Transition State above the HOCl minimum	3.28	3.21	3.98
Difference between HOCl and HClO minima	2.44	2.34	2.65

These two QCT calculations were carried out only on the $1^1A'$ PES. The cross sections and branching ratio obtained from the other two workers are shown in Table. 4.2. Kamisaka et al, using the PES reported in Ref.[14], however, have carried out a J=0 quan-

Table 4.2: Quasiclassical reactive cross Sections for O + HCl at (ν=0,j=0) initial state, E_{col} = 0.529 eV

	$\sigma_{ClO}(a_0^2)$	$\sigma_{OH}(a_0^2)$	σ_{ClO}:σ_{OH}
Christoffel et al Ref.[16]	2.34	45.06	0.0519
Martinez et al Ref.[17]	14.36	50.06	0.288

tum calculation on the $1^1A'$ surface as well as on the newly-obtained $1^1A''$ and $2^1A'$ surfaces. The quantum results for the three different surfaces are shown in Figs. 4.5, 4.6 and 4.7. One immediately striking observation from Fig. 4.6 is the sharp rise of the ClO products at higher energies at the point marked with the arrow B. Further discussion of the possible effects on the overall branching ratio is continued below.

4.4 METHOD OF CALCULATIONS

The quasiclassical method has been used to determine the DCS and other probability distribution functions on the $1^1A'$ ground potential surface [13, 16, 17]. I provide below the relevant formulation of the problem including the sampling of the initial conditions. This is done to make this chapter wholly self-contained and also because in chapter 2, a reference was made to this chapter as containing the full details of the quasiclassical techniques used throughout the extent of this thesis. The objective is to study an A + BC-type collision using a Monte-Carlo sampling to generate initial conditions for trajectories with specified initial quantized rotational and vibrational energies and fixed initial translational energy. These trajectories are propagated by integrating the equations of motion using any stable and efficient numerical recipe and at the end of reaction, one calculates the relevant probability distribution function from the bunch of such trajectories. It is conventional to work in terms of a generalized space-fixed coordinate of nine dimensions, which for the O + HCl system, can be written as $\mathbf{x} \equiv \{x_i; i = 1, \ldots, 3$ for O $, i = 4, \ldots, 6$ for H and $i = 7, \ldots 9$ for Cl.$\}$ with corresponding conjugate momenta, $\mathbf{p_x} \equiv \{p_{x_i}; i = 1, \ldots, 9\}$. The Hamiltonian is written in the form,

$$H(\mathbf{x}, \mathbf{p_x}) = T(\mathbf{p_x}) + V(x_i, i = 1, \ldots, 9), \tag{4.2}$$

where

$$T(\mathbf{p_x}) = \sum_{i=1}^{3}\Big(\frac{1}{2m_A}p_{x_i}^2 + \frac{1}{2m_B}p_{x_{i+3}}^2 + \frac{1}{2m_B}p_{x_{i+6}}^2\Big). \tag{4.3}$$

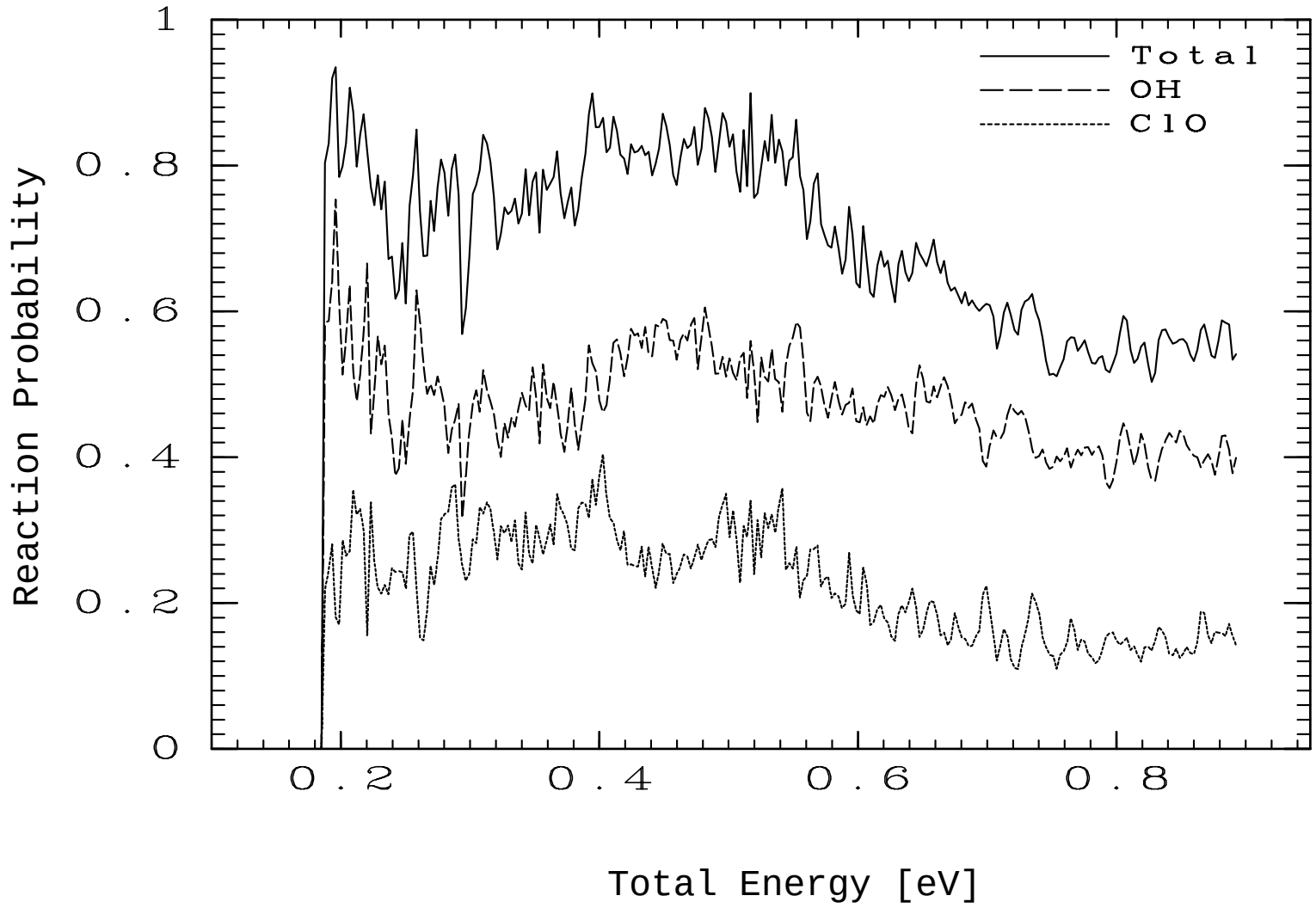

Figure 4.5: Quantum Mechanical reaction probabilities for the $O(^1D)$ + HCl(ν=0, j=0) reaction for J(total angular momentum) = 0 on the $1^1A'$ surface [Reproduced with the kind permission of Dr. Shinkoh Nanbu]

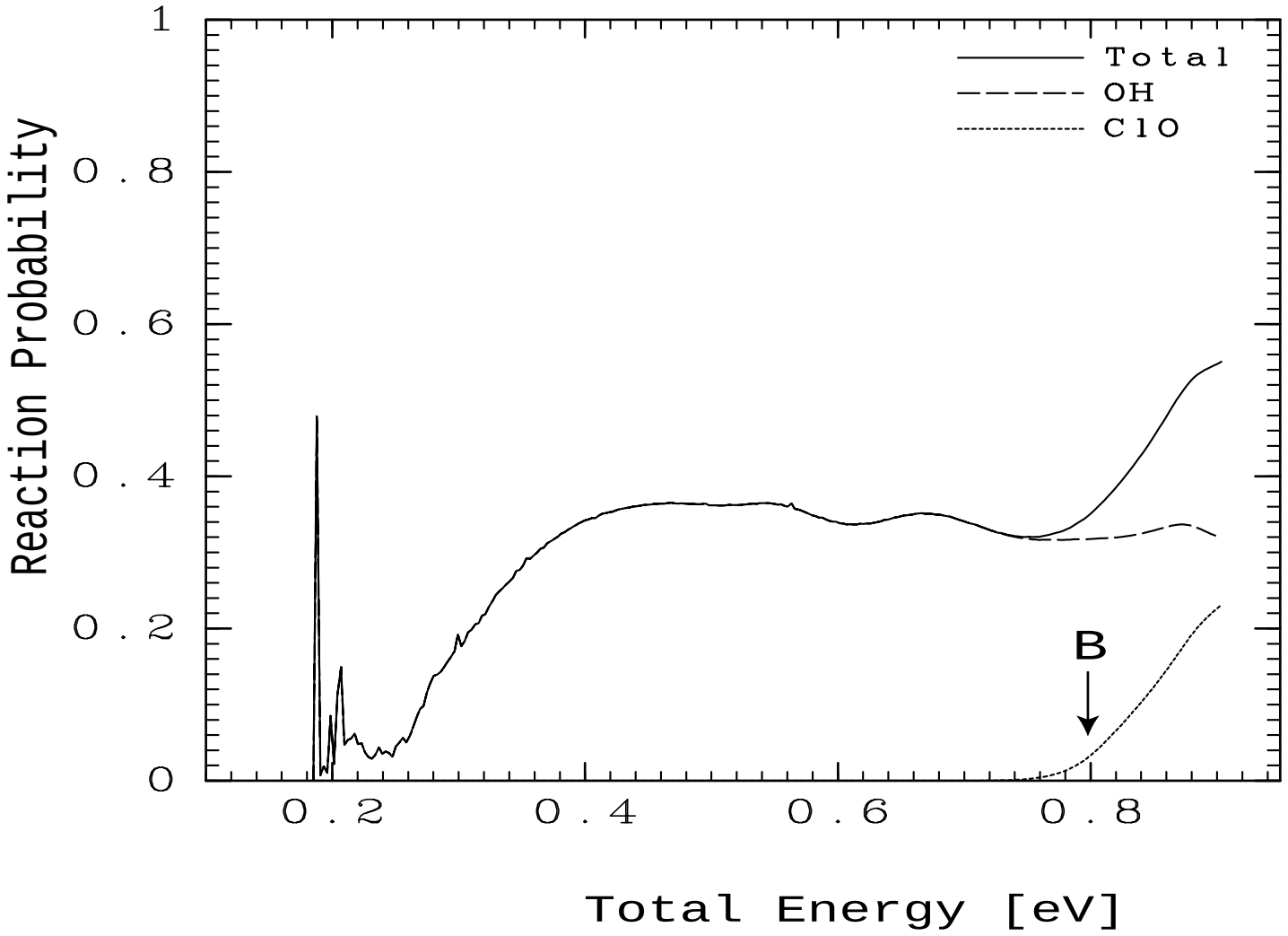

Figure 4.6: Quantum Mechanical reaction probabilities for the $O(^1D)$ + HCl(ν=0, j=0) reaction for J(total angular momentum) = 0 on the $1^1A''$ surface [Reproduced with the kind permission of Dr. Shinkoh Nanbu]

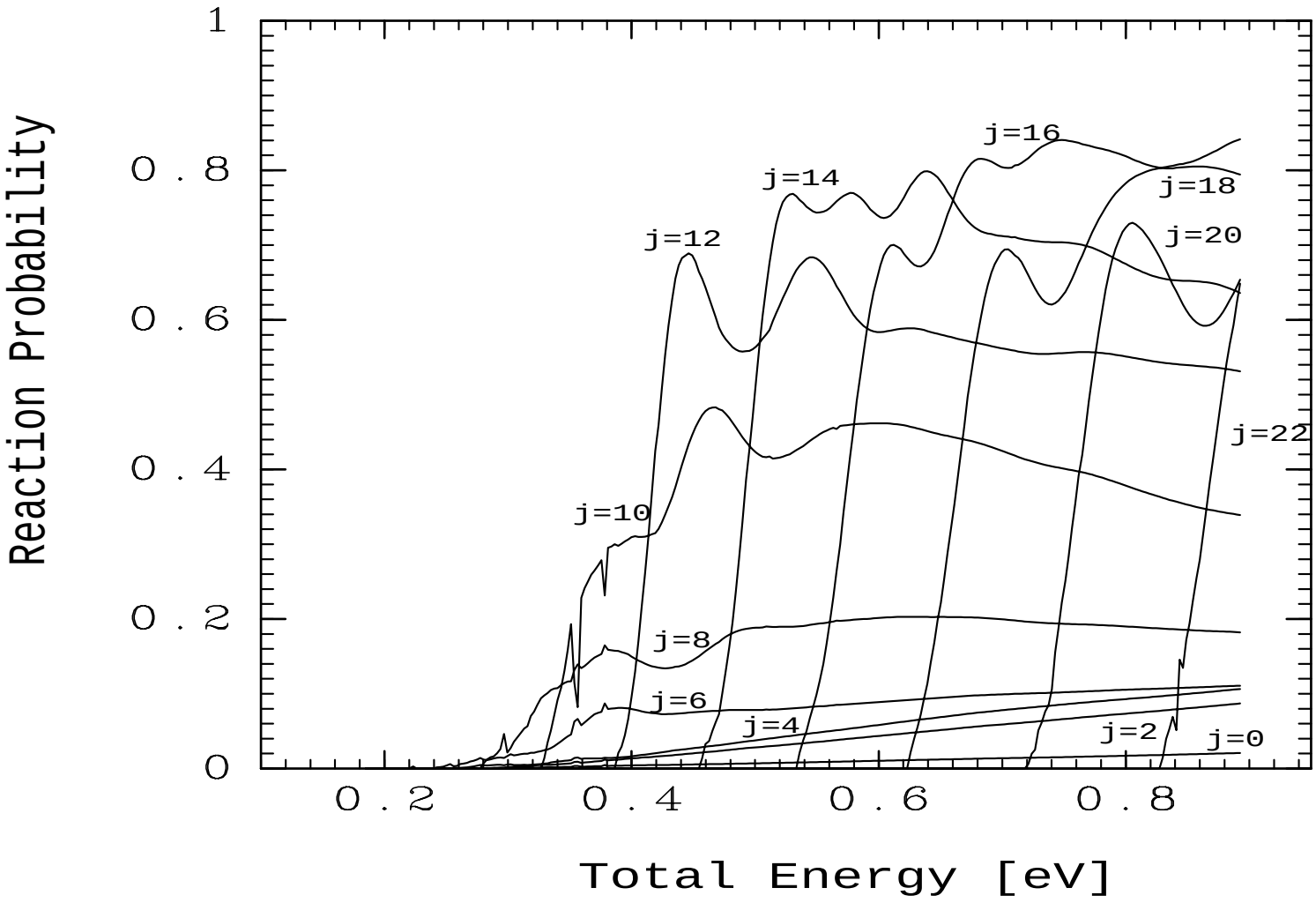

Figure 4.7: Quantum Mechanical reaction probabilities for the $O(^1D)$ + HCl(ν=0, j=0) reaction for J(total angular momentum) = 0 on the $2^1A'$ surface [Reproduced with the kind permission of Dr. Shinkoh Nanbu]

In this representation, Hamilton's equations of motion are,

$$\dot{x}_i = \frac{\partial H}{\partial p_{x_i}} = \frac{\partial T}{\partial p_{x_i}} (i = 1, \ldots, 9) \tag{4.4}$$

$$\dot{p}_{x_i} = -\frac{\partial H}{\partial x_i} = -\frac{\partial V}{\partial x_i} \tag{4.5}$$

It is conventional to employ a generalized coordinate system made up of

$$\begin{aligned} q_i &= x_{i+6} - x_{i+3} \\ Q_i &= x_i - \frac{1}{m_H + m_C l}[m_H x_{i+3} + m_{Cl} x_{i+6}] \\ S_i &= \frac{1}{M}[m_O x_i + m_H x_{i+3} + m_{Cl} x_{i+6}] \end{aligned} \tag{4.6}$$

where $M = m_O + m_H + m_{Cl}$ and q, Q and S are the internal, relative and the center of mass coordinates respectively and together are called the Jacobi coordinates.

Eqs. 4.4 and 4.5 together give a total of 18 coupled first-order differential equations which could be reduced to 12 equations using the variables of Eq. 4.6 and the arguments that the center of mass of the system, S_i is cyclic. Using the F_2 generating function[18],

$$F_2(p, P, P_S, \mathbf{x}) = \sum_{i=1}^{3} [p_i x_i + P_i x_{i+3} + P_{S_i} x_{i+6}] \tag{4.7}$$

and the relation $p_{x_i} = \frac{\partial F_2}{\partial x_i}$, the Hamiltonian, in terms of the generalized coordinates, becomes

$$H = T(\mathbf{p}, \mathbf{P}, \mathbf{P_S}) + V[R_1(\mathbf{q}, \mathbf{Q}), R_2(\mathbf{q}, \mathbf{Q}), R_3(\mathbf{q}, \mathbf{Q})], \tag{4.8}$$

where

$$T(p, P, P_s) = \sum_{i=1}^{3} \Big(\frac{1}{2\mu_H Cl} p_i^2 + \frac{1}{2\mu_{O,HCl}} P_i^2 + \frac{1}{2M} P_{S_i}^2 \Big),$$

$$\mu_{HCl} = \frac{m_H m_{Cl}}{(m_H + m_{Cl})} \qquad \text{(reduced mass of internal motion)}$$

and

$$\mu_{O,HCl} = \frac{m_O (m_H + m_{Cl})}{M} \qquad \text{(reduced mass of relative motion).}$$

In the generalized coordinate system, the 1^{st}-order Hamilton's equations are

$$
\begin{aligned}
\dot{q}_i &= \frac{\partial H}{\partial p_i} = \frac{\partial T}{\partial p_i} (i = 1, 2, 3), \\
\dot{Q}_i &= \frac{\partial H}{\partial P_i} = \frac{\partial T}{\partial P_i} (i = 1, 2, 3), \\
\dot{p}_i &= -\frac{\partial H}{\partial q_i} = -\frac{\partial V}{\partial q_i} = -\sum_{k=1}^{3} \frac{\partial V}{\partial R_k} \frac{\partial R_k}{\partial q_i}, \\
\dot{P}_i &= -\frac{\partial H}{\partial Q_i} = -\frac{\partial V}{\partial Q_i} = -\sum_{k=1}^{3} \frac{\partial V}{\partial R_k} \frac{\partial R_k}{\partial Q_i},
\end{aligned}
\tag{4.9}
$$

and the $\frac{\partial R_k}{\partial Q_i}$ and $\frac{\partial R_k}{\partial q_i}$ terms are evaluated from

$$
\begin{aligned}
R_{OH} &= \left[\sum_{i=1}^{3} \left(\frac{m_{Cl}}{m_H + m_{Cl}} q_i + Q_i \right)^2 \right]^{\frac{1}{2}}, \\
R_{HCl} &= \left[\sum_{i=1}^{3} q_i^2 \right]^{\frac{1}{2}}, and \\
R_{ClO} &= \left[\sum_{i=1}^{3} \left(\frac{m_H}{m_H + m_{Cl}} q_i - Q_i \right)^2 \right]^{\frac{1}{2}},
\end{aligned}
\tag{4.10}
$$

where R_{OH}, R_{HCl} and R_{ClO} being the distances between the atoms in the subscript.

The initial conditions sampled are:
b : impact parameter (the z component of the initial relative coordinate i.e., $Q^0_{e_z}$)
θ : initial azimuthal orientation angle of the HCl internuclear axis(angle between **q** and the +z axis)
φ : initial polar orientation angle of the internuclear HCl axis(angle between the projection of q onto the xy plane and the +x axis)
η : initial orientation angle of the HCl angular momentum(the angle between $\mathbf{q} \times \mathbf{p}$ and some reference vector normal to the HCl internuclear axis)
ξ : initial phase angle of the HCl vibration(defined to be zero and π at the inner and outer turning points respectively and varies linearly with time)

If R^0 is taken as the initial separation between O and the center of mass of HCl, then the initial conditions for the relative motion are,

$$
\begin{aligned}
Q^0_{e_x} &= 0 \\
Q^0_{e_y} &= b \\
Q^0_{e_z} &= -R^0
\end{aligned}
\tag{4.11}
$$

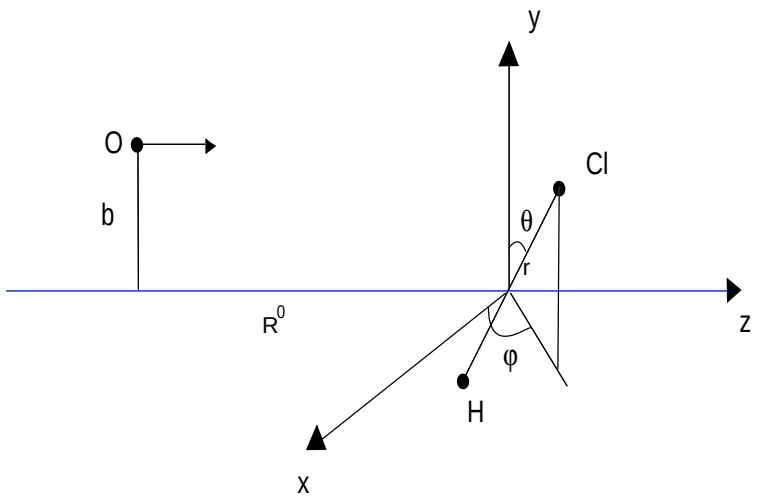

Figure 4.8: Specification of an initial coordinate system for a of an O + HCl reaction in the impact parameter picture.

$$\begin{aligned} P^0_{e_x} &= 0 \\ P^0_{e_y} &= 0 \\ P^0_{e_z} &= (2\mu_{O,HCl}E_{col})^{\frac{1}{2}} \qquad \text{(E_{col} is the initial collision energy),} \end{aligned}$$

while for the diatomic, letting $r \equiv |\mathbf{q}|$, and r^0 be the initial internuclear separation gives,

$$\begin{aligned} q^0_{e_x} &= r^0 \sin\theta\cos\phi, \\ q^0_{e_y} &= r^0 \sin\theta\sin\phi, \\ q^0_{e_z} &= r^0 \cos\theta. \end{aligned} \tag{4.12}$$

R^0 is chosen so large that interaction potential essentially vanishes while r^0 is placed at the inner turning point so that initial radial momentum of the diatomic is zero implying that all the initial momentum of the diatomic is angular momentum. In the figure below, the e_z vector defines the direction of approach of the O atom towards the HCl diatomic

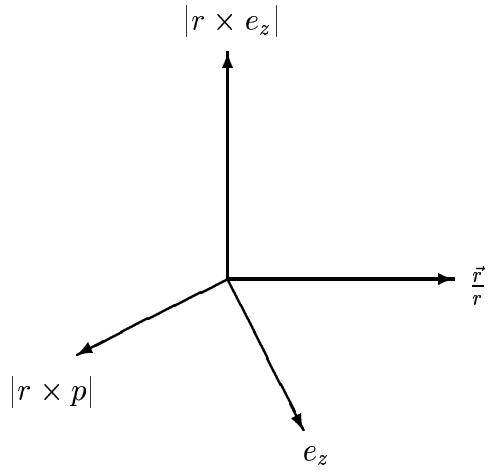

Figure 4.9: Initial orientation of the angular momentum vector.

and η defines the angle between the angular momentum vector $|r \times p|$, and a reference vector $|r \times e_z|$, normal to the BC internuclear axis. Solving for the components of p, one obtains

$$\begin{aligned} p^0_{e_x} &= J_r \frac{(\sin\varphi\cos\eta - \cos\theta\cos\varphi\sin\eta)}{r_-} \\ p^0_{e_y} &= -J_r \frac{(\cos\varphi\cos\eta + \cos\theta\sin\varphi\sin\eta)}{r_-} \\ p^0_{e_z} &= J_r \frac{(\sin\varphi\sin\eta)}{r_-} \end{aligned} \tag{4.13}$$

where J_r is taken to be the magnitude of the angular momentum of the diatomic and r_- is the inner turning point of the initial rovibrational level.

Choosing initial conditions as done above is equivalent to selecting points in collision parameter space in order to evaluate a multidimensional integral. For example, the reaction cross section σ_r, written in terms of the maximum impact parameter of collision, b_{max} is,

$$\sigma_r = \pi b^2_{max} < P_r(E_{col}, \nu, j) >, \tag{4.14}$$

where

$$\begin{aligned} < P_r(E_{col,\nu,j}) > = & \frac{1}{(2\pi)^3 b^2_{max}} \\ & \times \int_{b=0}^{b=b_{max}} \int_{\theta=0}^{\pi} \int_{\varphi=0}^{2\pi} \int_{\eta=0}^{2\pi} \int_{\xi=0}^{2\pi} P_r(b, \theta, \varphi, \eta, \xi; E_{col}, \nu, j) b \\ & \times \sin\theta db d\theta d\varphi d\eta d\xi. \end{aligned} \tag{4.15}$$

In the integral above, ν and j are the vibrational and rotational states respectively, and all the other parameters are as defined above. If the thermal rate constant is to be determined

as done in Sec. 2.4 of this thesis, then the expression need only be averaged over the collision energy to yield,

$$\begin{aligned} k_r(T) &= < v_{col}\sigma_r(E_{col,\nu,j}) >_T \\ &= \left(\frac{8kT}{\pi\mu_{A,BC}}\right)^{1/2}\pi b_{max}^2 \\ &\times \int_{E_{col}=0}^{\infty}\int_{b=0}^{b=b_{max}}\int_{\theta=0}^{\pi}\int_{\varphi=0}^{2\pi}\int_{\eta=0}^{2\pi}\int_{\xi=0}^{2\pi} P_r(b,\theta,\varphi,\eta,\xi;E_{col},\nu,j)b \\ &\times E_{col}\exp^{-\frac{E_{col}}{kT}}\sin\theta dE_{col}dbd\theta d\varphi d\eta d\xi, \end{aligned} \tag{4.16}$$

where k in the equation above is the Boltzmann constant. The Monte-Carlo approach is commonly employed in quasiclassical simulations to solve the integral in Eq. 4.15. This involves expressing the integral in terms of a probability integral and writing the parameters of the integral in terms of independent coordinates with well-defined distribution within a given interval. These coordinate transformations imply that the intergral can be rewritten as ,

$$< P_r(E_{col,\nu,j}) >= \int_0^1\int_0^1\ldots\int_0^1 f(\beta)d\beta, \tag{4.17}$$

where

$$\begin{aligned} \beta_1 &= \left(\frac{b}{b_{max}}\right)^2, \\ \beta_2 &= \frac{1}{2}(1-\cos\theta), \\ \beta_3 &= \frac{1}{2\pi}\varphi, \\ \beta_4 &= \frac{1}{2\pi}\eta, \\ and & \\ \beta_5 &= \frac{1}{2\pi}\xi. \end{aligned} \tag{4.18}$$

In actual computations, the procedures for selecting appropriate values of the collision parameters are to

1. Select a set of five random numbers $\beta_1, \beta_2, \ldots, \beta_5$ uniformly distributed in the interval (0,1), and

2. Obtain corresponding values of collision parameter by inverting the set of equations

above. This gives

$$\begin{aligned} b &= \beta_1^{1/2} b_{max}, \\ \theta &= cos^{-1}(1-2\beta_2), \\ \varphi &= 2\pi\beta_3, \\ \eta &= 2\pi\beta_4, \\ \xi &= 2\pi\beta_5. \end{aligned} \tag{4.19}$$

These values are then used to compose the initial condition of the trajectory to be propagated. After termination of trajectory propagation at a separation distance between the diatomic and the third body, where the interaction potential is almost non-existent, the probability distribution of interest can be obtained by manipulating the relevant data obtained from the final conditions of the reaction.

4.4.1 Differential Cross Section(DCS)

From N total trajectories, the value of $< P_r >$ of Eq. 4.14 is estimated to be

$$< P_r >= \frac{1}{N} \sum_{i=1}^{N_r} w_i = \frac{N_r(\nu, J, E_{col})}{N(\nu, J, E_{col})} \tag{4.20}$$

w_i is statistical weight of i^{th} trajectory and N_r is the number of reactive trajectory.

The distribution over different reaction/product variables can be used to provide useful information about the system of interest. Histogrammic representation over these variables consistent with σ_r provides a good choice. For a $f(x)$ vs x distribution, where $f(x)$ is related to σ_r via a weighting function, $g(x)$, one writes[23],

$$\sigma_r = \int_{x_{min}}^{x_{max}} f(x)g(x)dx \equiv \int_{G(x_{min})}^{G(x_{max})} f(x)dG \tag{4.21}$$

Dividing the intervals $[x_{min}, x_{max}]$ into n segments,

$$\begin{aligned} \sigma_r &= \sum_k^n \sigma_{rk} \\ &= \sum_k^n \int_k f\, dG = \sum_k^n f_k \int_k dG \\ &= \sum_k^n f_k \Delta G_k. \end{aligned} \tag{4.22}$$

In a QCT calculation, each trajectory may be identified with one of the Δx_k intervals, and

on grouping yields

$$\sigma_r = \sum_k \sigma_{rk} = \sum_k \sigma_r^0(\frac{A_k}{N}) \tag{4.23}$$

with

$$\left(\frac{A_k}{N}\right) = \frac{1}{N}\sum_i^{N_k} P_{ri} w_i = \frac{1}{N}\sum_i^{N_{rk}} w_i = \frac{N_{rk}}{N}, \tag{4.24}$$

where the latter summation is only over the (N_{rk}) reactive trajectories of the kth interval. The final expression is obtained by equating

$$\sigma_{rk} = f_k \Delta G_k = \sigma_r^0(\frac{A_k}{N}) \tag{4.25}$$

or

$$f_k = \frac{\sigma_r^0}{N\Delta G_k} A_k \tag{4.26}$$

The DCS with reference to the scattering angle is finally given by

$$\left(\frac{d\sigma_r}{d\theta'}\right)_k = \frac{\sigma_r^0}{2\pi\Delta\theta_k'}\frac{N_{rk}}{N} \tag{4.27}$$

where θ' is the final scattering angle and is obtained from the expression

$$\theta' = -\frac{P'_{e_z}}{\sqrt{P'^2_{e_x} + P'^2_{e_y} + P'^2_{e_z}}}. \tag{4.28}$$

All primed quantities denote the final conditions of the trajectory. Eq. 4.27 is the operational equation used to obtain the DCS results presented in this chapter.

4.4.2 Opacity Function

The integral in Eq. 4.15 as well as the probability of Eq. 4.20 both involve averaging over the entire parameters which define the collision. However, an important quantity– the opacity function which yields very important information– can be obtained if the averaging is not carried out over the impact parameter, b. The analogue of Eq. 4.20 for the opacity function is

$$P(\nu, j, E_{col}, b, db) = \frac{N_r(\nu, j, E_{col}, b, db)}{N(\nu, j, E_{col}, b, db)}, \tag{4.29}$$

where $N_r(\nu, j, E_{col}, b)$ being the number of reactive collisions at energy, E_{col} occuring at

impact parameters between b and b+db with molecule initially in the (ν,j) state.

The impact parameters of the population of the trajectories leading into a specific channels are paritioned into grids and are used to compose the opacity function of the respective reaction processes.

4.4.3 Internal Distribution of Products

The internal energy distribution of the products is composed from the sum of the internal energy of the product diatomic. This internal energy ϵ', is written as,

$$\epsilon' = \frac{1}{2\mu_{diatomic}} \sum_{i=1}^{3} p_i'^2 + V_D(r) \tag{4.30}$$

The p_i' are the components of momenta of the final diatomic and the $V_D(r)$ is the potential energy, which is equal to the potential energy of the whole system if the outgoing third-body is far enough from the diatomic that that all possibilities of interaction is eliminated.

4.5 COMPARISON WITH OTHER RESULTS: EXPERIMENTAL AND COMPUTATIONAL RESULTS

4.5.1 At Collision Energy of 0.529eV

QCT calculations were carried out for the O + HCl at the initial rovibrational state of (ν=0, j=0) system at a collision energy of 0.529 eV. This is the same energy at which the group of Balucani et al in Perugia, Italy have carried out experimental measurements [8] and also at which previous QCT studies have been done by Bowman and coworkers[16] and Martinez and coworkers[17]. The 3 QCT studies, including the present, have been carried out on different PES, although the PES used here is closer to that of Peterson et al as mentioned earlier in section 4.2. The data available for comparison between the three studies are the DCS and the branching ratio $\frac{\sigma_{ClO}}{\sigma_{OH}}$. The DCS for the two product channels from the present calculations are shown in Figs. 4.10 and 4.11 for the OH and ClO product channels respectively. The DCS for the OH product has similar qualitative features with that of Ref. [17] with both results showing a predominantly forward-backward scattering preference with strong dominance in the forward hemisphere. However, the ratio between the yields of the forward and backward hemispheres is different, being about 2.5 times for the present result while it is about 5 in Ref. [17]. Balucani et al did not publish experimental data for this channel.

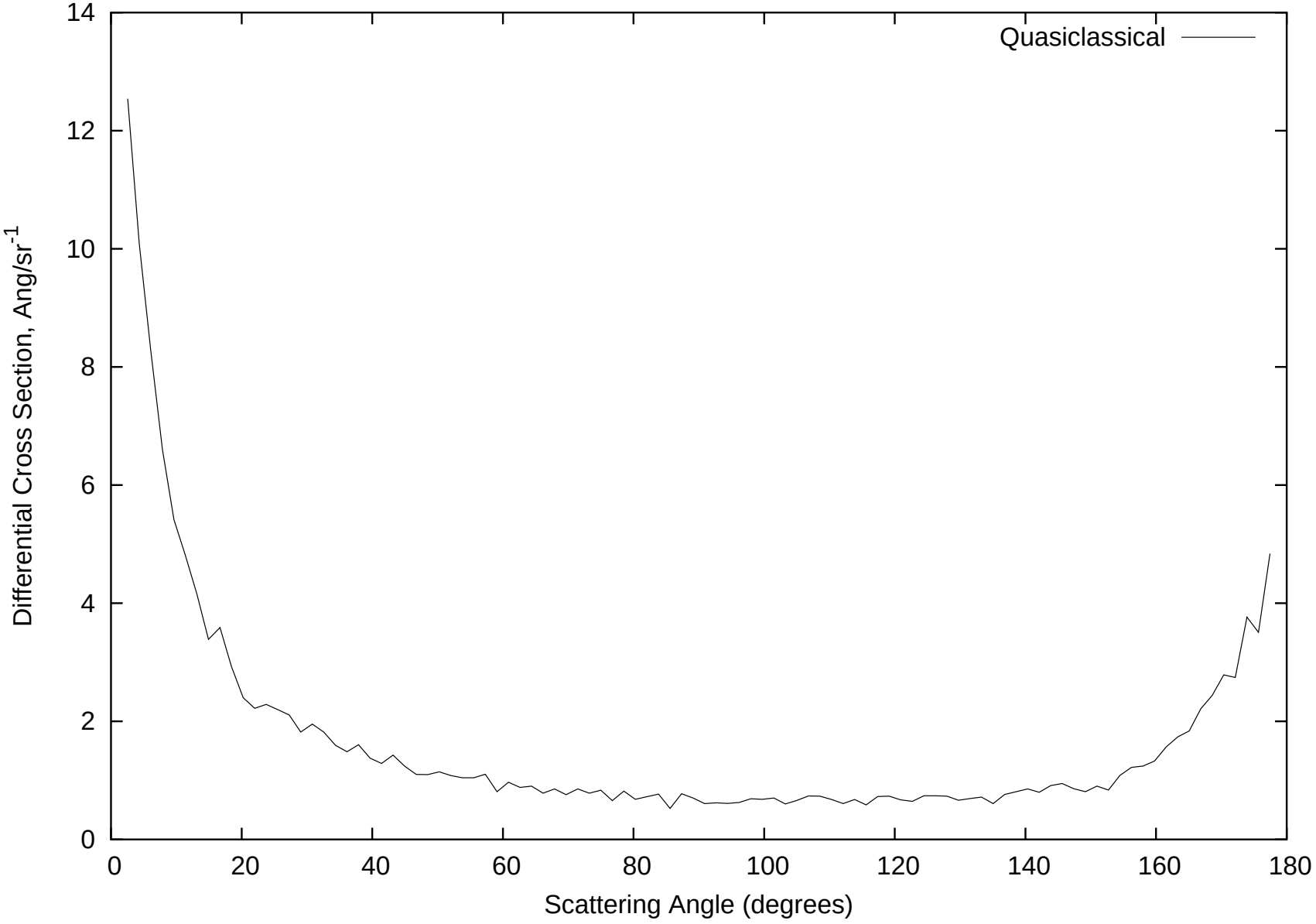

Figure 4.10: Differential Cross Section for OH + Cl product channel on the $1^1A'$ surface at Collision Energy 0.529eV

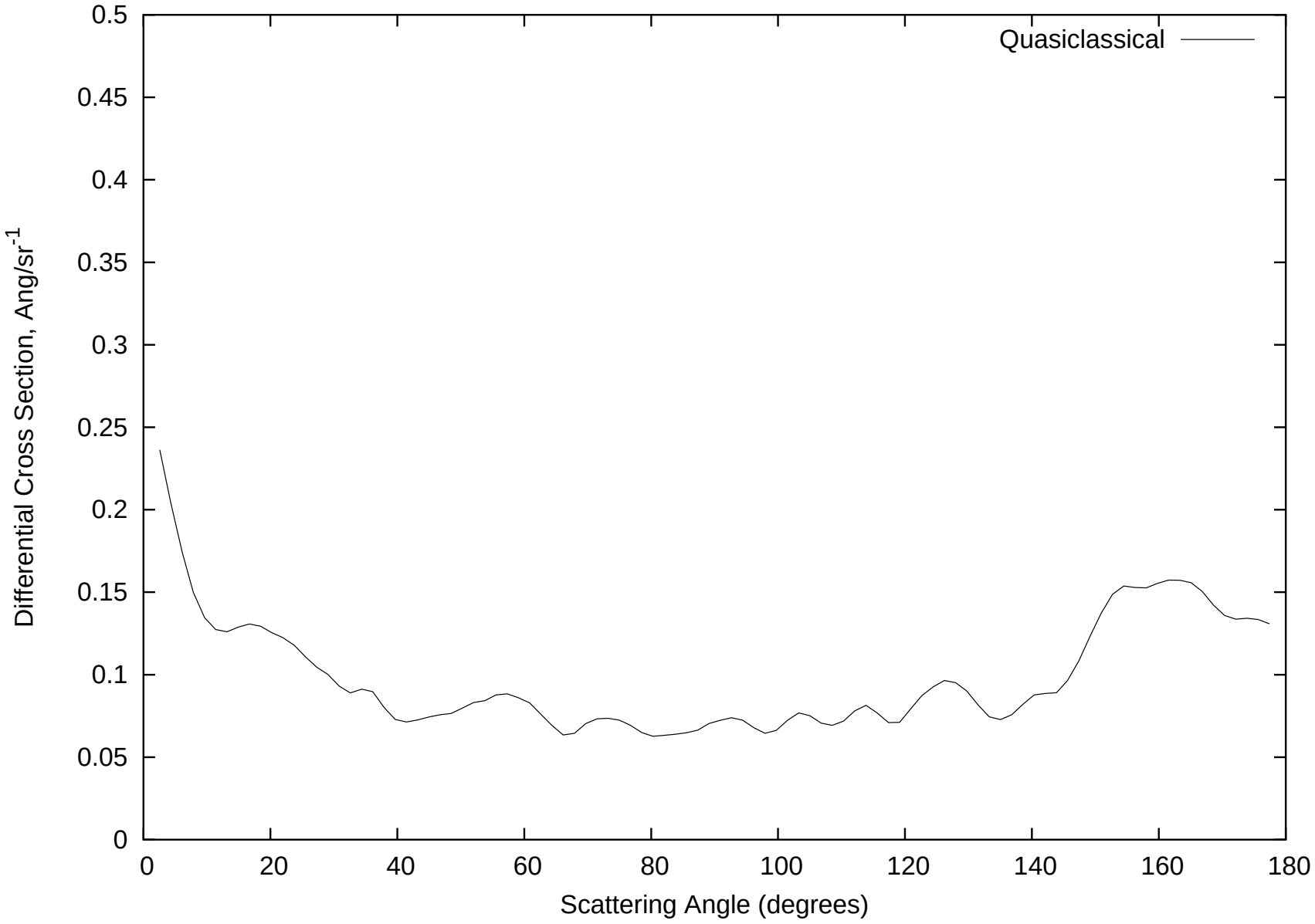

Figure 4.11: Differential Cross Section for ClO + H product channel on the $1^1A'$ surface at Collision Energy 0.529eV

In case of ClO product, the experimental DCS for the ClO product channel was measured[8] displaying a near backward-forward symmetry with a slight preference for the backward hemisphere. The present result, like that of Martinez et al is also nearly backward-forward symmetric but unlike in the experimental result, both QCT results display a bit of preference for the forward hemisphere. The values of DCS are also different, with the peak of Martinez et al being about $0.7\mathring{A}^2 sr^{-1}$ while the present calculation gives a peak of about $0.25\mathring{A}^2 sr^{-1}$. The experimental peak is at about 0.42 $\mathring{A}^2 sr^{-1}$. The final reaction probability for the present calculation on the $1^1A'$ surface for OH production, p_{OH} is 0.452 and p_{ClO} is 0.032. This gives a branching ratio of 0.071 compared with 0.052 for Bowman et al and 0.288 for Martinez et al while the experiment of Balucani et al gives a value of 0.34. The differences among the QCT results may basically be ascribed to the differences in the PES topography. However, in terms of comparison with experiment, the uncertainty in the distribution of the collision energy $\frac{\Delta E_{col}}{E_{col}}$, which may be as high as $\pm 30\%$, may contribute to an inadvertent overmeasurement of ClO. This is explained further with supporting figures in the section discussing the effect of excited states.

4.5.2 At Collision Energy of 0.26eV

At a collision energy of 0.26 eV, QCT calculations were similarly carried out for the O + HCl at the same initial rovibrational state, (ν=0, j=0) as was done for 0.529 eV. This enables a comparison with the experimental results obtained by the group of Toshinori Suzuki at RIKEN, Japan[27][1]. H. Koguchi and T. Suzuki measured two physical quantities, (1) the DCS of the OH product channel and (2) the distribution of the internal energy of the OH product. Fig. 4.12 shows very good agreement between the quasiclassical results and the experimental DCS . Fig. 4.13 shows comparison between experimental and theoretical distribution obtained for the internal energy distribution of the OH diatomic.[The QCT internal energy distribution was arbitrarily normalized to enable comparison with experiment]. The internal energy distribution from QCT is equally good, showing a peak-shift of less than 2000 cm^{-1} compared to experiment. Due to some experimental constraints, measurements have not been made for the ClO product channel and comparisons are thus not possible. However, results for ClO production obtained from the present QCT are shown in Figs. 4.14 for the DCS. It is seen from the internal energy distribution for the ClO displayed in Fig. 4.15 that the ClO is produced with a relatively narrow range of energy distribution, specifically within about 4000 cm^{-1}. The plots of the opacity function P(b)

[1]I am grateful to Drs. Koguchi and Suzuki for providing me with their unpublished results

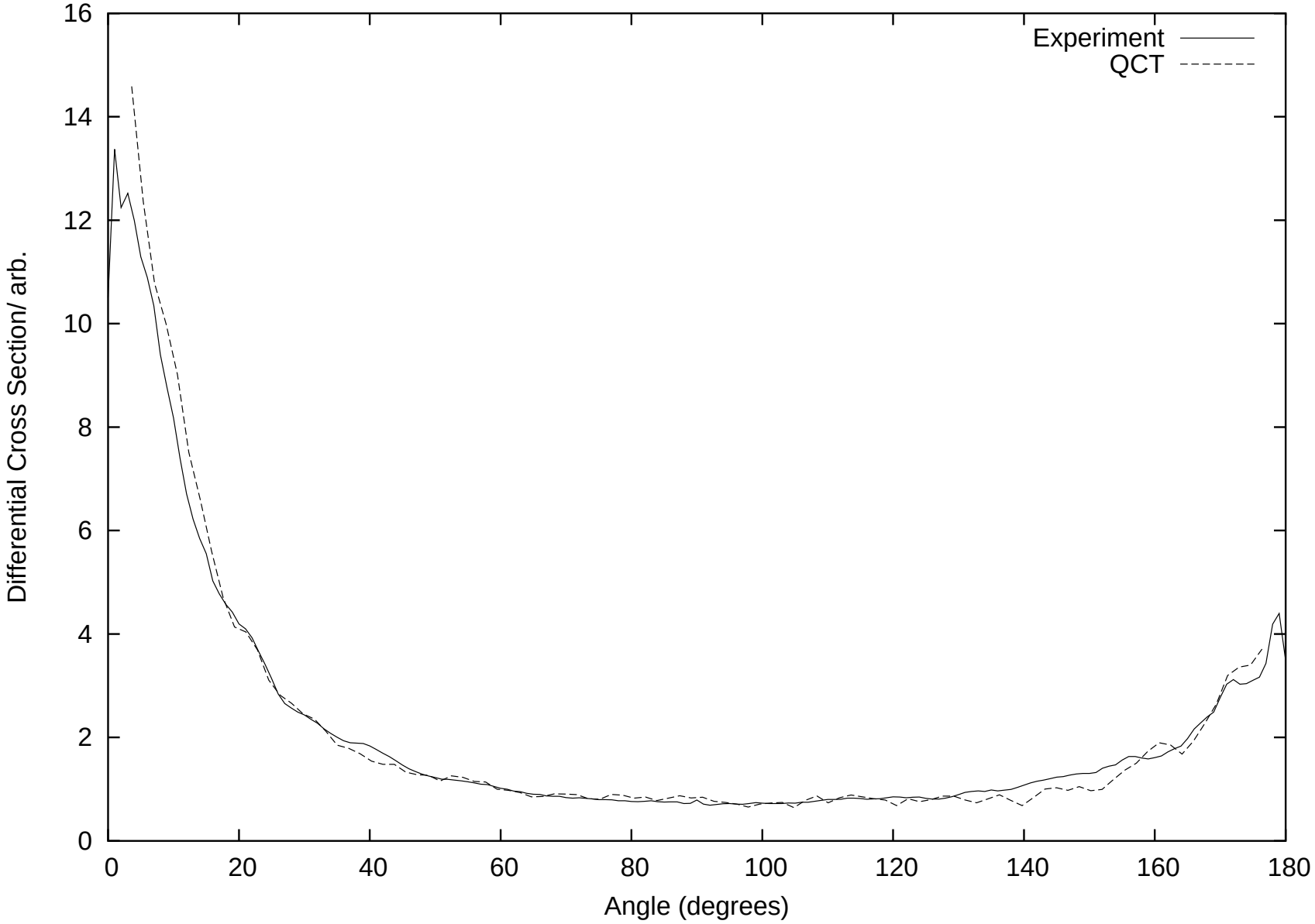

Figure 4.12: Differential Cross Section for OH + Cl product channel on the $1^1A'$ surface at Collision Energy 0.26eV

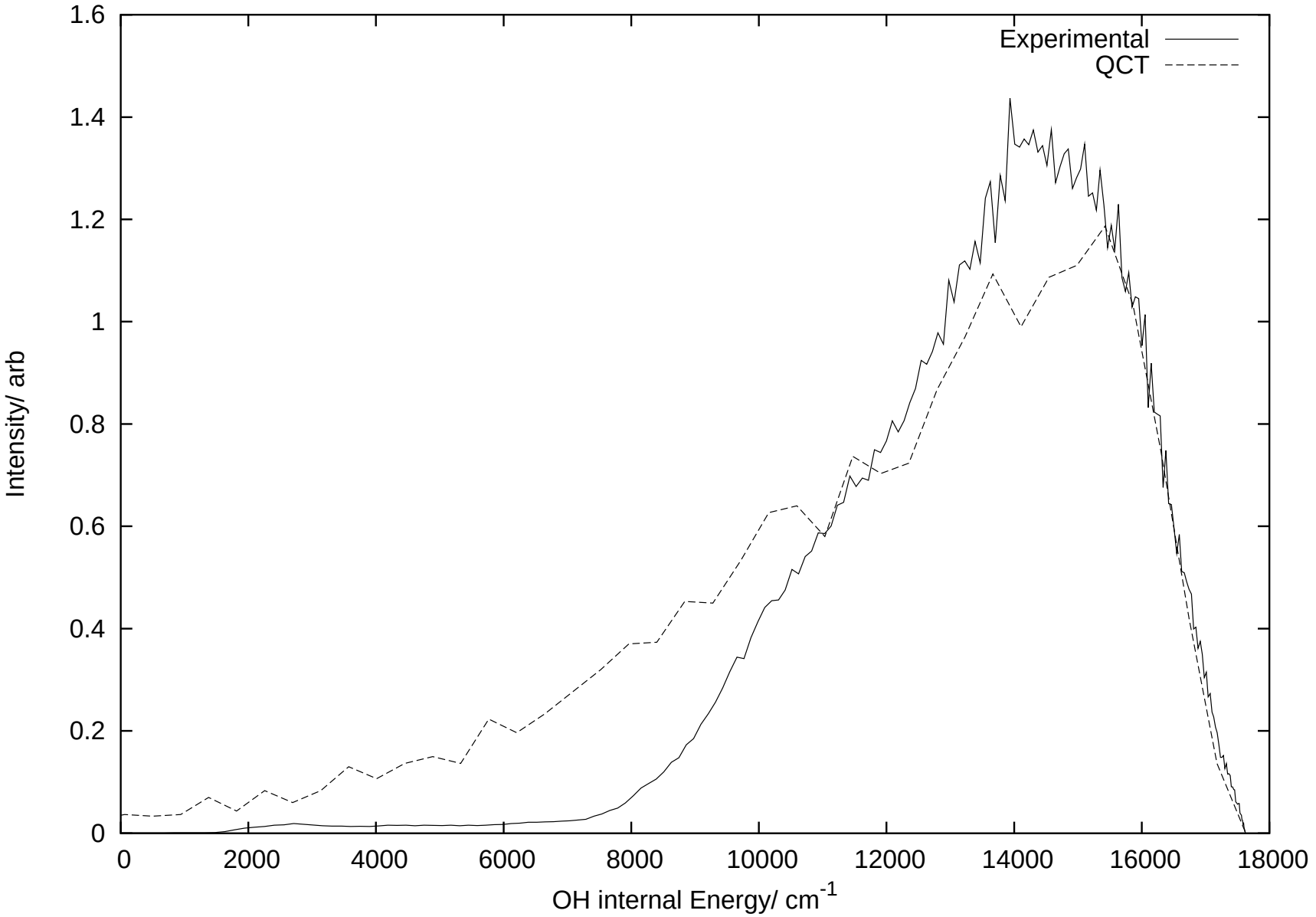

Figure 4.13: OH internal energy distribution for OH + Cl product channel on the $1^1A'$ surface at Collision Energy 0.26eV

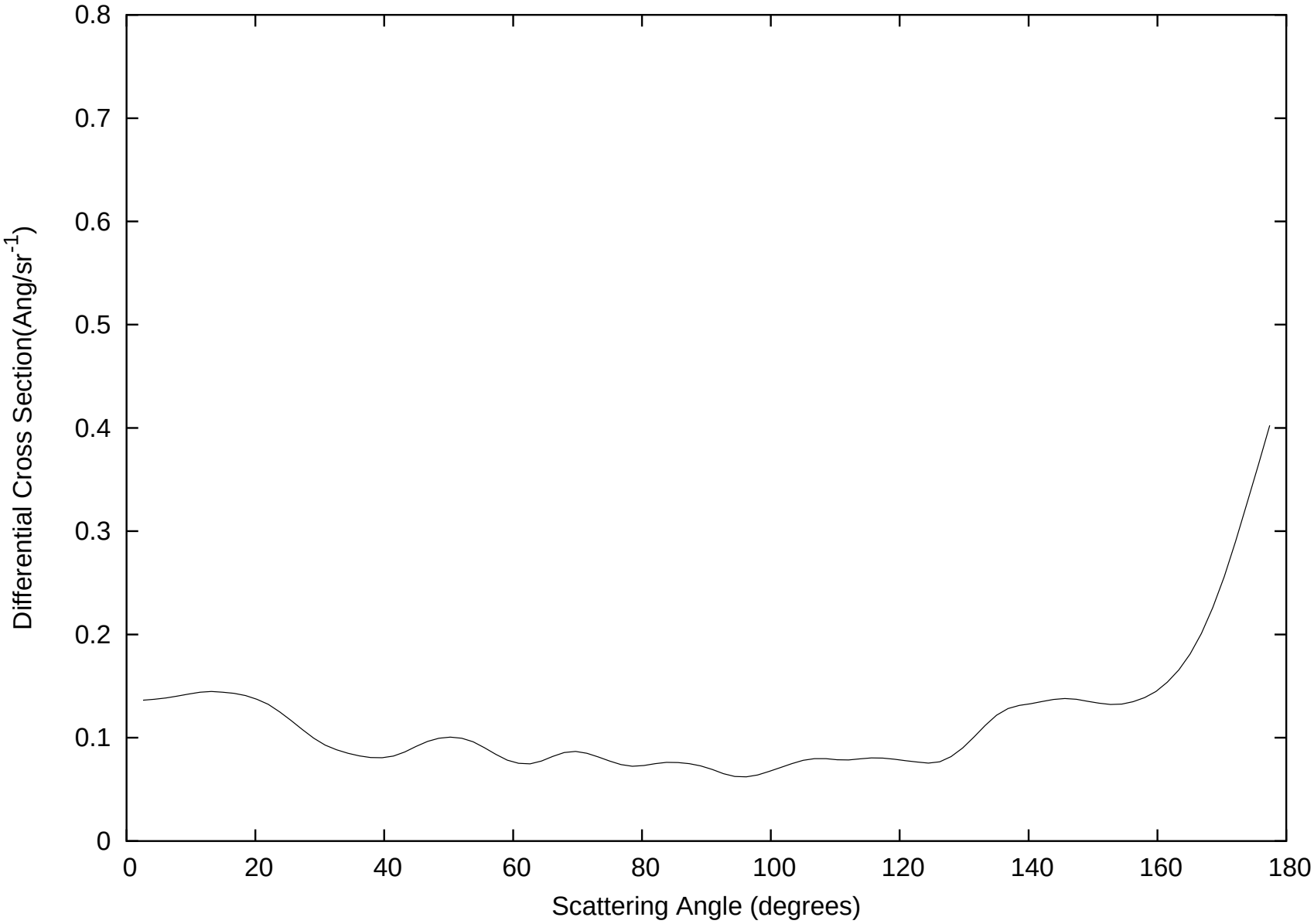

Figure 4.14: Differential Cross Section for ClO + H product channel on the $1^1A'$ surface at Collision Energy 0.26eV

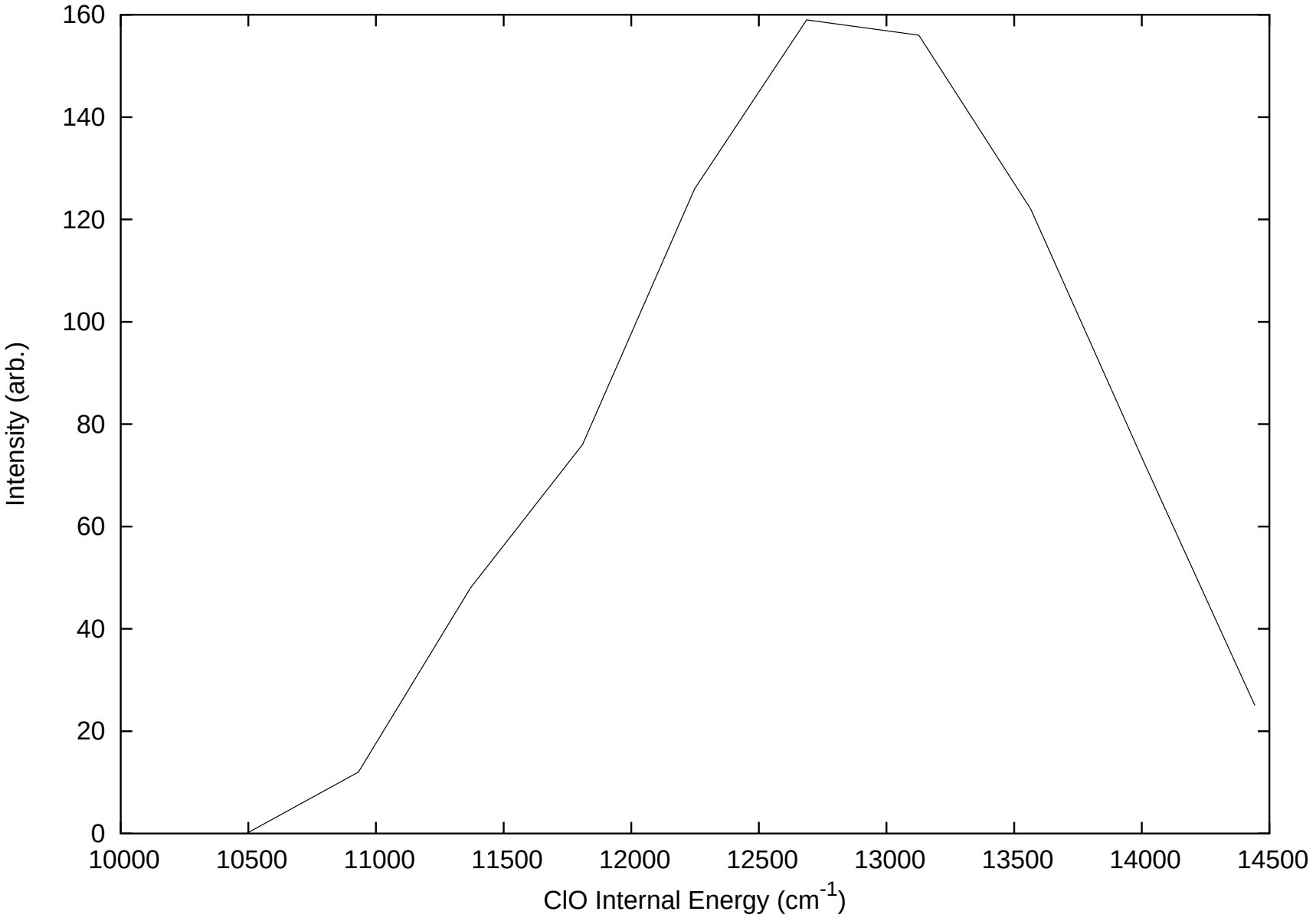

Figure 4.15: ClO internal energy distribution for OH + Cl product channel on the $1^1A'$ surface at Collision Energy 0.26eV

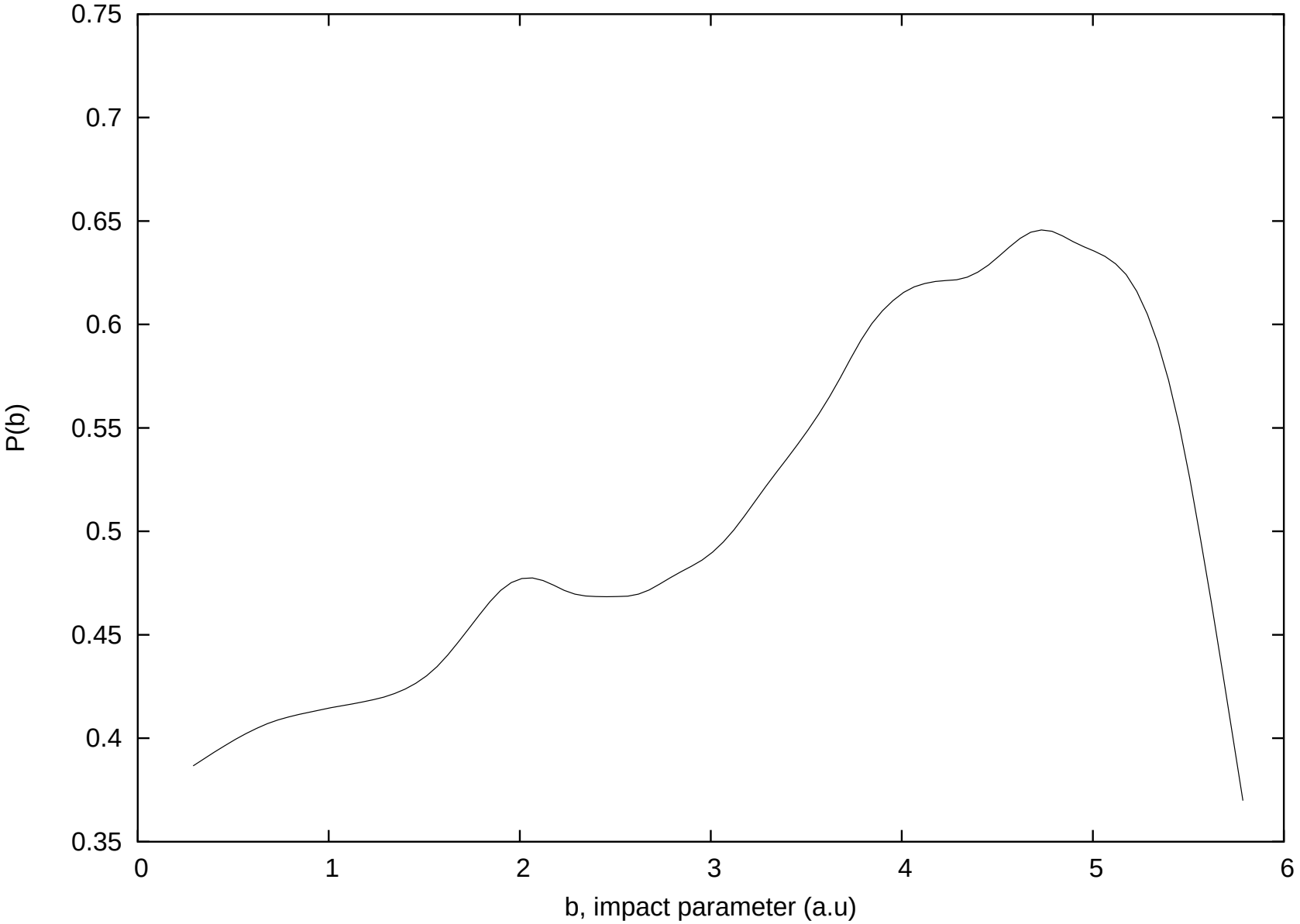

Figure 4.16: P(b) vs. b for the OH + Cl product channel on the $1^1A'$ surface at Collision Energy 0.26eV

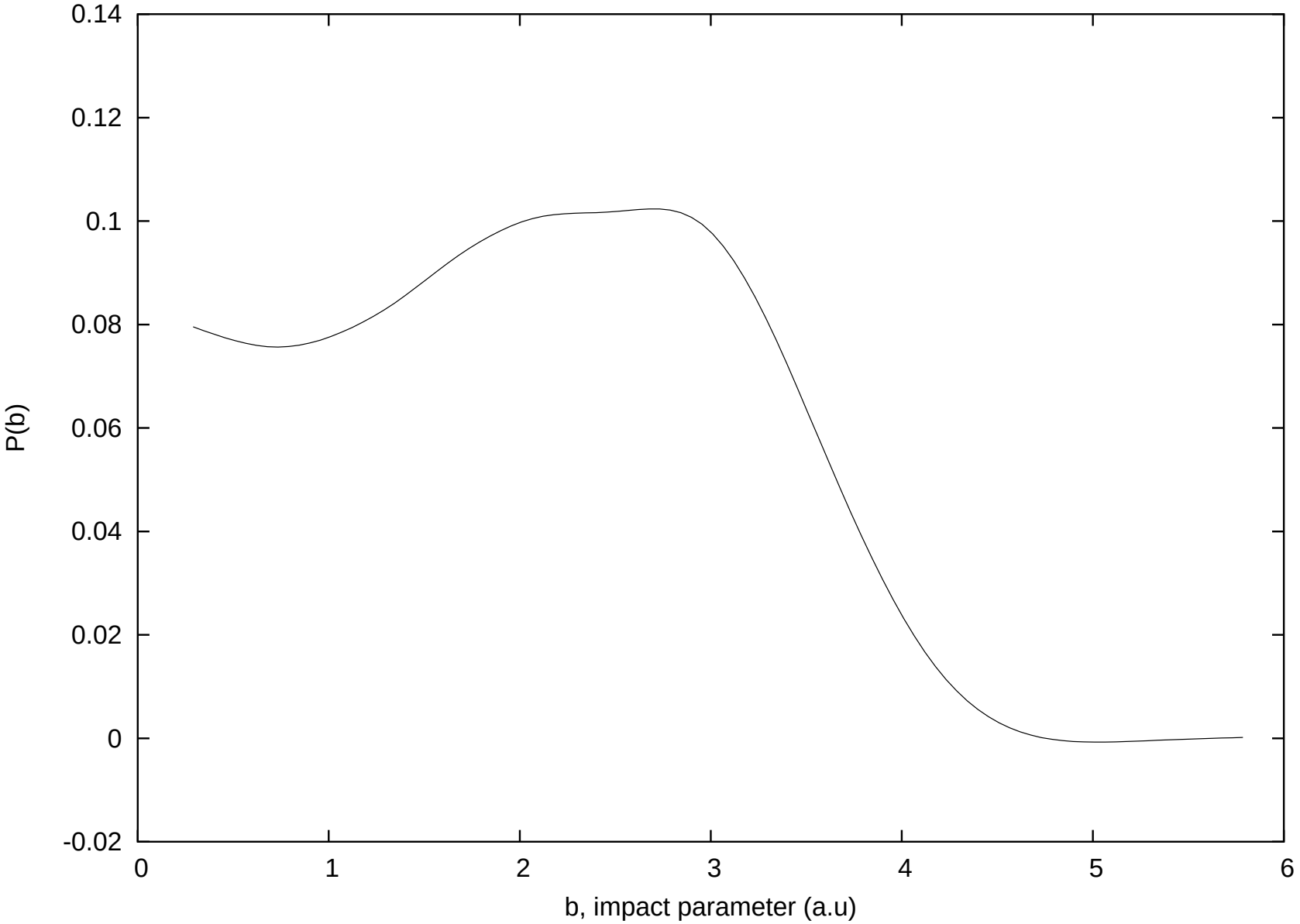

Figure 4.17: P(b) vs. b for the ClO + H product channel on the $1^1A'$ surface at Collision Energy 0.26eV

vs. b, for the two channels are presented in Figs. 4.16 and 4.17. The contribution of the high impact parameters dominates in the production of the OH product with a maximum at about 5 a.u. This behavior is a reflection of the smaller centrifugal barrier of the OH channel. With the cone of acceptance also smaller for the Cl side than the H side [13], the centrifugal barrier is smaller for an O atom attack on the H side of HCl than on the Cl side thereby favoring production of OH.

The branching ratio $\frac{\sigma_{ClO}}{\sigma_{OH}}$ at this collision energy is 0.073. At this energy, there is no data in literature with which I can make a comparison. However as explained later, the two excited PESs do not contribute much at this low energy and thus, this branching ratios is considered to be an appropriate value. In discussing the mechanism of these reactions, because of the two deep wells on the $1^1A'$ potential surface, the facile conjecture would be to regard the reactions as a purely insertion-type mechanism. In fact, it used to be considered as a prominent prototype of insertion reaction because of the presence of the HOCl intermediate which is strongly-bound in nature.[17]. However, the results shown in the accompanying figure dispute such a notion. It is seen that the bond distance of the HClO complex is almost the same as that of the isolated HCl molecule. It can then be suggested that the formation of the HClO complex would be facilitated by the entry of the O atom into the well region, forming the complex in the entrance channel. Looking at Fig. 4.18, it is easy to visualize the mediating effects of the potential well. In Fig. 4.18a and b, two deep wells are seen which correspond to the HO-Cl and the H-ClO intermediates. It is observed that the motion of the H atom in the direction of the hyperradius parameter η, dictates the formation of either the OH or the ClO product and the easy separation of the deep well seen in Fig. 4.18c and d, leads asymptotically to the H + ClO product. This supports the idea that unlike in typical insertion reaction, the trajectory is not trapped in the well long enough to cause an isotropic distibution of scattering angle. This is supported by the DCS plots where it is seen that the forward-backward scattering is favored. The single peak seen in the internal energy distribution also underlines the direct nature of the mechanism of these reactions.

4.6 EFFECTS OF EXCITED PES

4.6.1 $2^1A'$

The fact that $2^1A'$ surface is not correlated to the H+ClO channel means that, a purely quasiclassical approach yields zero probability for this product channel on this surface. This is confirmed from the calculations at both collision energies considered. However for the

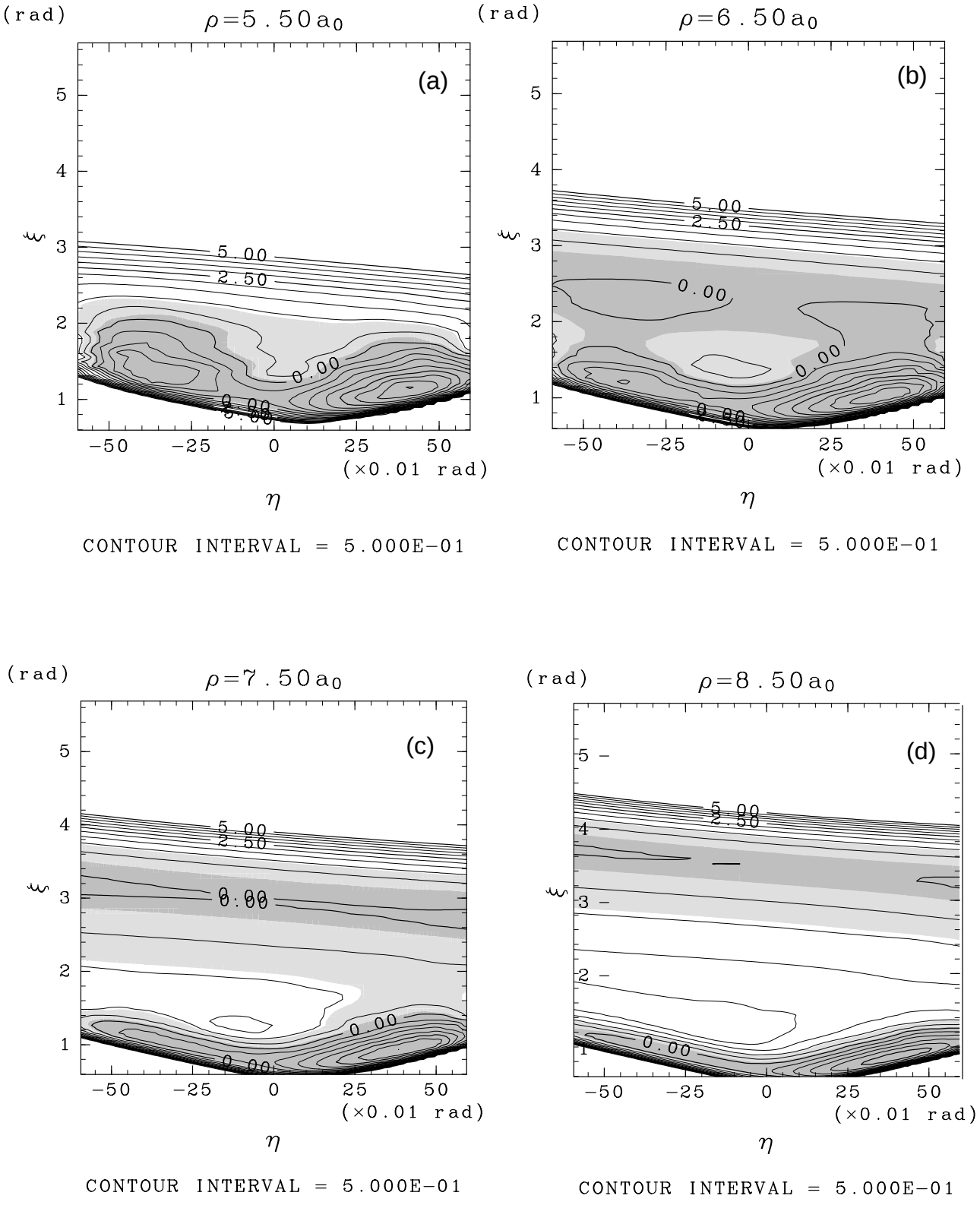

Figure 4.18: Contour plots of the $1^1A'$ potential surface in terms of the hyperradius (a) $\rho =$ 5.5 a_o (b) $\rho = 6.5$ a_o (c)$\rho = 7.5$ a_o and (d) $\rho = 8.5$ a_o. The left-bottom corner, right-bottom corner and mid-point at the upper edge corresponds to the united atom limit of HCl, OH and ClO respectively. [Reproduced with the kind permission of Dr. Shinkoh Nanbu]

OH + Cl product, on the $2^1A'$ surface at a collision energy of 0.529 eV, the reaction probability p_{OH}, is 0.018, confirming that the channel is open. In fact, with inclusion of tunneling, using the methods of Chapter 2, the probability showed an almost two-fold increase to 0.033, a scenario which was anticipated because of the presence of the barrier in the entrance channel. At 0.26eV collision energy, the inclusion of tunneling also boosts the production of the OH channel although the probability is quite small at this energy even with tunneling. Actually without tunneling at this energy, the channel is almost closed with the order of magnitude of the probability being about 10^{-4}. This trend of decreasing probability with decreasing energy on the $2^1A'$ surface is similar to the J= 0 quantum case shown in Fig. 4.7 but from the same figure, it is seen that a large contribution would arise when the initial reagent is rovibrationally excited.

4.6.2 $1^1A''$

On the $1^1A''$, the ClO channel is closed since the PES is not correlated to the ClO production. On the other hand, although tunneling effects do not contribute appreciably to the OH product reaction probability as it does on the $2^1A'$, using the ordinary QCT without tunneling yields a reaction probabilty p_{OH}, of 0.192 at 0.529 eV which is almost half the probability on the ground $1^1A'$ surface at 0.529 eV. This is striking because such contribution would alter the relative contributions of the two product channels especially since the ClO channel is completely closed on this surface. The probability p_{OH} at 0.26 eV is not similarly high, being about 0.039 showing that the reaction probabilities on this surface are much higher than those on the $2^1A'$ surface. Overall, at the collision energy of 0.26 eV, the two excited PES do not give any appreciable contribution to the reaction dynamics.

The discrepancy mentioned before between the experimental and the QCT branching ratio at the 0.529 eV collision enenrgy could also be regarded as an effect of the excited state. At this collision energy, the magnitude of uncertainty in the experimental collision energy means that the total energy could extend to more than 0.8 eV. At around this energy range, there is a sharp rise in the probability of ClO product which may lead to higher detection of ClO and consequent increase in the measured branching ratio.(See arrow labelled B in Fig. 4.6)

Another possible effect of the excited states is the possibility of nonadiabatic transition between the $1^1A'$ and the $2^1A'$ surfaces at higher energies which could lead to ClO products on the $2^1A'$ surface. Nanbu and coworkers have been able to compute the diabatic coupling terms and it would be very interesting to include simultaneously, both tunneling

and nonadiabatic transition, using the ideas expounded in Chapter 2 and 3 in the study of this important chemical system.

In conclusion, the excited states are certain to be quite important at high energies or for rovibrationally excited reactants(See Fig. 4.6 and 4.7). It would be especially interesting to investigate the internal state distribution of products under these conditions because the two excited PES depict very different dynamics i.e state-selectivity dynamics, from the ground-state PES.

4.7 CONCLUDING REMARKS

The quasiclassical method developed here with tunneling effects included has been applied to OHCl at the ν=0,j=0 rovibrational state with the use of the most accurate PES. The reaction mechansim at collision energies of 0.26 and 0.529 eV are clarified and it is deduced that the excited PES do not play crucial roles at these energies, although the effect of tunneling is significant on the $2^1A'$ PES. On this surface, the order of magnitude of reaction probability is one and two orders of magnitude smaller than that of $1^1A''$ at collision energies of 0.26 and 0.529 eV respectively. Although the ground PES is strongly attractive, the reaction proceeds by an abstraction-type mechanism rather than the insertion which would instead be the dominant mechanism at much lower energies.

Good agreement of the present QCT results have been obtained with experimental measurements of DCS and internal energy distribution. The branching ratio is predicted to be $\sim$ 0.08 at 0.26 eV. At 0.529eV, the product branching ratio is also $\sim$ 0.08 contrasting with the experimental value of $\sim$ 0.34. The disagreement between the QCT and the experiment, particularly regarding the branching ratio is ascribed to the $\sim$30% uncertainty of the initial experimental collision energy and the strong ClO production via the $1^1A''$ PES at $E_{col} \geq$ $\sim$ 0.6 eV.

For future work, I would like to investigate the effects of nonadiabatic coupling on the system. Although it may be present, the effects are not expected to be large since the PES are all correlated to the same asymptotic channels. Secondly, I intend to carry out a study to determine at which energy the mechanism transitions from abstraction to insertion. Also, because of the larger contributions of the excited PES, study of reactions at higher collision energies would be carried out most importantly for the branching ratio and the internal state distribution. And finally, I intend to investigate the effects of rovibrational excitation, motivated by the kind of effect seen in fig. 4.7.

REFERENCES

[1] J.A. Davidson, C.M. Sadowski, H.I. Schiff, G.E. Streit, C.J. Howard, D.A. Jennings and A.L. Schmeltekopf, J. Chem. Phys., **64**, 57, 1976.

[2] J.A. Davidson, H.I. Schiff, G.E. Streit, J.R. McAfee, A.L. Schmeltekopf and C.J. Howard, J. Chem. Phys., **67**, 5021, 1977.

[3] P.H. Wine, J.R. Wells and A.R. Ravishankara, J. Chem. Phys., **84**, 1349, 1986.

[4] N. Basco and R.G.W. Norrish, Proc. Roy. Soc. London, Ser. A, **260**, 293, 1961.

[5] A.C. Luntz, J. Chem. Phys., **73**, 5393, 1980.

[6] C.R. Park and J.R. Wiesenfeld, Chem. Phys. Lett., **163**, 230, 1989.

[7] E.J. Kruus, B.I. Niefer and J.J. Sloan, J. Chem. Phys., **88**, 985, 1988.

[8] N. Balucani, L. Beneventi, P. Casavecchia and G.G. Volpi, Chem. Phys. Lett., **180**, 34, 1991.

[9] Y. Matsumi, K. Tonokura, M. Kawasakai, K. Tsuji and K. Obi, J. Chem. Phys., **98**, 8330, 1993.

[10] M.J. Prather, Nature(London), **355**, 534, 1992.

[11] P.J. Crutzen, R. M*ü*ller, C. Bruhl and T. Peter, Geophys. Res. Lett., **19**, 1113, 1992.

[12] K.A. Peterson, S. Skokov and J.M. Bowman, J. Chem. Phys., **111**, 7446, 1999.

[13] T. Martinez, M.L. Hernandez, J. M. Alvarino, A. Lagana, F.J. Aoiz, V.S. Rabanos, J. Chem. Phys., **119**, 7871, 2000.

[14] S. Nanbu, M. Aoyagi, H. Kamisaka, H. Nakamura, W. Bian and K. Tanaka, J. Theo. Comp. Chem., **1**, 263, 2002.

[15] M. Bitterova, J.M. Bowman and K.A. Peterson, J. Chem. Phys., **113**, 6186, 2000.

[16] K.M. Chritoffel and J.M. Bowman, J. Chem. Phys., **116**, 4842, 2002.

[17] T. Martinez, M.L. Hernandez, J. M. Alvarino, A. Lagana, F.J. Aoiz, M. Menendez, E. Verdasco, Phys. Chem. Chem. Phys., **2**, 589, 2000.

[18] H. Goldstein, *Classical Mechanics*, (Addison-Wesley, Massachusetts, 1950)

[19] T. Ishida, G. C. Schatz, Chem. Phys. Lett., **314**, 369, 1999.

[20] C.M. Deeley and I.M. Mills, J. Mol. Spectrosc., **114**, 368, 1985.

[21] W.J. Lafferty and W.B. Olson, J. Mol. Spectrosc., **120**, 359, 1986.

[22] C.M. Deeley, J. Mol. Spectrosc., **122**, 481, 1987.

[23] M.B. Faist, J. T. Muckerman and F.E. Schubert, J. Chem. Phys., **69**, 4087, 1978.

[24] R. Schinke, J. Chem. Phys., **80**, 5510, 1984.

[25] H. Kamisaka, H. Nakamura, S. Nanbu, M. Aoyagi, W. Bian and K. Tanaka, J. Theo. Comp. Chem., **1**, 275, 2002.

[26] H. Kamisaka, H. Nakamura, S. Nanbu, M. Aoyagi, W. Bian and K. Tanaka, J. Theo. Comp. Chem., **1**, 285, 2002.

[27] H. Koguchi and T. Suzuki, unpublished results.

CHAPTER 5

CONCLUSION

In this thesis, the goal has been to extend the usefulness of quasiclassical methodologies in chemical dynamics. Methodologies which have been expounded upon here, like the caustics determination method and the generalized formulation of the Zhu-Nakamura Trajectory Surface Hopping method offer a viable path through which important chemical and biological processes in practically large systems could be studied.

The effiency of the caustics method developed in chapter 2 was checked using the well-known 2-dimensional Henon-Heiles potential and a triatomic reactive 3-dimensional system. A big selling-point of this method is that it works even in the chaotic regime. The utility of this method is further highlighted by its use in tunneling calculations for both the simple collinear and 3-D Jtotal angular momentum $\neq 0$ cases of the H_3 system to good effect. This makes it an important component in the continous task at describing tunneling with the semiclassical framework[1, 2, 3, 4].

In chapter 3, the trajetory-surface method is generalized with the use of the Zhu-Nakamura theory so as to be applicable to multi-dimensional system without prior knowledge of the crossing seam and irrespective of the type of crossing i.e. Landau-Zener(LZ) or Nonadiabatic tunneling(NT) types. The method is applied to the model CH_2 system and found to work nicely in comparison with the exact quantum mechanical results. The model system constructed in order to feature rich nonadiabatic dynamics has a conical intersection which provides both LZ and NT types. Even if the knowledge of the nonadiabatic coupling vector is not available, the direction of the nonadiabatic transition can be approximately estimated.

The caustics and straight-line tunneling method of chapters 2 is finally applied to the real triatomic reaction system O + HCl. Unfortunately, full inclusion of the effects of

nonadiabatic transitions could not be finished and included in this thesis. However, the reaction mechanism could be clarified and actually good agreement with experiment has been obtained. The predominantly forward scattering, and anisotropy seen from experiment is well-reproduced and the internal energy distribution agrees quite well, with a shift peak of less than 2000 cm^{-1}. Further thorough investigations of this system can clarify reaction dynamics in many respects such as the collision energy dependence, the effects of rovibrational excited reagents and the effects of nonadiabatic transitions and tunneling.

The new methodology developed in this thesis, namely the quasiclassical method with tunneling and nonadiabatic transition included can be useful and efficient in the investigation of large systems. The emergence of the Zhu-Nakamura theory should definitely drive these efforts because of its ease of inclusion in a variety of semiclassical methodologies and this is to the great benefit of ordinary quasiclassical methodologies when the system to be studied is too large to make full quantum calculations feasible. Although semiclassical theories including the effect of phases are more accurate[5, 7, 8, 9] than quasiclassical techniques, they are not yet straightforwardly applied to high-dimensional non-harmonic systems.

Since classical trajectories are easy to run as is evidenced by the surge in the various types of molecular dynamics(MD) simulation studies, this thesis advocates the incorporation of important quantum effects like tunneling and nonadiabatic transition to formulate a more useful modification of MD simulations.

Further necessary improvements include the formulation of better and more rigorous tunneling trajectories. These have been found for tunneling splitting and decay[10] but not for reaction. Also, the inclusion of such method should be incorporated into the methods which have been developed in this thesis.

REFERENCES

[1] A.J.C. Varandas and G.V. Mil'nikov, Chem. Phys. Lett., **259**, 605, 1996.

[2] G.V. Mil'nikov and A.J.C. Varandas, Phys. Chem. Chem. Phys., **1**, 1071, 1999.

[3] G.V. Mil'nikov and A.J.C. Varandas, J. Chem. Phys., **111**, 8302, 1999.

[4] F. Bezrukov, D. Levkov J. Expt. Theo. Phys., **98**, 820, 2004.

[5] M.F. Herman and E. Kluk, J. Chem. Phys., **91**, 27, 1984.

[6] E. Kluk, M.F. Herman and H.D. Davis, J. Chem. Phys., **84**, 326, 1986.

[7] E. Kluk, M.F. Herman and H.D. Davis, J. Chem. Phys., **84**, 326, 1986.

[8] X. Sun and W.H. Miller, J. Chem. Phys., **106**, 6346, 1997.

[9] A. Kondorskiy and H. Nakamura, J. Chem. Phys., **120**, 8937, 2004.

[10] G.V. Mil'nikov and H. Nakamura, J. Chem. Phys. **115**, 6881, 2001.